



UNIVERSITY OF TWENTE.



The silent force of the heart:
right ventricular energetics

*Validity and Feasibility of Cardiac Ultrasound for the
Determination of Right Ventricular – Pulmonary
Vasculature Coupling in Intensive Care Unit Patients*

M.J. Boonstra
Master thesis
18th July 2018

Graduation committee:

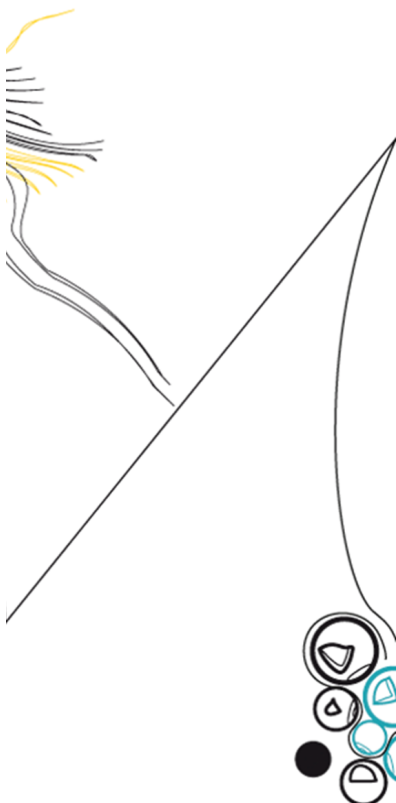
Chair and external member
prof. dr. ir. W. Steenberg

Clinical supervisor
dr. P.W.G. Elbers

Technical supervisor
dr. ir. W.L. van Meurs

Technical supervisor
drs. A.H. Jonkman

Process supervisor
drs. P.A. van Katwijk



Abstract

Introduction - Right heart failure is increasingly being recognized as an independent predictor of adverse outcome in the critically ill. Right ventricular (RV) - pulmonary artery (PA) coupling quantifies right heart efficiency and performance. Mechanical ventilation, pulmonary pathology, and cardiovascular support affect RV-PA coupling. Therefore, assessment of RV-PA coupling in ICU patients may yield important guidance for diagnosis and treatment. Theoretically, bedside determination of RV-PA coupling is possible using ultrasound, circumventing the need of MRI and/or right heart catheterization.

Objective - To determine validity and feasibility of ultrasound derived RV-PA coupling.

Methods - RV systolic pressure, RV stroke volume and RV end systolic volume were estimated from ultrasound measurements. Thereof RV-PA coupling was determined using a multiple beat method and a single beat method. Obtained estimates were compared against invasive pressure measurement and cardiac MRI. Besides, feasibility of the method was assessed in the intensive care unit.

Results - Using ultrasound, a systolic RV pressure profile as well as a systolic RV volumic profile could be obtained. However, ultrasound derived RV systolic pressure, RV stroke volume and RV end systolic volume showed poor correlation with gold standard invasive pressure measurements respectively MRI. Poor correlation existed between ultrasound derived single beat RV-PA coupling and gold standard single beat RV-PA coupling. In the ICU, ultrasound derived RV-PA coupling estimation was challenging. Tricuspid regurgitation was not always present and ultrasound views of the pulmonic valve could often not be obtained.

Conclusion - It is feasible to derive RV-PA coupling value from ultrasound measurements. Despite discrepancy between gold standard and ultrasound measurements, a single beat ultrasound method may provide patient specific guidance during ICU treatment and may therefore be of additional value. Future research should be aimed at the reduction of estimation errors and the ability of ultrasound derived RV-PA coupling to describe treatment effects.

Preface

Geachte lezer,

Voor u ligt mijn master thesis, het resultaat van mijn werk in het VU medisch centrum. Een jaar geleden toen besloot hier af te studeren, had ik nooit gehoopt op het jaar wat zou gaan komen. Ik heb ontzettend veel geleerd en mijn grenzen verlegd. Paul, bedankt voor alle mogelijkheden die je me hebt geboden. Het zelfstandig uit voeren van het onderzoek met jou als directe begeleider heeft me veel geleerd over mezelf en wat ik kan. Annemijn, bedankt dat je deur altijd voor me open stond en ik bij je terecht kon waar dat nodig was. Willem, bedankt voor de middagen overleg, je secure blik maar ook de rem die je soms op mijn enthousiasme wist te leggen. Paul, bedankt voor de inzichten die je me bood tijdens intervisiemomenten, maar ook daarbuiten. Door jouw begeleiding merk ik dat ik bewuster van mezelf ben en dat geeft vertrouwen.

Naast mijn directe begeleiding wil ik ook Erik bedanken. Jouw visie op het onderzoek, je antwoorden op mijn vragen, je pragmatische blik, de wetten van Lust en vooral het leren van echocardiografie hebben veel bijgedragen aan dit onvergetelijke jaar. De rustige, pragmatische en doelgerichte manier waarop jij aan het bed van een kritiek zieke patiënt staat is voor mij een groot voorbeeld. Pieter-Roel, bedankt voor het doorlezen van mijn warrige epistels, de feedback die jij me gaf heeft mij veel geleerd over duidelijk en compact schrijven. Voor u als lezer hoop ik dat dat ook te merken is. Bashar en Judith, bedankt voor alle mooie momenten in het lab, de goede gesprekken en het vertrouwen dat jullie in mij hebben waar ik dat zelf soms miste. En het pulmonale hypertensie team van de longziekten, met name Frank, Fred en Jan. Bedankt voor de dinsdagen, het enthousiasme en de vrijheid die jullie mij gaven mijn metingen te doen, het was machtig mooi.

Daarnaast wil ik ook mijn familie en vrienden bedanken voor de ontspanning, rust, vertrouwen en de mogelijkheid tot het afblazen van stoom. De artsen en de arts-assistenten van de afdeling die altijd enthousiast waren en me veel geleerd hebben op klinisch gebied. En bedankt aan mijn mede collega-studenten; de taartdagen, de grappen, de serieuze gesprekken en het samen genieten van het zachte, rustgevende en vooral oorstrelende geruis van de vriezer.

Veel plezier met lezen, Machteld

List of abbreviations

AP4CH	Apical four chamber
CO	Cardiac output
CW	Continuous Wave
Ea	Arterial elastance
EDV	End diastolic volume
Ees	Ventricular elastance
Ees/Ea	Right ventricular-Pulmonic vasuclar coupling
ESP	End systolic pressure
ESPiso	Isovolumic end systolic pressure
ESPVR	End systolic pressure volume relation
ESV	End systolic volume
ICU	Intensive Care Unit
MRI	Magnetic resonance imaging
PAC	Pulmonary arterial compliance
PCWP	Pulmonary capillary wedge pressure
PLAX	Parasternal long axis
PSAXao	Parasternal short axis at height of the aorta
PVR	Pulmonary vasculature resistance
PW	Pulsed Wave
RV	Right Ventricle
RV-PA	Right ventricular-Pulmonic vasuclar coupling
RVPes	End systolic right ventricular pressure
RVPmax	Maximal right ventricular pressure
RVSP	Right ventricular systolic pressure
SV	Stroke volume
US	Ultrasound

Contents

Abstract	ii
Preface	iv
List of abbreviations	vi
I Introduction	1
II Background	5
1 Physiological background	6
1.1 Physiology of RV systolic function	6
1.1.1 Right ventricular autoregulation	8
1.1.2 Interventricular interaction	8
1.2 Quantification of right ventricular systolic function	9
1.2.1 Stroke volume and ejection fraction	9
1.2.2 Isovolumic pressure change	9
1.2.3 End systolic pressure volume relationship and ventricular elastance	9
1.2.4 Chamber quantification	9
1.3 Physiology of RV afterload	10
1.4 Quantification of RV afterload	10
1.4.1 Pulmonary arterial compliance	11
1.4.2 Pulmonary impedance	11
1.4.3 Pulmonary vascular resistance	11
1.4.4 Pulmonary capillary wedge pressure	12
1.5 Right ventricular - pulmonary vasculature interactions	12
1.5.1 Pathophysiology of right ventricular - pulmonary vasculature interactions	12
1.6 Quantification of right ventricular – pulmonary vasculature interaction	13
1.6.1 Right ventricular pressure volume relation	13
1.6.2 Ventricular elastance and its relation to RV contractility	14

1.6.3	Arterial elastance and its relation to right ventricular afterload	15
1.7	Physiology of right ventricular – pulmonary vasculature coupling	15
2	Technical background	17
2.1	Ultrasound	17
2.2	Ultrasound right ventricular - pulmonary vasculature coupling	18
2.3	Ultrasound pressure estimation	18
2.3.1	Detection of tricuspid regurgitation	18
2.3.2	Bernoulli’s principle of fluid dynamics	19
2.3.3	Tricuspid regurgitation CW envelope	20
2.4	Ultrasound volume estimation	21
2.4.1	Stroke volume	21
2.5	End systolic volume	21
2.5.1	Right ventricular focused ultrasound protocol	22
III	Clinical studies	25
3	Validation of a cardiac ultrasound method to quantify right ventricular stroke volume and end systolic volume	26
3.1	Introduction	26
3.2	Methods	27
3.2.1	Study population	27
3.2.2	MRI	27
3.2.3	Ultrasound	27
3.2.4	Offline data analysis	30
3.2.5	Statistics	30
3.3	Results	30
3.3.1	Ejection fraction	32
3.3.2	Stroke volume and end systolic volume	32
3.4	Discussion	32
3.4.1	Ejection fraction	33
3.4.2	Stroke volume	36
3.4.3	End systolic volume	37
3.4.4	Overall implications for a ultrasound method to derive RV-PA coupling	37
3.4.5	Conclusion	38
4	Validation of a cardiac ultrasound method to quantify right ventricular systolic pressure	39
4.1	Introduction	39

4.2	Methods	39
4.2.1	Study population	39
4.2.2	Right heart catheterization	40
4.2.3	Ultrasound	40
4.2.4	Offline data analysis	41
4.2.5	Statistics	41
4.3	Results	41
4.3.1	Study population	41
4.3.2	RV systolic pressure	42
4.4	Discussion	47
4.4.1	RV systolic pressure	47
4.4.2	Automatic CW Doppler velocity profile detection	48
4.4.3	Invasive pressure measurements	48
4.4.4	Conclusion	49
5	The effect of passive leg raise on measured quantities and ultrasound estimated quantities	51
5.1	Introduction	51
5.2	Methods	52
5.2.1	Study population	52
5.2.2	Right heart catheterization and ultrasound	53
5.2.3	Offline data analysis	53
5.2.4	Statistics	54
5.3	Results	54
5.3.1	Study population	54
5.3.2	Measured RV pressure	54
5.3.3	Ultrasound estimated RV pressure	55
5.3.4	Ultrasound estimated stroke volume and end systolic volume	55
5.4	Discussion	56
5.4.1	RV systolic pressure	57
5.4.2	RV stroke volume and end systolic volume	58
5.4.3	Implications of observed effects on multiple beat RV-PA coupling	58
5.5	Conclusion	58
6	Determining right ventricular – pulmonary vascular coupling using ultrasound	59
6.1	Introduction	59
6.2	Methods	60
6.2.1	Study population	60
6.2.2	MRI, right heart catheterization and RV focused ultrasound	60

6.2.3	Offline data analysis	61
6.2.4	Statistics	61
6.3	Results	62
6.3.1	Study population	62
6.3.2	Ultrasound derived RV-PA coupling	62
6.4	Discussion	64
6.4.1	Single beat ultrasound derived RV-PA coupling	64
6.4.2	Multiple beat ultrasound derived RV-PA coupling	64
6.4.3	Study limitation	65
6.4.4	Added value of the determination of RV-PA coupling in the ICU	65
6.5	Conclusion	65
7	Preliminary investigation into the feasibility of ultrasound method to determine right ventricular pulmonary vasculature coupling in the ICU.	67
7.1	Introduction	67
7.2	Methods	68
7.2.1	Further data acquisition	68
7.2.2	Effect of cardiothoracic surgery	69
7.2.3	Screening adequacy	69
7.3	Results	69
7.3.1	Further data acquisition	70
7.3.2	Effect of cardiothoracic surgery	71
7.3.3	Screening adequacy	71
7.4	Discussion	71
7.5	Conclusion	72
IV	General discussion and conclusion	74
	Appendices	77
A	Descriptive diagrams	78
B	Framework for the automatic detection of PW Doppler velocity profile and CW Doppler velocity profile	82
B.1	Automatic R wave detection	82
B.2	Velocity profile extraction	83
C	Comparison manual and automatic PW profile	84
C.1	Manual PV Doppler velocity quantification	84
C.2	Automatic curve detection	84

C.3	Statistics	85
C.4	Results	86
C.5	Conclusion	86
D	Comparison manual and automatic CW Doppler profile	87
D.1	Manual tricuspid regurgitation Doppler velocity quantification	87
D.2	Automatic curve detection	87
D.3	Statistics	88
D.4	Results	88
D.5	Conclusion	89

Part I

Introduction

Patients admitted to the intensive care unit (ICU) require optimal personalized care for all organ systems. Interaction between organ systems is abundant and failure of one system can result in multiple organ failure. One of the most important systems is the circulatory system. The circulatory system is a closed system, which consists of the heart, systemic circulation and pulmonary circulation. It enables the transport of oxygenated blood and nutrients throughout the body and the removal of waste products from other organ systems. Left heart function is routinely evaluated in contrast to right heart function. However, right heart function is affected by mechanical ventilation. Therefore, frequent monitoring is important in an ICU setting.

In critically ill patients, the left heart function is often assessed to monitor hemodynamic treatment effects, whereas the right heart is not. The right heart is known for its high capability to adapt to fast fluctuations in venous return (VR) and to pressure or volume overload. A failing right heart is a strong predictor of poor outcome. Failure results in decreased cardiac output (CO), thereby diminishing organ perfusion. Severely diminished organ perfusion may result in failure of multiple organ systems and eventually to death. Over the last years, the acknowledgement of the importance of right heart evaluation in critically ill has increased. [1–4]

The interaction between RV systolic function and RV afterload (RV-PA interaction), is correlated with the capability of the RV to maintain cardiac output. RV to pulmonary artery (RV-PA) coupling may be mathematically defined as the ratio of RV end systolic elastance, or ventricular elastance, to pulmonary vasculature elastance, or arterial elastance. Ventricular elastance represents systolic contractile function and arterial elastance represents RV afterload. The ratio of ventricular elastance to arterial elastance describes the ability of the RV to meet RV afterload. When RV afterload increases, RV adaptational mechanisms increase RV systolic function to meet increased RV afterload, thereby maintaining RV-PA coupling. Decreased RV-PA coupling reflect the inability of adaptational mechanisms to compensate for further increasing RV afterload. [5]

In the current clinical practice, RV-PA coupling can only be measured using a combination of right heart catheterization (RHC) and cardiac MRI. However, RHC is highly invasive and MRI is expensive and cannot be performed bedside. Therefore, frequent assessment would result in high burden.

Cardiac ultrasound is often used to assess left and right heart systolic function. In depth right heart US evaluation consists of quantification of chamber dimension, systolic function, diastolic function, and afterload estimation [6]. A combination of these parameters provides insight into RV-PA coupling but does not quantify this interaction. To provide objective quantification of RV-PA interaction, we propose to use US to derive RV-PA coupling. Then, RV-PA coupling can be used as a new parameter to monitor right heart function. US provides a non-invasive, cheap, bedside and

frequent applicable technique. US is often used in the ICU setting, therefore this new parameter can be easily implemented in daily care. Frequent assessment of RV-PA interaction provides insight in direct effect of treatment alongside with additional insight in disease prognosis and outcome. Using US to determine RV-PA coupling, enables the intensivist to frequently assess RV-PA interaction.

The aim of this study is to determine whether an US method is valid and feasible in the ICU population. In the physiological background of RV-PA interaction and cardiac systolic function is further explained. In the technological background, the US method to determine RV-PA coupling is explained with underlying technical assumptions. In the chapter 3 and 4, validity of the US method is tested. In chapter 5, the effect of a passive leg raise maneuver on ultrasound quantities and invasive RV pressure is determined. In chapter 6, RV-PA coupling is determined using a multiple and single beat method. In chapter 7, feasibility of the methodology in the ICU population is described.

Part II

Background

Chapter 1

Physiological background

The right ventricle (RV) is connected in series with the pulmonary circulation, left ventricle and systemic circulation. To maintain cardiac output, adequate left and right systolic function is required. The ability of the RV to maintain cardiac output is determined by RV systolic function and afterload.

The RV is a thin walled, elastic structure and consists of an RV body and RV outflow tract. The RV body contains approximately 80% of total RV volume. These two parts differ in fiber orientation as well as in timing of contraction. Compared to the left ventricle, the RV contracts in a more peristaltic motion from the apex to the RV outflow tract, predominantly facilitated by longitudinal oriented muscle fibers.

Systolic function of the heart is determined by intrinsic ventricular contractility and afterload. Right ventricular afterload depends on a combination of pulmonary artery compliance, pulmonary vascular resistance and left atrial pressure. Changes in compliance, resistance and left atrial pressure are reflected in pulmonary arterial pressure and RV stroke volume. RV systolic function compensates for fast fluctuations in venous return and RV afterload via autoregulation. The physiology of the RV is outlined in the following sections. [7, 8]

1.1 Physiology of RV systolic function

The cardiac cycle consists of four phases, the isovolumic contraction, ejection, isovolumic relaxation and filling (Figure 1.2c). During isovolumic contraction, pressure builds up in the RV without RV outflow over the pulmonic valve. When RV pressure exceeds PA pressure, the pulmonic valve opens and RV ejection begins. After ejection, RV pressure decreases, the pulmonic valve closes and isovolumic relaxation starts. The tricuspid valve opens when right atrial pressure exceeds RV pressure and ventricular filling begins. The phases in the cardiac cycle are affected cardiac muscle properties. [9–11]

Cardiac muscle cell fibers consist of sarcomeres, which are the smallest contractile units of the

cardiac muscle. Sarcomeres are connected to each other by the Z-discs and consist of actin, titin and myosin filaments. During contraction, Z-discs move to each other because myosin filaments slide between actin filaments and cross bridges are formed. Active myosin ATPase initiates movement. Titin filaments attach myosin filaments to the Z-discs and contain several spring sections. Titin filaments are the main determinants of diastolic stiffness.

Depolarization of cardiac muscle cells causes the influx of calcium ions, which triggers further release of calcium ions from the sarcoplasmic reticulum. Calcium ions also interact with myosin ATPase whereby sarcomere shortening is initiated. After sarcomere shortening, calcium ions are removed from the cytosol into the sarcoplasmic reticulum or extracellular fluids. Removing calcium ions from the cytosol allows the sarcomeres to relax to their initial length.

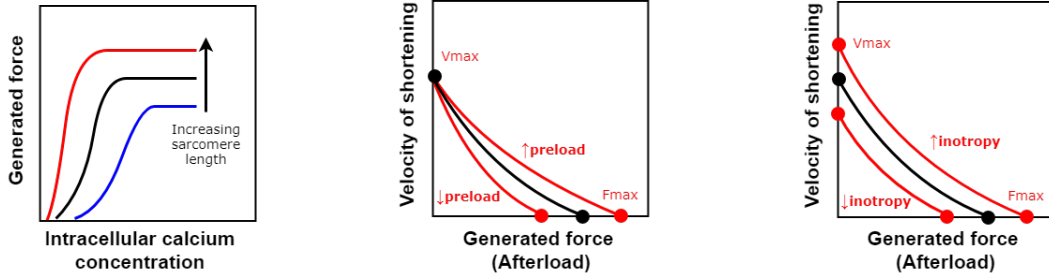
The magnitude of the force during contraction is determined by sarcomere length and by the intracellular calcium ion concentration, which can be described by a sigmoidal curve (Figure 1.1a). An increase in intracellular available calcium ions causes positive inotropic effect. Due to the increased availability of calcium ions, the amount of formed cross bridges increases thereby increasing contraction force. An increase in sarcomere length causes increased sensitivity of the actin and myosin filaments for calcium ions and causes a left- and upward shift of the curve. The effect of increase in sarcomere length forms the basis of the Frank-Starling law of the heart. [12, 13]

Another characteristic of the cardiac muscle cell is the inverse relation between force and velocity of shortening. As force increases, velocity of shortening decreases. Maximal shortening velocity occurs when stress on the sarcomeres is zero, and is not affected by sarcomere length, but is affected by intracellular calcium availability. Alterations in preload and inotropy are known to affect the force-velocity relationship.

With increased preload, the length tension relationship increases contractile force (Figure 1.1b). The sarcomere can generate higher force, the velocity of shortening is increased and thus the sarcomere contracts faster against constant RV afterload. Increased preload also increases maximal isometric force, but maximal shortening velocity remains the same. Decreased preload results in the opposite effect.

With increased inotropy, both maximal isometric force and shortening velocity increase (Figure 1.1c). Due to the increased inotropic state, force generation by the sarcomere increased due to the increased amount of formed cross bridges against constant RV afterload.

Figure 1.1: Schematic representations of cellular mechanisms determining RV systolic function.



(a) A schematic representation of the interaction between intracellular calcium concentration (x-axis) and sarcomere length (black arrow) on ventricular contractile force (y-axis). Contractile force increases with sarcomere length and intracellular calcium concentration. [10–12].

(b) A schematic representation of the effect of increased preload on the relation between afterload (x-axis) and velocity of shortening (y-axis) of the cardiac muscle cell. The black curve represents initial condition and the red curves represent the conditions with increased respectively decreased preload. As preload increases, maximal velocity of shortening remains the same whereas maximal generated force increases. [10, 11]

(c) A schematic representation of the effect of positive inotropy and negative inotropy on the relation between afterload (x-axis) and velocity of shortening (y-axis) of the cardiac muscle cell. The black curve represents initial condition and the red curves represent the conditions with increased respectively decreased inotropy. Positive inotropy causes both maximal velocity of shortening and maximal generated force to increase. [10, 11]

1.1.1 Right ventricular autoregulation

Two autoregulatory mechanisms exist to maintain cardiac output after changes in preload or afterload in the RV; heterometric and homeometric autoregulation. Heterometric autoregulation is a fast mechanism based on the length-tension relationship. It is also known as the Frank-Starling law of the heart. Homeometric autoregulation is a slower mechanism based on changes in contractility. In case of increased RV afterload, homeometric autoregulation induces a positive inotropic effect, also known as the Anrep-effect. [7, 14]

These mechanisms are not completely independent. For example, if an increase in RV afterload occurs, heterometric autoregulation immediately responds by increasing end diastolic volume, thereby altering the length tension properties of the muscle cell. If increased RV afterload persists, homeometric autoregulation allows for an increase in muscle cell contractility.

1.1.2 Interventricular interaction

As the RV is connected in series with the left ventricle via the pulmonary vasculature, RV stroke volume will influence left ventricular stroke volume. Via the interventricular septum a more direct

interaction between the left ventricle and RV exists. During systole, left ventricular contraction affects RV contraction. Left ventricular contraction contributes up to 40% to RV contraction. Another direct interaction is due to the stiffness of the pericardium. Because the pericardium limits all outer ventricular walls to expand, pressure and volume overload of the RV affect left ventricular function via the interventricular septum. [15]

1.2 Quantification of right ventricular systolic function

1.2.1 Stroke volume and ejection fraction

Stroke volume is the amount of blood ejected by the RV in the pulmonary vasculature. Ejection fraction is defined as the ratio of stroke volume to end diastolic volume and describes the fraction of ejected blood from the RV into the pulmonary vasculature. Both stroke volume and ejection fraction are affected by preload, afterload and contractile force of the ventricle. In a failing RV, these parameters strongly reflect decreased RV systolic function.

1.2.2 Isovolumic pressure change

Maximal positive pressure change in the ventricle during the isovolumic contraction and maximal negative pressure change during the isovolumic relaxation phase is determined as dP/dt_{max} respectively dP/dt_{min} . Increase in RV inotropy is reflected in increased dP/dt_{max} . However, dP/dt_{max} is also influenced by preload, afterload, heart rate and the myocardial hypertrophy. An increase in lusitropy (relaxation) is reflected by increased dP/dt_{min} . Therefore, both dP/dt_{max} and dP/dt_{min} can not serve as a quantity to solely describe RV contractile function. [10, 11, 16]

1.2.3 End systolic pressure volume relationship and ventricular elastance

The end systolic pressure volume relation (ESPVR) describes the relation between generated pressure at given ventricular volume. ESPVR reflects intrinsic contractile state of the cardiac muscle. The slope of ESPVR represents ventricular elastance (E_{es}). Ventricular elastance is merely insensitive to changes in preload, afterload and heart rate. Due this relative insensitivity, using ventricular elastance to describe RV contractility is superior to the use of dP/dt_{min} , dP/dt_{max} , stroke volume and ejection fraction. Ventricular elastance will be further addressed in section 1.6.1. [17]

1.2.4 Chamber quantification

To gain insight in the occurrence of RV dilatation and the effect of volume and pressure overload on the left ventricle, cardiac ultrasound or MRI can be performed. Septum deviation as well as increased RV volume can be determined and gives a global information about RV systolic function and its effect on left ventricular function. [6]

1.3 Physiology of RV afterload

The RV generates pressure to eject blood into the pulmonary vasculature. The amount of pressure generated by the RV depends on pulmonary vascular resistance, pulmonary arterial compliance, wave reflections, left atrial pressure (or pulmonary capillary wedge pressure (PCWP)) and blood inertance. Respiration is known to affect both pulmonary vascular resistance and venous return.

During a respiratory cycle total lung volume changes. With changing total lung volume, pulmonary vascular resistance is affected. Total pulmonary vascular resistance is determined by extra-alveolar and alveolar pulmonary vascular resistance. Alveoli expand during inspiration thereby compressing alveolar capillaries whereas during expiration, pressure on alveolar capillaries decreases. In extra-alveolar vessels, resistance decreases during inspiration. Extra-alveolar vessels become less tortuous due to increased lung volume. The interaction between lung volume and total pulmonary vascular resistance is displayed in Figure 1.2a. In mechanically ventilated patients, positive end expiratory pressure (PEEP) is applied to prevent alveoli from collapsing. With the application of PEEP, end expiratory volume is increased, thereby increasing pulmonary vascular resistance. [10,15]

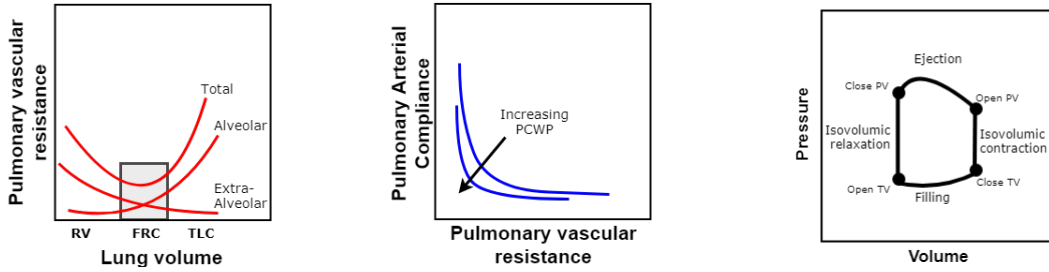
Respiration affects venous return due to the change in intrathoracic pressure. During inspiration, intrathoracic pressure decreases also causing right atrial pressure to decrease. This decrease increases the pressure gradient between the systemic venous system and the right atrium thereby increasing venous return. During expiration, intrathoracic pressure increases, thereby decreasing the pressure gradient and decreasing venous return. In mechanically ventilated patients, this effect is reversed. Air is pushed into the lungs with a positive pressure instead of sucked into the lungs with a negative pressure. Therefore, intrathoracic pressure is higher during inspiration and lower during expiration. [18–20]

Interaction factors determining RV afterload is displayed in Figure 1.2b. In a system with high compliance, resistance is low but a slight change in resistance causes a significant change in compliance. This inverse relation between resistance and compliance is defined as RC-time (= compliance*resistance). RC-time is constant but can be affected by PCWP. [5]

1.4 Quantification of RV afterload

RV afterload consists of a steady and pulsatile component. RV afterload is mainly determined by its steady component, the pulsatile component accounts 25-30% of RV afterload [21,22].

Figure 1.2: Schematic representations of factors affecting RV afterload and the cardiac cycle.



- (a) A schematic representation of the interaction between total lung volume (x -axis) and pulmonary vascular resistance (y -axis). Total pulmonary vascular resistance consists the summation of alveolar resistance and extra-alveolar resistance. [10]
- (b) A schematic representation of the effect of increased pulmonary capillary wedge pressure (PCWP) on the interaction between pulmonary vascular resistance (PVR, x -axis) and pulmonary arterial compliance (PAC, y -axis). At low PVR, slight changes in PVR have a major impact on PAC. At high PVR, major changes in PVR slightly affect PAC. As PCWP increases, the relation between PVR and PAC is affected. [5, 10]
- (c) A schematic representation of the four phases of a cardiac cycle, as presented by a pressure (y axis) volume (x axis) loop. The four phases of contraction and opening and closing of the pulmonic valve and tricuspid valve are displayed. [10]

1.4.1 Pulmonary arterial compliance

Pulmonary arterial compliance gives a measure of the arterial distensibility of the arterial tree of the pulmonary vasculature. Compliance is defined as the ratio of volume change to pressure change. Therefore, pulmonary arterial compliance is defined as stroke volume to pulmonary artery pulse pressure (= pulmonary artery systolic pressure – pulmonary artery diastolic pressure). [10, 15, 23]

1.4.2 Pulmonary impedance

Pulmonary impedance describes RV afterload in the frequency domain. Fourier analysis is applied to simultaneous pulmonary artery pressure and flow measurements. Pulmonary impedance contains information about the resistance, timing of arterial wave reflections, arterial stiffness and pulse wave velocity. [21]

1.4.3 Pulmonary vascular resistance

To describe resistance of laminar flow of a Newtonian fluid in a circular rigid tube, the Hagen-Poiseuille law must be applied. This law illustrates the sensitivity of resistance to radius of a tube and thus explains the effect of narrowing of the pulmonary vasculature. However, a healthy

pulmonary vasculature does not contain rigid tubes with equal radius, flow is not laminar but pulsatile and blood viscosity depends on flow velocity. Therefore, pulmonary vascular resistance is often determined by Ohm's law. Ohm's law states that the ratio of voltage across a resistor to current is proportional to resistance. In the pulmonary circulation, pressure is analogous to voltage and cardiac output to current:

$$R = \frac{U}{I} \quad - > \quad PVR = \frac{\text{meanPAP} - \text{PCWP}}{CO} \quad (1.1)$$

where *PVR* represents pulmonary vascular resistance, *mean PAP* represents mean pulmonary artery pressure, *PCWP* represents pulmonary capillary wedge pressure and *CO* represents cardiac output. [10, 11, 15]

1.4.4 Pulmonary capillary wedge pressure

PCWP gives an estimation of left atrial pressure. It is determined using a fluid filled catheter which is introduced in the pulmonary artery via the right heart. A small artery of the pulmonary arterial branch is occluded by balloon inflation. When the balloon is inflated, left atrial pressure is measured through the static fluid column behind the balloon to the left atrium. If left atrial pressure is increased due to left heart failure RV afterload will increase, thereby stressing the RV. [15]

1.5 Right ventricular - pulmonary vasculature interactions

Interaction between the RV and PA is determined by parameters determining RV systolic function and RV afterload. Where increased SV increases RV afterload, increased RV afterload changes RV systolic function. A concise representation of RV-PA interaction gives insight in RV systolic function and RV afterload. Frequent quantification of RV-PA interaction provides insight in deteriorating or improving RV-PA interaction. The ability of the RV to maintain CO is described and therapy directed on RV-PA coupling can be quantified and objectively adjusted. [5, 24]

1.5.1 Pathophysiology of right ventricular - pulmonary vasculature interactions

Increased RV afterload can be caused by narrowing of the pulmonary arterial vasculature, left heart failure, chronic lung disease, chronic embolisms in the pulmonary vasculature or systemic diseases like sarcoidosis or thyroid disease. Pulmonary hypertension is defined as a resting mean pulmonary artery pressure is at or above 25 mmHg, which reflects increased RV afterload. [15, 25]

If the cause of pulmonary hypertension is adequately treated, RV afterload decreases or remains the same and the RV does not have to compensate further to maintain stroke volume. To compensate for chronic increased RV afterload, the RV may become hypertrophic. When the cardiac muscle remains well perfused and an appropriate capillary bed develops, RV hypertrophy does not necessarily result in RV failure. In case of cardiac malperfusion, RV failure can be induced. With

therapy targeting RV afterload, RV hypertrophy can be reversed. [26,27]

RV failure can also be induced by its inability to further compensate increasing RV afterload. Consequently, stroke volume will decrease. The RV then tries to compensate by dilation to maintain stroke volume. However, RV dilation and increased RV pressure results in increased wall stress. With increasing wall stress, deviation of the interventricular septum is induced which interferes with left ventricular function. End stage pulmonary hypertension is associated with a vicious circle of further decreasing stroke volume and increasing RV dilation.

1.6 Quantification of right ventricular – pulmonary vasculature interaction

RV systolic function depends on a combination of intrinsic contractility, afterload, preload and heart rate. Intrinsic contractility defines the contractile force of the muscle to overcome RV afterload. RV preload defines wall stress and affects the length-tension interaction of sarcomere. Heart rate and heart rhythm affects filling and contraction time, thereby affecting preload and afterload. A pressure volume loop represents the cardiac cycle and can be used to describe ventriculo-arterial interaction. [5,24]

1.6.1 Right ventricular pressure volume relation

A pressure volume loop gives insight in the change in pressure and volume during a cardiac cycle (Figure 1.2c). Pressure volume loop analysis reflects systolic function. Ejection fraction, stroke volume, stroke work, contractility, afterload and preload can be derived from a pressure volume loop. Ventriculo-arterial coupling is described by the ratio of ventricular elastance to arterial elastance. Sunagawa et al [28,29] were the first to describe this concept in the left ventricle. Ventricular contractility is described by maximal elastance during contraction, occurring at end systole. [30,31] The concept of ventriculo-arterial coupling was tested in the RV and proven applicable. [32–35]

Multiple beat methods and single beat methods have been designed to determine right ventricular-pulmonary vasculature (RV-PA) coupling. A multiple beat method depends on a change in venous return, thereby affecting RV preload. Via the Frank-Starling law of the heart, RV stroke volume, RV pressure and RV end systolic volume are affected, without a change in RV contractility. From a set of pressure volume loops at different preload conditions, RV-PA coupling is derived. A single beat method obviates the need for a change in preload. Using the isovolumic contraction and relaxation phases, maximal isovolumic pressure is extrapolated and used to derive single beat RV-PA coupling. The following section contains a more comprehensive description of both methods.

1.6.2 Ventricular elastance and its relation to RV contractility

Cardiac contractility depends on sarcomere length and intracellular calcium availability. At end systole, sarcomeres are fully contracted and all myofilaments contain bound calcium. Contracted sarcomeres generate force (pressure) against end systolic volume. At end systole, sarcomeres are neither lengthening or shortening. Therefore, end systolic pressure reflects to which extent the cardiac muscle can generate force and thus provides a surrogate for contractility.

An acute increase in venous return increases end diastolic volume. Increase in end diastolic volume increases sarcomere length and sarcomere sensitivity to calcium without changing intracellular calcium concentration. This is related to the Frank-Starling law of the heart. The pressure volume loop shifts to the right and due to increased stroke volume, RV afterload increases, also causing an upward shift (Figure 1.3a). From these two pressure volume loops, end-systolic pressure volume relation (ESPVR) can be derived. The slope of ESPVR reflects ventricular contractility and is defined as end systolic ventricular elastance. Increased inotropy is related to a change in the slope of the ESPVR (Figure 1.3a). At constant RV afterload, the RV can eject increased stroke volume into the pulmonary vasculature.

Ventricular elastance is mathematically defined as:

$$Ees = \frac{ESP}{ESV - V_0} \quad (1.2)$$

where Ees is ventricular elastance in mmHg/ml, ESP is end systolic pressure in mmHg, ESV is end systolic volume in ml and V_0 is the volume of the unstressed and unloaded ventricle in ml. [28]

The multiple beat method relies on the acquisition of multiple pressure volume loops under different preload conditions. This method obviates the need of V_0 estimation and ventricular elastance is determined as the slope of the line between the end systolic pressure volume point of two pressure volume loops (Figure 1.3a). Multiple beat ventricular elastance (Ees,mb) is mathematically defined as:

$$Ees,mb = \frac{ESP_2 - ESP_1}{ESV_2 - ESV_1} \quad (1.3)$$

where 1 (red in Figure 1.3a) indicates the first loading condition and 2 (blue in Figure 1.3a) the second loading condition.

In animal studies, preload was decreased by the inflation of a balloon in the inferior vena cava. The Valsalva maneuver was proposed and proven applicable as a non-invasive alternative to obviate the need for inferior vena cava occlusion. [36, 37]

The single beat method obviates the need to alter preload to determine ventricular elastance [16, 38]. The isovolumic phases of the cardiac cycle are used to extrapolate maximal end systolic pressure

(ESP_{iso}) as would occur when the RV contracts and no blood is ejected (see left panel Figure 5.1b). Single beat ventricular elastance (E_{es,sb}) is mathematically defined as:

$$E_{es, sb} = \frac{ESP_{iso} - ESP}{SV} \quad (1.4)$$

The single beat method has been validated in dogs by pulmonary arterial occlusion. Linear correlation between extrapolated isovolumic pressure and measured isovolumic pressure existed. Extrapolated isovolumic pressure overestimated measured isovolumic pressure by approximately 15%. Positive inotropy affected estimated ventricular elastance, whereas changes in preload did not. [16]

1.6.3 Arterial elastance and its relation to right ventricular afterload

Afterload is defined as the wall stress during ventricular ejection and can be thought of the load the RV faces during ejection. The RV generates pressure to eject blood in the pulmonary vascular system, this pressure is generated to overcome the pressure to initiate blood flow. Therefore, pressure generated in the ventricle during ejection is often thought of as afterload.

RV afterload consists of a pulsatile and steady component. Both components of RV afterload can be described using arterial elastance (E_a) [39]. Arterial elastance is defined as:

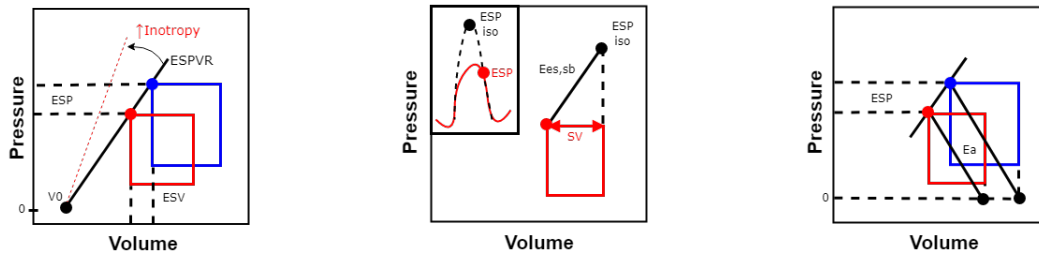
$$E_a = \frac{ESP}{SV} \quad (1.5)$$

where *ESP* is end systolic pressure in mmHg and *SV* is stroke volume in ml. Arterial elastance can be determined from pressure volume loops (Figure 1.3c). Under different preload conditions, E_a remains constant. Although E_a is more sensitive for changes in pulmonary vasculature resistance than pulmonary arterial compliance [40–42], arterial elastance gives information about both RV afterload components and can be compared to ventricular elastance.

1.7 Physiology of right ventricular – pulmonary vasculature coupling

The dimensionless ratio of ventricular elastance to arterial elastance (E_{es}/E_a) is defined as RV-PA coupling and describes RV-PA interaction. When the ratio is bigger than 1, the RV provides enough energy to overcome RV afterload. When the ratio becomes smaller than 1, the system becomes uncoupled. A ratio below 1 reflects the inability of the RV to compensate further for increased RV afterload. Consequently, stroke volume decreases. [5, 24, 36, 43, 44]

Figure 1.3: Schematic representations the derivation of ventricular elastance and arterial elastance from pressure volume loops.



- (a) A schematic representation of the end systolic pressure volume relation (ESPVR, black solid line) and its estimation from multiple pressure volume loops (blue and red rectangle). Ventricular elastance is determined as the slope of ESPVR. Increase in inotropy causes the slope of the ESPVR line to increase, as indicated with the arrow. End systolic pressure (ESP) and end systolic volume (ESV) are used to determine ESPVR. [32]
- (b) A schematic representation of the single beat estimation of ventricular elastance. In the upper left panel, extrapolation of isovolumic pressure (black dot) from the isovolumic phases of the pressure curve (red line) is displayed. Stroke volume (SV) and the difference between end systolic pressure (ESP, red dot) and ESP_{iso} are used to determine ventricular elastance ($E_{es, sb}$) [16]
- (c) A schematic representation of the derivation of arterial elastance (E_a , black solid lines) from pressure (y axis) volume (x axis) loops. Arterial elastance is determined as the ratio of end systolic pressure (ESP) to stroke volume. [16, 28, 32]

Chapter 2

Technical background

With ultrasound, RV function can be described. Systolic RV function is affected by RV afterload. However, ultrasound quantities used in a clinical setting only describe systolic RV function or RV afterload. A combination of these parameters provides insight in RV-PA interaction but does not quantitatively describe this interaction. Therefore, ultrasound derived RV-PA coupling is proposed as an additional ultrasound quantity to describe RV-PA interaction. The method relies on a combination of RV fractional area changes, RV systolic pressure and pulmonic valve flow. These quantities are often assessed in extensive cardiac ultrasound, but not in the clinical setting at the ICU. [6]

2.1 Ultrasound

The active element of the ultrasound probe consists of piezoelectric elements. A piezoelectric element converts electrical signals to mechanical vibrations and vice versa. This element can send and receive signals. Transmitted mechanical vibrations, or sound waves, are conducted through tissues and are partly reflected at boundaries between different kinds of acoustic impedance. The reflected wave is received by the piezoelectric element and converted to an electrical signal. [45]

Two-dimensional images are constructed from an array of piezoelectric elements. Received sound waves are reconstructed to depth and intensity values. Apart from two dimensional images, an ultrasound probe can also determine velocity of flow based on the Doppler effect. The Doppler effect describes that a change in frequency of the sound wave is equal to relative motion between the source and receiver of the sound:

$$v = \frac{cf_d}{2f_0\cos\Theta} \quad (2.1)$$

where v is blood flow velocity, c is speed of sound in tissue ($= 1540$ m/s), f_d is frequency shift, f_0 is frequency of transmitted ultrasound wave and Θ is the angle between the ultrasound scan line and direction of blood flow velocity. [10, 45]

On the cardiac ultrasound machine three Doppler modes exist; color Doppler, pulsed wave (PW)

Doppler and continuous wave (CW) Doppler. Color Doppler provides an overview of the velocity profile of a two-dimensional image, whereas PW Doppler and CW Doppler measure the velocity over the scan line. The difference between PW Doppler and CW Doppler that PW Doppler measures velocity at a specified depth of the image whereas CW Doppler detects all velocities over the complete scan line. With CW Doppler, all velocities can be detected, PW Doppler is limited to a velocity range based on the depth of the velocity measurement. [6,46]

2.2 Ultrasound right ventricular - pulmonary vasculature coupling

RV-PA coupling can be determined using a multiple beat or single beat method. Determining RV-PA coupling requires the estimation of end systolic volume (ESV), stroke volume (SV) and end systolic pressure (ESP). Using US, these parameters can be determined and theoretically RV-PA coupling can thus be determined using US. To visualize required estimates to determine RV-PA coupling using ultrasound, a descriptive diagrams are added to this thesis in Appendix A. The following sections discusses ultrasound derived RV systolic pressure, RV stroke volume and RV end systolic volume.

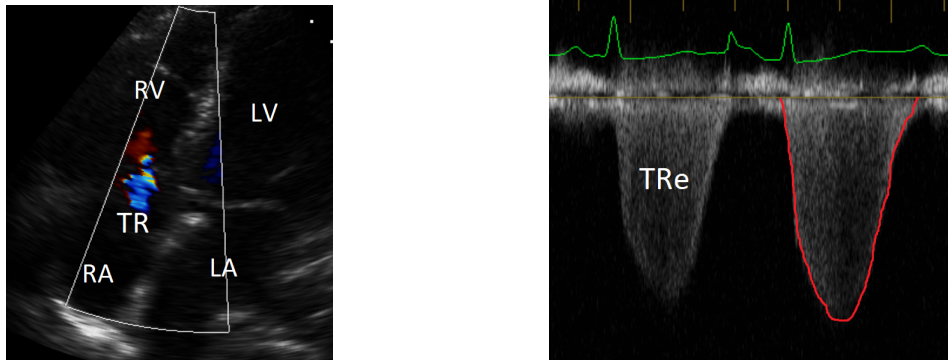
2.3 Ultrasound pressure estimation

Ultrasound estimation of RV systolic pressure relies on the occurrence of tricuspid regurgitation. Maximal velocity detected in the tricuspid regurgitation orifice allows the computation to pressure by the use of Bernoulli's principle. Thereby RV systolic pressure is estimated. [46]

2.3.1 Detection of tricuspid regurgitation

Tricuspid regurgitation occurs during systole. The RV contracts and via a small deficit in the tricuspid valve, blood from the RV flows back into the right atrium. In healthy subjects the prevalence of physiological tricuspid regurgitation is 65-75%. The prevalence of tricuspid regurgitation increases with age and with the presence of a catheter through the tricuspid valve. Physiological tricuspid regurgitation is often not holosystolic. The more severe tricuspid regurgitation becomes, the better tricuspid regurgitation can be imaged. Using ultrasound, tricuspid regurgitation can be detected using Color Doppler in the parasternal short axis views at height of the aorta (PSAXao), in the subcostal view and in the apical four chamber view (AP4CH). Figure 2.1a displays the detection of tricuspid regurgitation in the AP4CH view. Subsequently, the CW Doppler scan-line can be aligned with the jet and a time-velocity profile of tricuspid regurgitation can be acquired (Figure 2.1b). The red line represents maximal measured tricuspid regurgitation velocity. From maximal tricuspid regurgitation velocity, the RV systolic pressure profile is estimated using a simplified version of Bernoulli's principle of fluid dynamics. [46-53]

Figure 2.1: An example of acquired images to detect tricuspid regurgitation and measure its maximal velocity profile.



(a) Color Doppler image of tricuspid regurgitation in the apical four chamber view. The right ventricle (RV), right atrium (RA), left ventricle (LV) and left atrium (LA) can be observed in the image. Inside the white box in the image, the Color Doppler profile of tricuspid regurgitation is displayed (TR).

(b) CW Doppler image of tricuspid regurgitation velocity as measured in the apical four chamber view. The ECG is displayed as the green line. The horizontal plane of the image represents time and velocities are detected in the vertical plane in cm/s. The tricuspid regurgitation envelope (TRe) is imaged and the red line represents the maximal velocity profile.

2.3.2 Bernoulli's principle of fluid dynamics

In fluid dynamics, Bernoulli's principle of fluid dynamics describes that in a steady flow, the sum of all forms of energy is constant. It states that in any point along a stream line, the sum of kinetic ($\frac{1}{2}\rho v^2$), internal (ρgh) and potential (p) energy is constant:

$$constant = \frac{1}{2}\rho v^2 + \rho gh + p \quad (2.2)$$

where v is fluid flow speed, g is acceleration due to gravity, h is the elevation of the point above a reference plane opposite to gravitational force, p is pressure and ρ is density. [10, 11]

The amount of each type of energy in a stream line depends on the diameter. In a horizontal narrowing pipe with equal gravitational force of the complete pipe, flow velocity increases and pressure decreases over the stream line. Bernoulli's principle can be applied when flow is steady, the fluid is incompressible and friction forces are negligible. [54]

The sum of all types of energy is constant at any point of the stream line according to Bernoulli's principle. Therefore, these points can be set equal. The points at the tricuspid regurgitation stream line from RV to right atrium via the tricuspid regurgitation orifice can thus be described using Bernoulli's principle. Maximal conversion of the types of energy exist between the smallest and biggest diameter along the stream line. The tricuspid regurgitation orifice has the smallest

diameter and the RV the biggest. The sum of all energies is calculated by:

$$\frac{1}{2}\rho v_{RV}^2 + \rho gh_{RV} + p_{RV} = \frac{1}{2}\rho v_{TRO}^2 + \rho gh_{TRO} + p_{TRO} \quad (2.3)$$

where *RV* is the point at the stream line in the right ventricle, and *TRO* is the point at the stream line in the tricuspid regurgitation orifice.

Assuming equal gravitational force in the RV and the tricuspid regurgitation orifice, Bernoulli's principle can be simplified to:

$$p_{RV} - p_{TRO} = \frac{1}{2}\rho(v_{TRO}^2 - v_{RV}^2) \quad (2.4)$$

Thereby describing the pressure gradient between the tricuspid regurgitation orifice and the RV. Assuming the complete conversion from potential to kinetic energy in the tricuspid regurgitation orifice during tricuspid regurgitation, the equation can be further simplified to:

$$p_{RV} = \frac{1}{2}\rho(v_{TRO}^2) \quad (2.5)$$

Equation 2.5 describes the pressure gradient between RV and right atrium instead of absolute pressure. Adding right atrial pressure (or central venous pressure) to the equation, results in absolute RV systolic pressure:

$$p_{RV} = \frac{1}{2}\rho(v_{TRO}^2) + RAP \quad (2.6)$$

Using Color Doppler, tricuspid regurgitation is be detected. Alignment of the CW Doppler scan line allows for the acquisition of maximal tricuspid regurgitation velocity. Even though RV contraction does not provide constant steady flow, applicability of Bernoulli's principle of fluid dynamics is proven applicable for the estimation of RV systolic pressure. [46,48,55,56] RV systolic pressure can be computed by the use of the simplified Bernoulli equation. Correct alignment of the CW scan line is important, otherwise RV systolic pressure will be underestimated. [50]

2.3.3 Tricuspid regurgitation CW envelope

Severity of tricuspid regurgitation and alignment of the CW Doppler scan line alter the CW envelope of tricuspid regurgitation. Tricuspid regurgitation is graded absent, physiological, mild, moderate or severe and with severity density of the CW envelope increases. Ultrasound imaging of the RV is often difficult because the RV is located behind the sternum and the RV is enclosed by the left ventricle and lung tissue. These anatomical structures limit acoustic windows in which the RV can be completely observed. Therefore, alignment of the CW Doppler scan line along the tricuspid regurgitation stream line may be difficult. Also, respiratory heart movement can cause misalignment of the CW Doppler scan line with the direction of tricuspid regurgitation flow. Consequently, maximal velocity is underestimated. [50,57]

2.4 Ultrasound volume estimation

2.4.1 Stroke volume

Stroke volume estimation using ultrasound is based on the measurement of systolic flow over the aortic or pulmonary valve. In the parasternal short axis view at height of the aorta (PSAXao), the pulmonary artery can be visualized. After the identification of the pulmonic valve, the PW Doppler scan line is aligned parallel to the expected flow direction and the velocity sample volume is placed at height of the pulmonic valve. Then the pulmonic valve flow profile is acquired. [58–60]

Assuming a flat flow profile over the pulmonic valve and a circular anatomical shape of the PV, stroke volume is computed via:

$$SV = VTI_{pv} * 2\pi\left(\frac{d}{2}\right)^2 \quad (2.7)$$

Where VTI_{pv} is the velocity time integral over the pulmonic valve and d is the diameter of the pulmonic valve.

An example of the pulmonic valve velocity time integral can be observed in Figure 2.2a. Using PW Doppler the gray flow velocity profile is acquired. The opening and closing clicks of the pulmonic valve are imaged as narrow peaks with a high spectral density (white in the image). Between the opening and closing click, the velocity time integral is determined as the red area. The diameter of the pulmonic valve is determined in the PSAXao, as displayed in Figure 2.2b. The diameter of the pulmonic valve is assumed not to change during systole.

2.5 End systolic volume

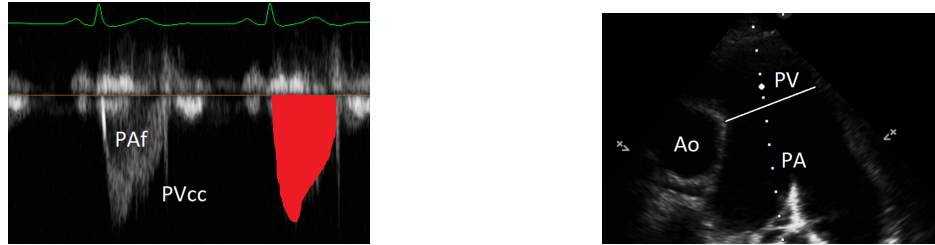
End systolic volume is determined using a combination of ultrasound derived stroke volume and ejection fraction. Ejection fraction is defined as the ratio of stroke volume to end diastolic volume. Residual fraction is defined as the ratio of end systolic volume to end diastolic volume or as 1 minus ejection fraction.

As discussed further in this thesis, volumic estimation of the RV is difficult. Therefore, a combination of ultrasound derived stroke volume and an estimation of ejection fraction by the use of fractional area changes is used to compute end systolic volume:

$$ESV = \frac{(1 - EF)SV}{EF} \quad (2.8)$$

where ESV is end systolic volume, EF is ejection fraction and SV is stroke volume. In chapter 3, the estimation of these quantities using ultrasound is further discussed.

Figure 2.2: An example of acquired images to determine right ventricular stroke volume.



(a) PW Doppler image of pulmonic valve flow velocity as measured in the parasternal short axis view at height of the aorta. The ECG is displayed as the green line. The horizontal plane of the image represents time and velocities are detected in the vertical plane in cm/s. The pulmonic artery flow velocity envelope (PAf) is displayed. The closing click of the pulmonic valve (PVcc) is also observed as a fast fluctuation in the velocity profile. The pulmonic valve velocity time integral is displayed as the red area in the image.

(b) Two-dimensional image of the pulmonary artery (PA) and the bifurcation into the left pulmonary artery and right pulmonary artery. The pulmonic valve (PV) is located next to the aorta (Ao) and the diameter of the pulmonic valve is measured.

This computation assumes that ejection fraction only consists of forward flow through the pulmonic valve, which is not the case when tricuspid regurgitation exists. Also, in case of pulmonary hypertension, stroke volume can be severely overestimated due to the occurrence of retrograde flow. In Chapter 3, these subjects will be further discussed. [61–66]

Two-dimensional ultrasound ejection fraction may be estimated by uniplanar and multiplanar indices. Fractional area change of the RV body is assessed in the apical four chamber (AP4CH) view, fractional area change of the RV outflow tract is assessed in the parasternal long axis (PLAX) view. The fractional shortening indices of RV length and width are assessed in the AP4CH view. The fractional shortening index of the RV outflow tract is assessed in the PLAX view.

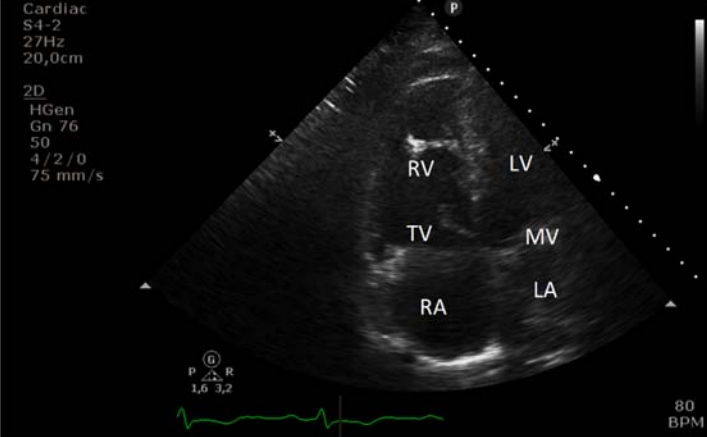
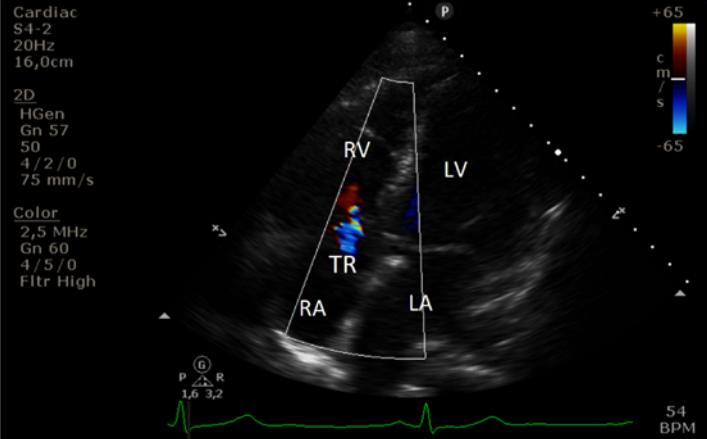
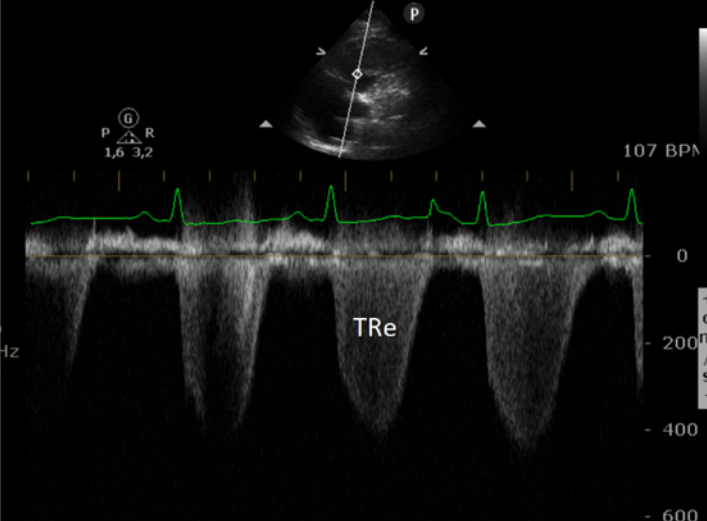
2.5.1 Right ventricular focused ultrasound protocol

The RV focused ultrasound protocol consists of three views; the apical four chamber view (AP4CH), the parasternal long axis (PLAX) and parasternal short axis at height of the aortic valve (PSAXao). In each view, two-dimensional images, PW Doppler images and CW Doppler images were acquired. An example of the images obtained during the RV focused ultrasound protocol are displayed in Figure 2.3 and 2.4.

Figure 2.3: RV focused ultrasound protocol, part 1.

PLAX	Abbreviation	Measurement
	<p>Right Ventricular Outflow Tract</p> <p>Aortic Valve</p> <p>Aorta</p> <p>Left Ventricle</p> <p>Left Atrium</p> <p>Mitral Valve</p>	<p>Fractional RV outflow tract shortening (FSI RVOT)</p> <p>Fractional RVOT area change (FAC RVOT)</p>
PSAXao	Abbreviation	Measurement
	<p>Aorta</p> <p>Pulmonary Artery</p> <p>Pulmonic Valve</p>	<p>Pulmonary valve diameter (PVD)</p>
	<p>Pulmonary Artery flow</p> <p>Pulmonary Valve closing click</p>	<p>Pulmonary artery velocity time integral (PA VTI)</p>

Figure 2.4: RV focused ultrasound protocol, part 2.

AP4CH	Abbreviation	Measurement
	<p>Right Ventricle</p> <p>Left Ventricle</p> <p>Right Atrium</p> <p>Left Atrium</p> <p>Tricuspid Valve</p> <p>Mitral Valve</p>	<p>Fractional RV length shortening (FSI RVI)</p> <p>Fractional RV width shortening (FSI RVw)</p> <p>Fractional RV body area change (FAC_AP4CH)</p>
	<p>Tricuspid Regurgitation</p> <p>Right Ventricle</p> <p>Left Ventricle</p> <p>Right Atrium</p> <p>Left Atrium</p>	<p>-</p>
	<p>Tricuspid Regurgitation envelope</p>	<p>Tricuspid regurgitation derived RV-RA pressure gradient</p>

Part III

Clinical studies

Chapter 3

Validation of a cardiac ultrasound method to quantify right ventricular stroke volume and end systolic volume

3.1 Introduction

To establish a pressure volume loop using ultrasound, RV pressure changes and RV volume changes during the cardiac cycle must be determined. To determine RV-PA coupling, both end systolic volume and stroke volume must be determined. In this chapter, an ultrasound method to determine these quantities is described and compared to gold standard MRI.

Volumic quantification of the RV using ultrasound is often debatable in its use due to complex RV shape and RV contraction profile. [6, 67–69] Two-dimensional ultrasound is based on many assumptions and at individual level these assumptions become erroneous. For example, RV dilatation due to pulmonary hypertension, alters RV shape. Therefore, a geometric model based on the healthy RV becomes less applicable. [70–73] The use of multiplanar indices improves the description of RV shape. The description of RV global function is improved by the use of multiplanar indices. [74–76]

In clinical practice, PW Doppler is used to determine the velocity time integral over the pulmonic valve during systole. In combination with the radius of the pulmonic valve, pulmonic valve area is determined. Then, stroke volume is computed as the product of pulmonic valve velocity time integral and pulmonic valve area.

A new method to determine end systolic volume using ultrasound is elaborated. Therefore, combination of ultrasound ejection fraction and ultrasound stroke volume is used. End systolic volume is computed by:

$$ESV = \frac{(1 - EF)SV}{EF} \quad (3.1)$$

where ejection fraction (EF) is estimated using two-dimensional ultrasound indices and stroke volume (SV) is computed by the product of pulmonic valve velocity time integral (VTI_{pv}) and pulmonic

valve area:

$$SV = VTI_{pv} * 2\pi\left(\frac{d}{2}\right)^2 \quad (3.2)$$

using the diameter (d) of the pulmonic valve as measured using two-dimensional ultrasound.

Ultrasound derived end systolic volume and stroke volume are compared to the MRI gold standard. In multiple slices of MRI recordings, RV border is manually drawn and end systolic volume and end diastolic volume are calculated by the integration over the slices consisting the RV border. Thereof stroke volume and ejection fraction are computed as:

$$SV = EDV - ESV \quad EF = \frac{EDV - ESV}{EDV} \quad (3.3)$$

where EDV is end diastolic volume and ESV is end systolic volume.

3.2 Methods

3.2.1 Study population

Retrospective analysis and prospective analysis was performed. Retrospective analysis was performed at the Cardiology department in the Amsterdam UMC, location Amsterdam Medical Center. Subjects screened prior to a MitraClip procedure who underwent cardiac MRI and RV focused US from June 2015 to December 2016 were included. Prospective analysis was performed at the Pulmonary Diseases department in the Amsterdam UMC, location VU University Medical Center. Subjects with a clinical indication for right heart catheterization for the follow-up of pulmonary hypertension from January 2018 to May 2018 were asked for informed consent. Ultrasound measurements were performed under the wings of the OPTIEK 2 study.

3.2.2 MRI

Standardized clinical cardiac MRI was performed to quantify RV end diastolic and end systolic volume. First end systolic and end diastolic frames were determined. Then the borders of the RV were manually drawn in all slices. End systolic volume is calculated by the addition of all determined volumes of the slices in the end systolic frame. End diastolic volume is calculated the same in the end diastolic frame. From the MRI images, RV end systolic volume, RV end diastolic volume and RV stroke volume were determined. RV ejection fraction was determined as the ratio of stroke volume to end diastolic.

3.2.3 Ultrasound

Ultrasound was performed using a clinical CX50 (PHILIPS, Eindhoven, The Netherlands) or Vivid E9 (GE Healthcare, Horten, Norway) ultrasound machine. The clinical cardiac probe (S5-1, M5S-D) was used in two-dimensional and PW Doppler mode to obtain required images. Briefly, the RV

focused ultrasound protocol consisted of three views (see section 2.5.1): the parasternal long axis (PLAX), parasternal short axis at height of the aortic valve (PSAXao) and the apical four chamber (AP4CH) view. Two-dimensional images of at least two subsequent heartbeats in the PLAX and AP4CH view were acquired. PW Doppler images of the pulmonic valve velocity profile of at least three subsequent heartbeats were acquired. Images were saved on the ultrasound machine and exported as DICOM from the PHILIPS CX50 or loaded into the electrical ultrasound database. From the ultrasound images, RV ejection fraction, RV stroke volume and RV end systolic volume were determined.

Ejection fraction

From two-dimensional ultrasound, three fractional shortening indices and two fractional area changes were determined (Figure 3.1). In the apical 4 chamber view (AP4CH) RV length, RV width and RV body area are determined. In the parasternal long axis (PLAX) RV outflow tract diameter and area are determined. All indices were determined at end systole and end diastole. Thereof fractional shortening indices and fractional area change are computed by:

$$Fractionalchange(\%) = \frac{Index_{enddiastole} - Index_{endsystole}}{Index_{enddiastole}} \quad (3.4)$$

Stroke volume

RV stroke volume was estimated from acquired PW Doppler velocity profiles. The velocity profile was automatically detected and smoothed using a cubic spline interpolation. A more detailed description of the automatic Doppler velocity profile detection is depicted in in Appendix B and C. After obtaining systolic flow profile, stroke volume was computed with Equation 3.2.

End systolic volume

To estimate end systolic volume, a combination of RV ejection fraction and RV stroke volume is used. Three models derived using multiple linear regression were compared. The first model consisted of three fractional shortening indices, the second of two fractional area change and the third of one fractional area change. fractional area change and fractional shortening indices were manually determined in MATLAB using the tool *imfreehand*. An example of these indices is displayed in Figure 3.1.

The model with the highest R-squared value to estimate ultrasound derived ejection fraction was used to determine RV end systolic volume. End systolic volume was computed according to Equation 3.1. Where stroke volume was computed according to Equation 3.2 and ejection fraction was estimated using the chosen multiple linear regression model.

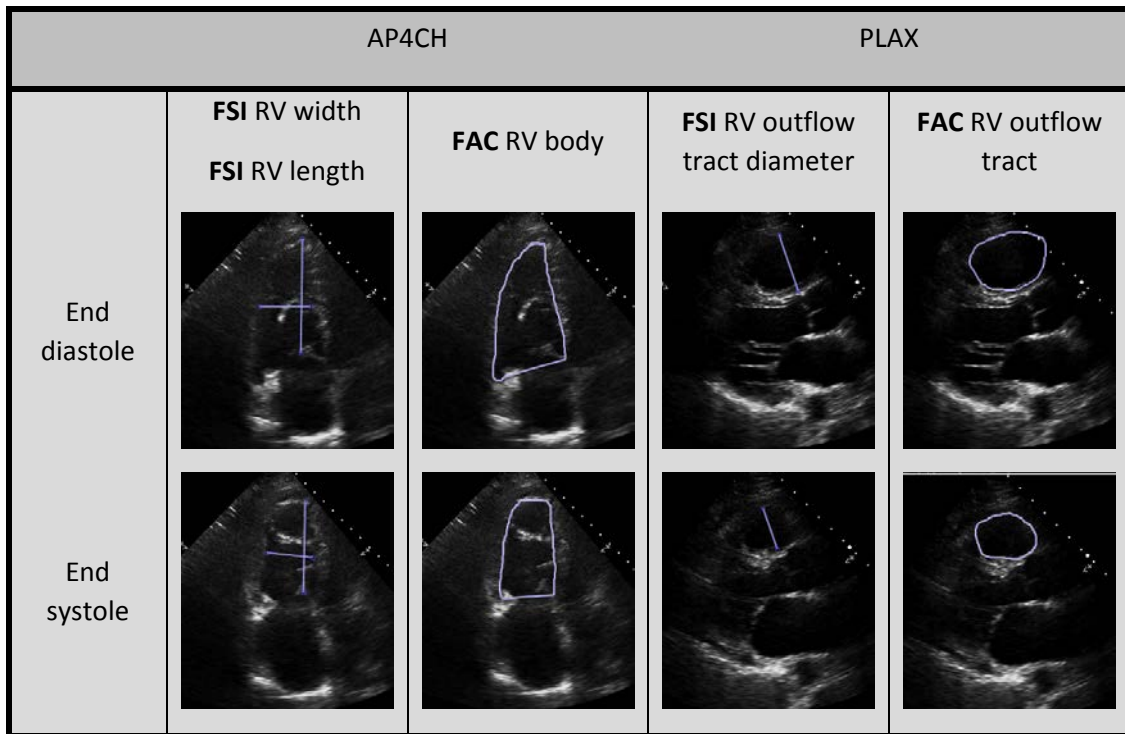


Figure 3.1: Example of the determination of fractional shortening indices (FSI) and fractional area changes (FAC) from two-dimensional images. The left four images display the apical four chamber (AP4CH) view, the right four display the parasternal long axis (PLAX) view. In the upper row end diastolic images are displayed with their determined indices and in the lower row the same indices were determined at end systole. [74]

3.2.4 Offline data analysis

Using MATLAB (release 2017b, The Mathworks, Inc., Natick, Massachusetts, United States), fractional area change, fractional shortening indices, stroke volume and end systolic volume were estimated. Manually, fractional area change and fractional shortening indices were determined. First, the end diastolic ultrasound frame and end systolic US frame were determined. Then all indices were manually drawn in the ultrasound frame using the tool *imfreehand*.

Adequate PW Doppler envelopes were included for analysis based on visual inspection. If the PW Doppler profile contained a closing click and the border of the profile was not affected by aliasing, the PW Doppler envelope was included for analysis. Automatic detection of systolic PW Doppler profile was performed. A detailed description of automatic PW Doppler velocity profile detection and comparison of different processing methods is included in Appendix B and C. Shortly, the algorithm is based on the detection of maximal PW Doppler velocity based on pixel intensity. The obtained signal was smoothed using cubic spline interpolation.

3.2.5 Statistics

Statistical analysis was performed in MATLAB (version 9.3, 2017b, MathWorks, Eindhoven, The Netherlands). Multiple linear regression was performed to determine a model between two dimensional fractional changes and MRI ejection fraction. Linear regression was performed to determine correlation between MRI stroke volume and end systolic volume and ultrasound derived stroke volume and end systolic volume. Sufficient fit of an obtained model is achieved when R-squared >0.8 . In our dataset, derived model with highest R-squared was used as a model to estimate RV ejection fraction. Correlation between maximal RV systolic pressure and MRI stroke volume was determined. Regression was determined using the function *regress*. R-squared and regression coefficients were determined. Bland-Altman analysis was performed to determine the difference between MRI stroke volume and end systolic volume and ultrasound derived stroke volume and end systolic volume. Average difference between the measurement methods and corresponding limits of agreement (± 1.96 SD) were determined and plotted.

3.3 Results

For retrospective analysis, 19 subjects were included. For prospective analysis, 15 subjects were included. Clinical characteristics of the complete population are displayed in Table ???. MRI and ultrasound evaluation were on average 11 days apart.

Table 3.1: Clinical characteristics of the complete study population, $n = 34$. Subjects underwent RV US evaluation and RV MRI evaluation. Values are displayed as mean (standard deviation).

Clinical characteristics	
Age, years	69 (19)
Gender, Male, n	12
NYHA class	3 (1)
Body mass index	24.7 (4.8)
Arterial blood pressure	
Systolic, mmHg	124 (20)
Diastolic, mmHg	73 (12)
Mean, mmHg	90 (13)
Hemoglobin concentration	8 (1.4)
Arterial saturation	95 (4)
Primary cause pulmonary hypertension	
Group 1 - Pulmonary arterial hypertension, n	10
Group 2 - Left heart disease, n	21
Group 3 - Lung disease or chronic hypoxia, n	0
Group 4 - Chronic thromboembolic pulmonary hypertension, n	2
Group 5 - Blood, metabolic or systemic disorders, n	0
Atrial fibrillation	3
Cardiac output L/min	5.3 (1.4)
Echocardiographic indices	
Heart rate, bpm	78 (13)
Left ventricle	
Degree MI	3 (1)
E/A	4.2 (4.6)
Right ventricle	
TAPSE, cm	1.9 (0.5)
E/e'	6.4 (3.0)
RVSP, mmHg	44 (18)
PV VTI, cm	16.2 (5.6)
Diameter PV, cm	2.8 (0.7)
Cardiac output, L/min	8.6 (3.8)
Degree TR	2 (1)
Fractional area change	
RV body	31 (11)
RV outflow tract	33 (12)
Fractional shortening indices	
RV width, %	16 (13)
RV length, %	16 (6)
RVOT diameter, %	19 (9)
MRI indices	
Heart rate, bpm	74 (14)
RV end diastolic volume, ml	142 (50)
RV end systolic volume, ml	75 (41)
RV stroke volume, ml	67 (20)
RV ejection fraction, (%)	50 (12)
Pulmonary forward flow, ml	59 (16)

Table 3.2: Multiple linear regression model of multiplanar fractional area change (FAC) to cardiac MRI EF. Regression coefficients with their corresponding 95% confidence interval are displayed. R-square and partial correlation of the regression coefficients were determined.

Multiple linear regression	Regression coefficient	95% CI
FAC RV body	0.37	-0.02 - 0.75
FAC RV outflow tract	0.28	-0.06 - 0.61
Constant	0.29	0.16 - 0.42
Statistics		P-value
R-squared	0.26	<0.05
Partial correlation	0.37	<0.05

Table 3.3: MRI and ultrasound derived stroke volume (SV), end systolic volume (ESV) and heart rate during MRI respectively ultrasound evaluation. Mean (standard deviation) values and [range] is displayed. No significant difference was determined with a paired t-test.

	US		MRI	
SV, ml	118 (87)	[37-373]	64 (17)	[41-116]
ESV, ml	117 (86)	[35-436]	71 (43)	[31-201]
HR, bpm	77 (13)		74 (14)	

3.3.1 Ejection fraction

Three models describing the correlation between MRI ejection fraction and ultrasound derived linear fractional changes were established using multiple linear regression. The use of a combination of fractional area changes of the RV outflow tract and RV body yielded the best correlation with MRI ejection fraction, but correlation remained poor. Regression coefficients R-squared and partial correlation of the selected model are stated in Table 3.2. Both the model based on fractional area change of the RV body and the model based on three fractional shortening indices, yielded a R-squared of 0.19. Dispersion of the measurement data around the model based on the fractional area changes of the RV body and RV outflow tract is displayed in Figure 3.2.

3.3.2 Stroke volume and end systolic volume

In 24 subjects the US PV velocity profile and PV diameter were acquired. In this subset, correlation and agreement between MRI SV and US SV and MRI ESV and US ESV were determined. Results are displayed in Figure 3.3. As can be observed in Table 3.3, ultrasound stroke volume overestimates gold standard MRI stroke volume. Increasing RV pressure seems to decrease stroke volume as determined using MRI (Figure 3.5). A not significant trend can be observed.

3.4 Discussion

All models to estimated ejection fraction from ultrasound fractional changes obtained poor correlation to measurement data. Stroke volume and end systolic volume were overestimated and underestimated by the described method. A large range in agreement between MRI derived stroke

Multiple linear regression model fractional area change

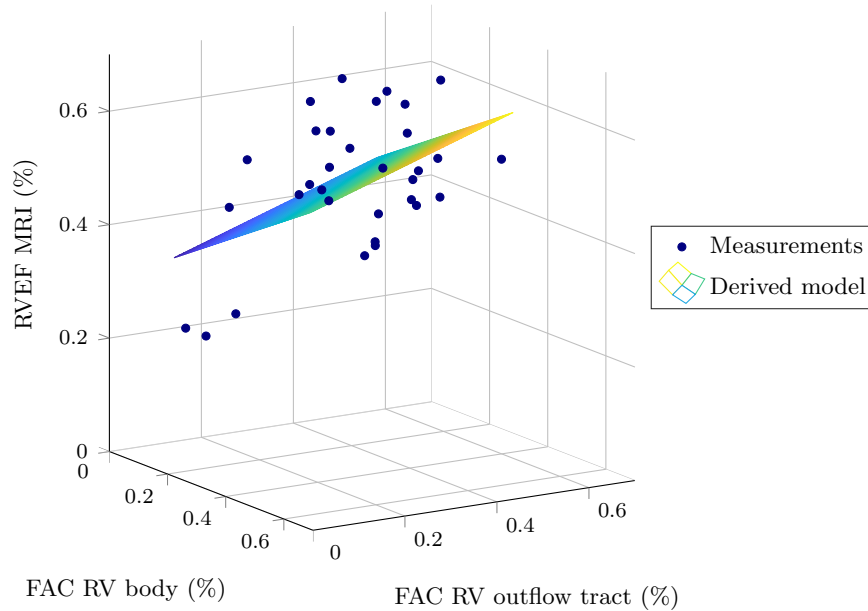


Figure 3.2: Three dimensional representation of the multiple linear regression model and the dispersion of data around the model. Fractional area change of the RV outflow tract and RV body are represented at the horizontal axes and MRI derived EF is represented at the vertical axis. Units of all measures are percentages. The blue dots represent obtained data per subject, whereas the colored plotted plane represents the model.

volume and end systolic volume implicate a large estimation error.

3.4.1 Ejection fraction

Results obtained in this small cohort underline the improved description of RV ejection fraction using multiplanar fractional change indices instead of uniplanar fractional change indices. [74–77] Further improvement of ultrasound RV systolic evaluation may be achieved by the use of two-dimensional indices instead of one dimensional indices. Expansion of the model cohort and a distinct validation cohort is recommended for future research. As correlation of all models was poor, the model based on two fractional area changes provided the best fit. However, a large estimation error remained.

A large variation in RV shape is expected in the population included in this small cohort study. The population consisted solely of patients with pulmonary hypertension, which is known to affect RV shape. Based on RV remodeling capacity and RV cardiac reserve, the effect of pulmonary hypertension on RV shape and systolic function differs amongst this population. The derivation of a model on a more general population is therefore recommended. [67, 72, 73]

The derived model was a fit for the measurement data and real ejection fraction was both overestimated and underestimated. A maximal overestimation of 20% and a maximal underestimation

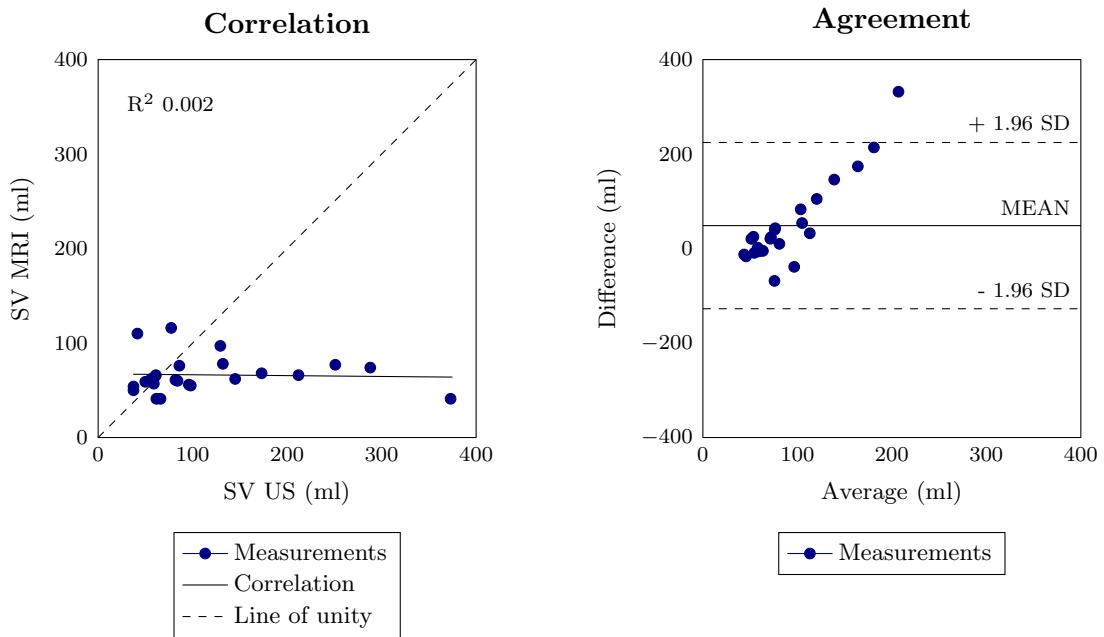


Figure 3.3: Correlation (left) and Bland-Altman (right) analysis between MRI derived stroke volume (SV) and US derived SV in milliliters (ml). **Left panel:** Correlation plot. The blue dots represents measurement data, the solid line represents correlation line and the dashed line represents the line of unity. R-squared value is displayed in the plot area. **Right panel:** Bland-Altman analysis. The blue dots represent measurement data, the solid line represents mean mean difference between the two measurement methods and the dashed lines represents limits of agreement.

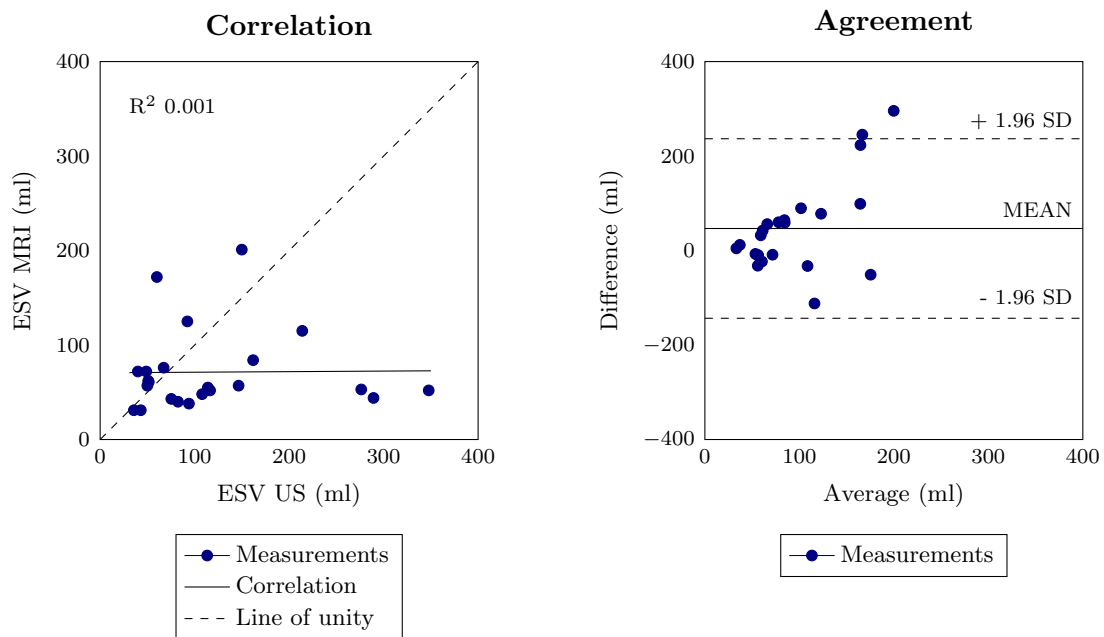


Figure 3.4: Correlation (left) and Bland-Altman (right) analysis between MRI derived end systolic volume (ESV) and US derived ESV in milliliters (ml). **Left panel:** Correlation plot. The blue dots represents measurement data, the solid line represents correlation line and the dashed line represents the line of unity. R-squared value is displayed in the plot area. **Right panel:** Bland-Altman analysis. The blue dots represent measurement data, the solid line represents mean mean difference between the two measurement methods and the dashed lines represents limits of agreement.

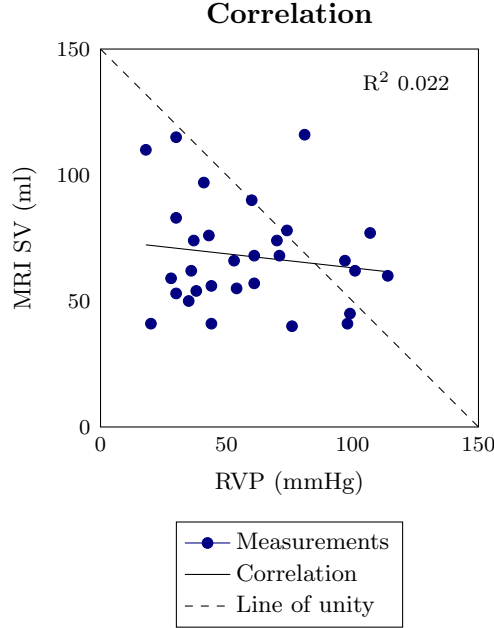


Figure 3.5: The effect of RV pressure (RVP) in mmHg on measured MRI stroke volume (SV) in ml. At the x-axis RV pressure in mmHg is displayed, at the y-axis SV in ml as measured using MRI is displayed. The blue dots represents measured data points of all subjects. The solid line represents correlation between RV pressure and MRI estimated stroke volume. Poor negative correlation exists, the line of unity (dashed line) is therefore displayed with a negative slope.

of 15% were obtained. Normal ejection fraction values range between 55 and 75%. [67] Due to the range of overestimation and underestimation of ejection, subjects may be incorrectly assigned to a decreased ejection fraction group.

Precise estimation of ejection fraction using multiplanar fractional area changes remains not recommended. Expansion of the model cohort and a second cohort to validate a model based on a larger cohort will demonstrate whether RV ejection fraction can be estimated using two dimensional ultrasound indices within clinical acceptable limits. Also, the effect of sub optimal ultrasound views at the ICU due to patient position, presence of thoracic drains and inability of the subject to cooperate during ultrasound evaluation should be investigated. [78]

3.4.2 Stroke volume

In a clinical setting, stroke volume and cardiac output are estimated using ultrasound. Precise sampling volume placement in the middle of the vascular trunk at height of the valve and alignment of the scan line with flow direction are important to obtain accurate measurements. Sample volume placement at the cross sectional area which changes the least during the cardiac cycle, introduces the least error. [58–60] However, cardiac output estimated using ultrasound overestimates and underestimates gold standard cardiac output, as was also observed in our results. [79–83] Obtain-

ing view of the pulmonary trunk to obtain pulmonic valve diameter is also known to be difficult. [84]

Due to pulmonary hypertension, systolic pulmonic valve flow is affected. PW Doppler velocity profile shape changes and systolic retrograde flow from the pulmonary artery into the RV occurs. [61–66] The occurrence of retrograde flow implicates the violation of the assumption that the PW Doppler scan line represents the complete pulmonic valve velocity profile. The amount, onset and velocity of retrograde flow is affected by individual pulmonary vascular characteristics and the magnitude of the effect of retrograde flow cannot be easily incorporated in ultrasound stroke volume estimation.

A combination of retrograde flow and pulmonary artery dilatation might induce overestimation of RV stroke volume. Healthy RV stroke volume ranges from 65-105 ml [67]. This range was also expected in this cohort, because the RV is known for its high capability to adapt for increased RV afterload. However, ultrasound derived RV stroke volume ranged from 33 to 373 ml and compared to MRI, ultrasound overestimates stroke volume. This might be the effect a large area of the pulmonic valve in combination with altered flow profile. [81]

The main pulmonic artery and the RV outflow tract dilate due to pulmonary hypertension, thereby also affecting PV diameter. The pulmonic valve can be visualized using transthoracic ultrasound. However accurate pulmonic diameter may be difficult. [85, 86]

3.4.3 End systolic volume

End systolic volume was determined from a combination of ejection fraction and stroke volume. Comparing ultrasound estimated ejection fraction and stroke volume to MRI showed large discrepancy and poor correlation. This implicates erroneous end systolic volume estimation which is reflected in the results. Healthy end systolic volume ranges from 40 to 120 ml and in pulmonary hypertension end systolic volume may increase. However, obtained ultrasound derived end systolic volume ranges from 35 to 436 ml and compared to MRI ultrasound mainly overestimates end systolic volume. In some cases, estimated RV end systolic was higher than RV volume and left ventricular volume together. Therefore, there results are classified as inaccurate. [67, 68]

3.4.4 Overall implications for a ultrasound method to derive RV-PA coupling

MRI or three-dimensional ultrasound remain superior to two-dimensional ultrasound for the volumic quantification of RV. [6, 72, 73, 87, 88] However, two-dimensional US is a bedside, non-invasive, cheap and easy applicable technique. Operator dependency, training intensity and the amount of post processing of two-dimensional ultrasound is lower compared to three-dimensional ultrasound. Due to these properties, feasibility of a two-dimensional ultrasound method to determine RV-PA coupling in an ICU setting is expected to be superior and further research for the two-dimensional ultrasound estimation of ejection fraction, stroke volume and end systolic volume is encouraged.

However, as the results also implicate, a large estimation exist in ultrasound estimation of all quantities. Therefore, cautious use of ultrasound derived estimates is important.

3.4.5 Conclusion

It is evident that ultrasound derived stroke volume and end systolic volume overestimate gold standard stroke volume and end systolic volume. These results implicate cautious use of ultrasound derived stroke volume and end systolic volume. Inter subject comparison of ultrasound derived stroke volume and end systolic volume might result in poor decision making. However, individual comparison of ultrasound derived stroke volume and end systolic volume may yield further information about disease progression and the effect of therapeutic strategies.

Chapter 4

Validation of a cardiac ultrasound method to quantify right ventricular systolic pressure

4.1 Introduction

To establish a pressure volume loop using ultrasound, RV pressure changes and RV volume changes during the cardiac cycle have to be determined. To determine RV-PA coupling, end systolic RV pressure and isovolumic RV pressure must be obtained. In this chapter, a ultrasound method to determine these parameters is described and compared to RV pressure measurements.

In clinical practice, a first screening tool for the possibility of pulmonary hypertension is ultrasound. Maximal RV systolic pressure is then estimated by the measurement of maximal velocity of tricuspid regurgitation. The velocity profile of tricuspid regurgitation can be obtained using CW Doppler ultrasound. In the vena contracta of the tricuspid regurgitation orifice, complete conversion of potential energy (pressure) to kinetic energy (velocity) is assumed. The simplified Bernoulli equation is then used to compute the pressure gradient over the tricuspid valve. A complete velocity profile of tricuspid regurgitation may be used to derive a complete systolic pressure profile of the systolic RV-RA pressure gradient.

RV-PA coupling can be determined using a single beat method or a multiple beat method. The single beat method requires adequate measurement of the isovolumic contraction and relaxation curve and an estimation of RV end systolic pressure. The multiple beat method requires an estimation of RV end systolic pressure under different preload conditions.

4.2 Methods

4.2.1 Study population

The study population consisted of twenty-three subjects diagnosed with pulmonary hypertension. Between January 2018 and May 2018, subjects underwent right heart catheterization for the follow

up of pulmonary hypertension in the Amsterdam UMC, location VU University Medical Center, Amsterdam.

4.2.2 Right heart catheterization

Clinical right heart catheterization was performed by a trained medical specialist using a balloon-tipped thermodilution 7F Swan-Ganz catheter with three lumina. The Swan-Ganz catheter was introduced via the right internal jugular vein and threaded through the right atrium and right ventricle into the pulmonary artery. After the introduction of the tip of the catheter into the pulmonary artery and measuring pulmonary capillary wedge pressure, the catheter was fixed. The pressure transducer was then leveled at heart height. Heart height was defined at the midaxillary line at the height of the nipple.

ECG, right atrial pressure, RV pressure and pulmonary artery pressure were simultaneously recorded and stored using LabChart reader (Version 5, update 8.1.1, ADInstruments, Dunedin, New Zealand). The continuous measurements were sampled with frequency of 1000 Hz. Pulmonary capillary wedge pressure (PCWP) was obtained by balloon inflation. Recordings were exported from LabChart as *.adicht files and converted to *.mat files.

4.2.3 Ultrasound

The RV focused ultrasound protocol (see Section: 2.5.1) was performed using a CX50 (PHILIPS, Eindhoven, The Netherlands) ultrasound machine. The clinical cardiac probe (S5-1) was used in two-dimensional color Doppler mode and CW Doppler mode. CW Doppler images of tricuspid regurgitation velocity of at least three subsequent heartbeats were acquired. Images were saved at the ultrasound machine and exported as DICOM images. From the ultrasound images, systolic RV-RA pressure gradient and maximal isovolumic RV pressure were determined. CW Doppler pressure measurements were performed at a maximum of 10 minutes before or during invasive pressure measurements.

Systolic RV pressure

From CW Doppler images, systolic RV-RA pressure gradient was determined. Addition of RA pressure to these curves yielded the systolic RV pressure profile. From the CW Doppler pressure measurements and invasive pressure measurements maximal RV systolic pressure and end systolic RV pressure were determined. End systolic RV pressure was determined as RV pressure occurring 30 ms before maximal negative pressure change in the isovolumic relaxation phase of the RV pressure curve.

Isovolumic RV pressure

Maximal isovolumic RV pressure was estimated by the extrapolation of the isovolumic phases of the cardiac cycles. First maximal pressure change (dP/dt_{max}) in the contraction phase of the RV pressure curve was estimated, thereafter maximal negative pressure change (dP/dt_{min}) was determined in the relaxation phase of the RV pressure curve. For fitting purposes, the length of the isovolumic pressure phases were equalized and maximal isovolumic RV pressure was estimated using the non-linear Levenberg-Marquardt fitting technique. Isovolumic phases were fitted to a sine wave:

$$\text{Isovolumic pressure curve} = a + b\sin(ct + d) \quad (4.1)$$

with a , b , c and d the fitting parameters and t time.

4.2.4 Offline data analysis

Using MATLAB (release 2017b, The Mathworks, Inc., Natick, Massachusetts, United States), systolic RV-right atrial pressure gradient was estimated. When an adequate CW Doppler profile was obtained, the CW Doppler profile was included for analysis. Adequacy of CW Doppler profiles was based on visual inspection. If the CW Doppler envelope was visually detectable over at least half of systole, the CW Doppler envelope was adequate. Then, automatic detection of systolic CW Doppler profile was performed. A detailed description of automatic CW Doppler velocity profile detection and comparison of different processing methods is included in Appendix B and D. Shortly, the algorithm used during data analysis is based on the detection of maximal CW Doppler velocity based on pixel intensity. The obtained signal was smoothened using cubic spline interpolation.

4.2.5 Statistics

Statistical analysis was performed in MATLAB (release 2017b, The Mathworks, Inc., Natick, Massachusetts, United States). Linear regression was performed to determine correlation between gold standard maximal RV pressure and end systolic RV pressure and ultrasound derived maximal RV pressure and end systolic RV pressure. Regression was determined using the function regress and R-square was determined. R-squared >0.8 implicates proper correlation between estimated values. Bland-Altman analysis was performed to determine the difference between gold standard pressure measurement and ultrasound pressure estimation. Maximal RV pressure, end systolic RV pressure (as defined 30 ms before dP/dt_{min}) and isovolumic pressure were compared.

4.3 Results

4.3.1 Study population

Twenty-three subjects were included from January to May 2018. Clinical characteristics are displayed in Table ???. Thirteen subjects had adequate CW envelopes and were included for analysis.

Table 4.1: Clinical characteristics of the complete study population, $n = 23$. Subjects underwent RV US evaluation and right heart catheterization.

Clinical characteristics	n = 33
Age	57 (15)
Gender (Male)	8
NYHA class	3 (1)
Body mass index	26.8 (5.8)
Arterial blood pressure	
Systolic	125 (25)
Diastolic	78 (14)
Mean	94 (17)
Hemoglobin concentration	9.2 (1.1)
Primary cause pulmonary hypertension	
Group 1 - Pulmonary arterial hypertension	13
Group 2 - Left heart disease	4
Group 3 - Lung disease or chronic hypoxia	1
Group 4 - Chronic thromboembolic pulmonary hypertension	4
Group 5 - Blood, metabolic or systemic disorders	0
Atrial fibrillation	0
Echocardiographic indices	
Heart rate	76 (14)
RVSP	62 (31)
PV VTI	19.8 (4.6)
Diameter PV	3.2 (0.7)
Degree TR	2 (1)
Fractional area change	
RV body	0.27 (0.11)
RV outflow tract	0.31 (0.12)
Invasive pressure measurements	
Heart rate	79 (12)
Mean PAP	46.2 (19.3)
Mean RVP	26.9 (7.9)
Mean RAP	7.8 (5.1)
Pulmonary capillary wedge pressure	11.2 (6.6)
Cardiac output	5.3 (1.4)
Pulmonary vascular resistance	520 (351)
Arterial saturation	91 (8)
Venous saturation	66 (16)

One subject was excluded from analysis based on the presence of atrial fibrillation. A mean maximal RV systolic maximal pressure was 55 mmHg, with an average intra subject variation of 10 mmHg.

4.3.2 RV systolic pressure

In Table 4.2, difference between ultrasound derived RV pressure parameters and gold standard derived RV pressure parameters is depicted. As can be observed in Figure 4.1, ultrasound derived maximal RV pressure caused an overall underestimation of invasive measured maximal RV pressure. In two subjects, similar maximal RV systolic pressure and extrapolated isovolumic RV pressure were determined by both methods. Correlation and agreement of ultrasound estimated RV pressure was poor, as can be observed in Figure 4.2-4.4.

Table 4.2: RV pressures derived from CW Doppler ultrasound (US) and invasive pressure measurements (Invasive). Maximal RV systolic pressure (RVPmax), end systolic RV pressure (RVPes), maximal pressure change during contraction (dP/dtmax) and maximal pressure change during relaxation (dP/dtmin), extrapolated isovolumic RV pressure (ESPiso) and heart rate depicted. Results are displayed in mean (standard deviation). To illustrate comparability of the measurements, heart rate is also depicted. CW Doppler pressure measurements were performed maximal 10 minutes before or during invasive pressure measurements.

	US	Invasive
RVPmax, mmHg	56 (34)	80 (29)
RVPes, mmHg	49 (31)	45 (19)
dP/dtmax, mmHg/s	733 (322)	469 (203)
dP/dtmin, mmHg/s	-2139 (3674)	-628 (293)
ESPiso, mmHg	57 (32)	115 (49)
HR, bpm	73 (17)	77 (13)

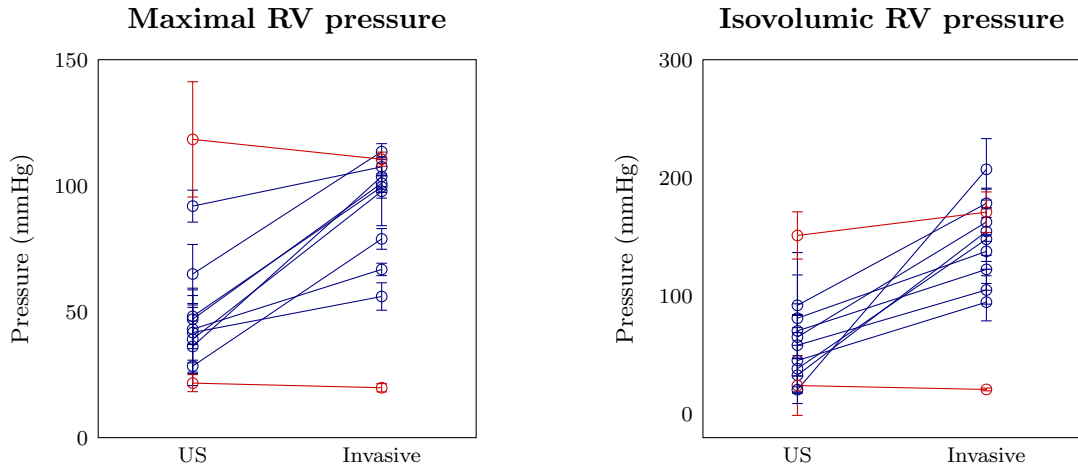


Figure 4.1: Visual representation of maximal RV pressure and isovolumic RV pressure estimated using ultrasound and measured using invasive pressure measurements per subject. The x-axis represents measurement method, the y-axis represents pressure in mmHg. A dot represents mean value, the errorbar represents standard deviation and the line connects pressure measured with two measurement methods. As can be observed, ultrasound underestimated measured maximal RV pressure in all cases except two, which are highlighted with a red line. As can be observed, when the difference between estimated RV maximal pressure is lower, the difference in extrapolated isovolumic RV pressure is also lower.

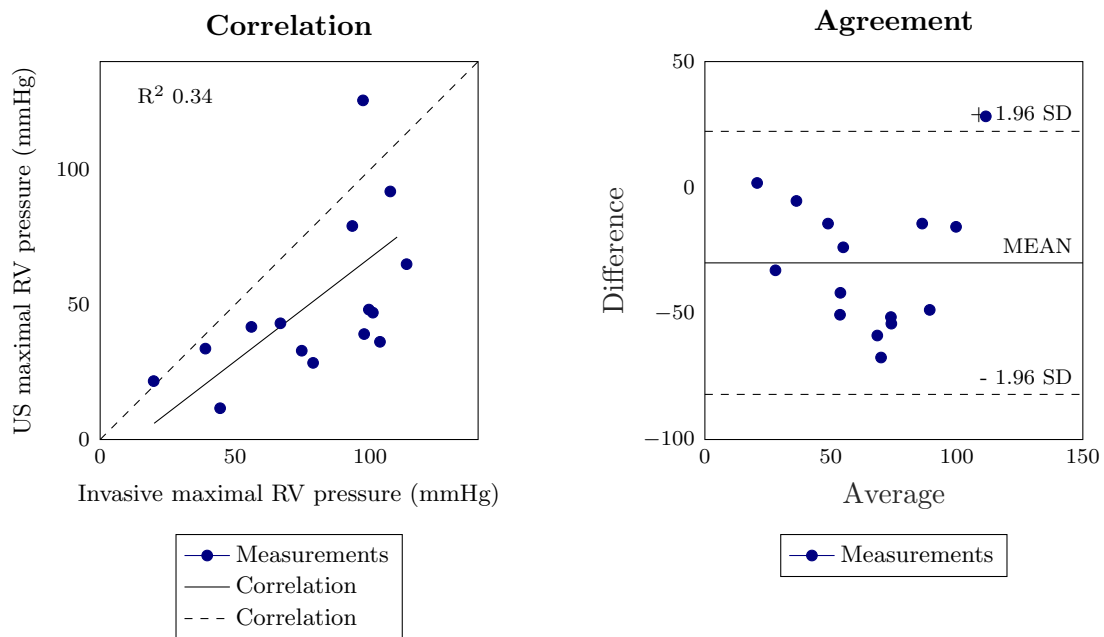


Figure 4.2: Correlation (left) and Bland-Altman (right) analysis between invasive pressure measurement and US derived pressure in mmHg in obtained maximal RV pressure. **Left panel:** Correlation plot. The blue dots represents measurement data, the solid line represents correlation line and the dashed line represents the line of unity. R-squared value is displayed in the plot area. **Right panel:** Bland-Altman analysis. The blue dots represent measurement data, the solid line represents mean mean difference between the two measurement methods and the dashed lines represents limits of agreement.

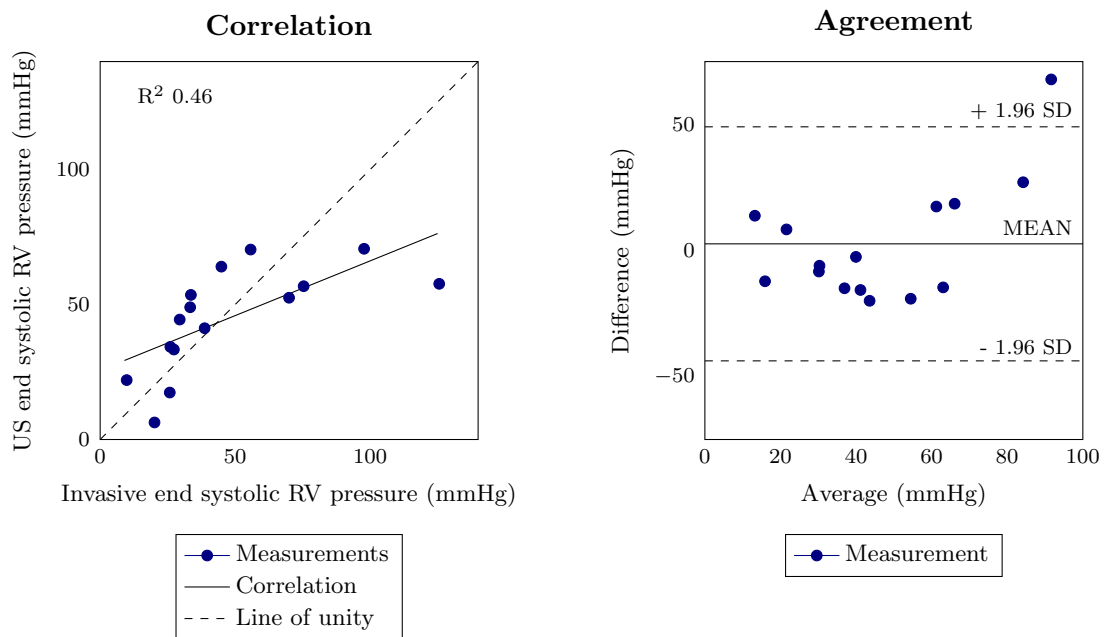


Figure 4.3: Correlation (left) and Bland-Altman (right) analysis between invasive pressure measurement and US derived pressure in mmHg in obtained end systolic RV pressure. **Left panel:** Correlation plot. The blue dots represents measurement data, the solid line represents correlation line and the dashed line represents the line of unity. R-squared value is displayed in the plot area. **Right panel:** Bland-Altman analysis. The blue dots represent measurement data, the solid line represents mean mean difference between the two measurement methods and the dashed lines represents limits of agreement.

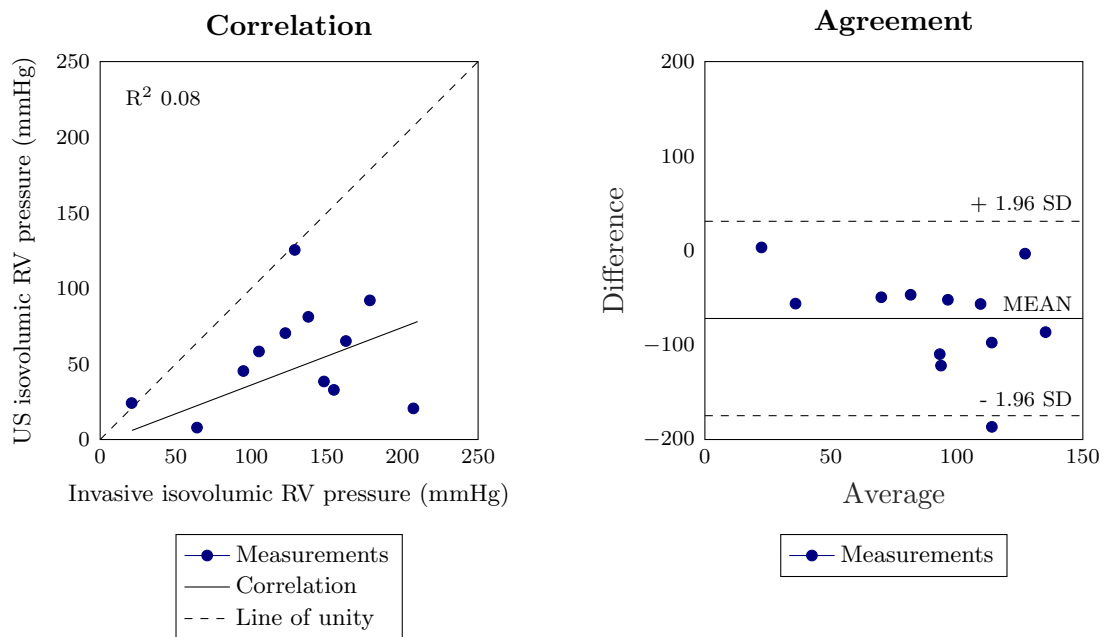


Figure 4.4: Correlation (left) and Bland-Altman (right) analysis between invasive pressure measurement and US derived pressure in mmHg in extrapolated isovolumic RV pressure. **Left panel:** Correlation plot. The blue dots represents measurement data, the solid line represents correlation line and the dashed line represents the line of unity. R-squared value is displayed in the plot area. **Right panel:** Bland-Altman analysis. The blue dots represent measurement data, the solid line represents mean mean difference between the two measurement methods and the dashed lines represents limits of agreement.

4.4 Discussion

4.4.1 RV systolic pressure

In our results, ultrasound derived RV pressure underestimates invasive RV pressure measurements. Overestimation and underestimation of ultrasound derived pressure measurements is often reported in literature. [47, 55, 81, 89–92] Overestimation and underestimation ranges from 10 mmHg to 40 mmHg, the latter can be observed in ultrasound derived of end systolic RV pressure, whereas maximal RV pressure was consistently underestimated.

In literature, underestimation was often accused to be the effect of misalignment of the CW Doppler scan line or inadequate CW Doppler envelopes. [47, 55, 81, 89, 91, 92] As can be observed from Equation 2.1, the frequency shift of the transmitted beam also depends on the angle between the ultrasound beam and direction of flow. If this angle increases, frequency shift decreases and without correction real velocity is underestimated. Respiratory movements or slight probe movements may cause slight changes in this angle. Average intra subject variation of estimated ultrasound pressure was 10 mmHg in this study, implicating these slight variations. For future research, it is thus recommended to obtain the tricuspid regurgitation profile over at least one complete respiratory cycle. [57]

A second explanation is the use of the simplified Bernoulli equation. The simplified equation neglect viscous and inertial forces, anatomical variation of the tricuspid regurgitation orifice, fluid viscosity, severity of tricuspid regurgitation, right atrial size, interaction of the tricuspid regurgitation jet with right atrial wall, mean right atrial pressure and potential pressure recovery. If potential energy is not completely converted to kinetic energy but is partially lost, obtained velocity is lower and therefore RV pressure is underestimated. [90, 93] However, intra subject changes of these factors is expected to be low and monitoring of hemodynamic treatment during ICU admittance may provide clinically relevant additional information. [47, 92, 94–98]

Overestimation was often accused to be the effect of a dynamic RA pressure profile with a high v-wave. [47, 81, 98, 99] However, in vitro studies [95] and in vivo studies [92] show that tricuspid regurgitation orifice size is associated with overestimation of RV pressure derived using ultrasound. In a large tricuspid regurgitation orifice, laminar flow occurs which is associated with pressure recovery and low viscous/inertial energy losses. [54, 100–102] Also small right atrial size is thought to induce overestimation [90, 95]

In this study, tricuspid regurgitation was always assessed in the apical four chamber view. This view is recommended by the European Association of Echocardiography [50] and often used in clinical studies. [48, 55, 56] However, in a clinical setting and in these studies, subjects are often positioned in lateral decubitus position. Subjects in this study remained in supine position, thereby increasing

the change of underestimation. [48, 55, 56]

In patients with pulmonary hypertension, ultrasound is often referred to as the initial screening tool, or considered to be complementary to right heart catheterization. However, to avoid misclassification and mismanagement due to incorrect derived pressure, CW Doppler is not recommended to be used as a replacement of right heart catheterization.

As can be observed in Figure 4.1, a proper estimation of RV pressure using ultrasound, also results in a better estimation of RV isovolumic pressure. The underestimation of the complete velocity profile thus also reflects on the isovolumic phases, resulting in underestimated isovolumic pressure. However, in two subjects, adequate isovolumic RV pressure indicates validity of an ultrasound derived isovolumic pressure.

4.4.2 Automatic CW Doppler velocity profile detection

Spectral density of a signal describes the power of a frequency occurring in the reflected frequency spectrum. The more a specific frequency is present in the reflected signal, the higher its power. In an CW image, spectral density is reflected in pixel intensity, higher power corresponds to a brighter pixel. The algorithm designed in this study relies on this difference in pixel intensity of the obtained CW Doppler spectrum and background noise. In an ultrasound image, gain can be increased to amplify the displayed power of weakly present frequencies in the reflected signal. Increasing gain also amplifies the power of background noise, thereby increasing background intensity of the CW image. In this study a set threshold of 10% pixel intensity was used to distinguish between background noise and reflected ultrasound signals. Consequently, increasing gain would cause the algorithm to detect background noise as spectral information resulting in the inadequate detection of the velocity profile.

A more robust method using an adaptive threshold based on image characteristics is recommended. A straightforward solution could be an adaptive threshold based on the lower quantile range of pixel intensity of the CW image. More sophisticated algorithms have been tested and would further improve the algorithm. [103, 104] Also signal enhancement using microbubbles could improve the detection of CW Doppler profiles in the case of mild regurgitation. [105]

4.4.3 Invasive pressure measurements

In healthy subjects, the prevalence of tricuspid regurgitation is 65-75%. However, often tricuspid regurgitation does not extend throughout systole and spectral density of the obtained CW Doppler profile is low. Pathological conditions such as RV dilation due to increased RV afterload or pathology of the tricuspid valve can increase incidence and severity of tricuspid regurgitation. Then tricuspid regurgitation extends throughout systole and the density of the CW Doppler profile increases. If tricuspid regurgitation does not extend throughout systole, an incomplete RV pressure profile will

be obtained. If the pressure profile is incomplete, isovolumic phases, maximal systolic RV pressure and end systolic RV pressure are inadequately acquired.

During the measurements, a catheter was introduced through the tricuspid valve. The presence of the catheter is shown to increase the incidence of tricuspid regurgitation. Also, the introduction of the catheter through the tricuspid valve is expected to affect regurgitation orifice. Interaction of the jet with the catheter affects detection of tricuspid regurgitation. In most cases, tricuspid regurgitation may be induced, but tricuspid regurgitation may also become undetectable due to catheter presence. [46–53, 90]

Another important factor is the induction of a change in hemodynamic profile of the right heart due to catheter introduction. Tricuspid regurgitation and pulmonic regurgitation may be induced or aggravated by the introduction of a catheter. Consequently, ventricular volume changes and ventricular pressure changes may be affected for the complete cardiac cycle. However, ultrasound measurements were most often performed when a catheter was present. Therefore, measured pressure profile and estimated ultrasound pressure profile are expected to be comparable. [46]

4.4.4 Conclusion

A complete CW envelope provides the ability to determine systolic RV pressure. A tricuspid regurgitation velocity profile can be used to estimate RV systolic pressure. However, cautious use of ultrasound derived pressure is recommended. Underestimation of systolic RV pressure affects estimated RV afterload and RV systolic function.

Chapter 5

The effect of passive leg raise on measured quantities and ultrasound estimated quantities

5.1 Introduction

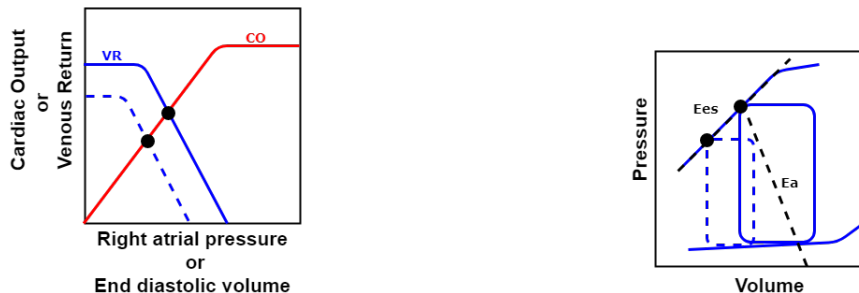
In an ICU setting, a passive leg raise maneuver is used to determine fluid responsiveness. During a passive leg raise maneuver, volume from the lower body compartment is transferred towards the right heart. This increase in venous return increases cardiac output in fluid responsive patients without a change in heart rate. The Frank-Starling law of the heart describes this observed phenomena, which is displayed in Figure 5.1a. In mechanically ventilated patients and spontaneously breathing patients, cardiac output increases in fluid responsive patients as an effect on passive leg raising. The autotransfusion effect of passive leg raising disappears after several minutes and is not accompanied with increase in RV contractility. Therefore, passive leg raising can be theoretically used to determine ventricular elastance using a multiple beat method. [106–114]

Due to the increase in preload, contractile force of the RV is increased and stroke volume increases. Contractility is defined as the intrinsic ability of the heart muscle to generate force and to shorten. The ability of the RV to generate additional force with increasing venous return, reflects contractility of the RV. The acquisition of pressure volume loops under different preload conditions may therefore be used to describe ventricular contractility. Using passive leg raising to alter preload and obtain multiple pressure volume loops is addressed in this chapter.

In a clinical setting, the effect of passive leg raise maneuver is determined using calibrated pulse contour analysis or cardiac ultrasound. Calibrated pulse contour analysis is minimally invasive and assesses changes in pulse pressure, reflecting changes in stroke volume. Cardiac ultrasound is non-invasive; using PW Doppler, change in the velocity time integral over the aortic and pulmonic valve can be determined, reflecting changes in stroke volume. [113,115,116]

Passive leg raising increases RV systolic pressure [107]. Whether this change in RV pressure can

Figure 5.1: The effect of a passive leg raise maneuver on cardiac output, venous return and beat to beat right ventricular pressure and volume.



(a) A schematic representation of the effect of increased venous return (VR) on cardiac output (CO). The x-axis represents right atrial pressure or end diastolic volume and the y-axis represents VR and CO. The blue dashed line represents VR in baseline condition. As an effect on passive leg raising, VR increases, as represented with the solid blue line. The working point, represented as the black dot, is shifted upwards the CO curve. [13]

(b) A schematic representation of the effect of a passive leg raise maneuver on a pressure volume loop. The dashed loop represents a pressure volume loop in the baseline condition, the solid loop represents a pressure volume loop in leg raise condition. As venous return increases, stroke volume, end systolic volume and systolic pressure increases. Arterial elastance (E_a) and ventricular elastance (E_{es}) are expected to remain the same and the pressure volume loop makes a rightward shift. [13]

be assessed using cardiac ultrasound, remains inconclusive. RV pressure can be estimated using cardiac ultrasound by the assessment of the velocity profile of tricuspid regurgitation. Therefore, estimated ultrasound RV pressure was compared to measured RV pressure.

5.2 Methods

5.2.1 Study population

The effect of passive leg raising on invasive pressure measurements, ultrasound pressure estimations and ultrasound volume estimations were determined. Therefore, three subsets of the population described in Chapter 4 were formed.

The first subset consisted of subjects with invasive RV pressure measurements who underwent passive leg raising. The second subset consisted of subjects who underwent invasive RV pressure measurement, passive leg raising and had adequate CW Doppler envelopes. The third subset consisted of subjects who underwent invasive RV pressure measurements, passive leg raising and had adequate PW Doppler envelopes.

5.2.2 Right heart catheterization and ultrasound

Clinical right heart catheterization and RV focused ultrasound was performed as described in Chapter 3 and 4. The RV-focused ultrasound protocol was performed prior to and during passive legs raised. Using the algorithms described in Chapter 3 and 4, ultrasound derived stroke volume, end systolic volume and RV systolic pressure were determined.

5.2.3 Offline data analysis

Using MATLAB (release 2017b, The Mathworks, Inc., Natick, Massachusetts, United States), ultrasound derived systolic RV-RA pressure gradient was determined. The outer border of the systolic CW Doppler profile was automatically detected. A detailed description of automatic CW Doppler velocity profile detection and comparison of different processing methods is included in Appendix B and D. Shortly, the algorithm used during data analysis is based on the detection of maximal PW Doppler velocity based on pixel intensity. The obtained signal was smoothed using cubic spline interpolation.

Invasive derived quantities

From the invasive RV pressure measurements, systolic RV pressure, systolic pulmonary arterial pressure, diastolic RV pressure, diastolic pulmonary arterial pressure, mean right atrial pressure and pulmonary capillary wedge pressure were obtained. During the measurement, the time at which passive leg raising was performed was annotated. Manually, prior to passive leg raising and during passive legs raised, the time interval for analysis was specified and all parameters were automatically obtained.

Ultrasound derived quantities

CW Doppler images and PW Doppler images were obtained prior to passive leg raising and during passive legs raised. Adequacy of CW Doppler profiles and PW Doppler profiles were based on visual inspection. If the CW Doppler envelope was visually detectable over at least half of systole, the CW Doppler envelope was included for analysis. If the PW Doppler profile contained a closing click and the border of the profile was not affected by aliasing, the PW Doppler envelope was included for analysis.

Automatic detection of the pulmonic valve velocity time integral as described in Chapter 3 was performed to obtain stroke volume. Manually fractional area shortening of the RV outflow tract and RV body were determined and end systolic volume was estimated. Automatic detection of maximal RV systolic pressure and end systolic pressure was performed as described in Chapter 4.

Table 5.1: Invasive pressure measurement prior to passive leg raising and during passive legs raised. Systolic and diastolic right ventricular pressure (RVP), systolic and diastolic pulmonary artery pressure (PAP), mean right atrial pressure (RAP) and pulmonary capillary wedge pressure (PCWP) are depicted. Values are displayed as mean (standard deviation) for the baseline condition, passive leg raised condition and difference between the two conditions. A paired t test was performed to determine whether baseline condition significantly different from passive legs raised condition. Significance level is displayed by the P -value, all values were statistically significant with a confidence interval of 95%.

	Baseline	Passive leg raise	Mean difference	P-value
RVP, mmHg				
Systolic	76.5 (25.7)	82.2 (24.3)	5.6 (5.3)	<0.005
Diastolic	1.6 (4.0)	3.4 (4.3)	1.8 (1.6)	<0.005
PAP, mmHg				
Systolic	79.6 (26.1)	84.3 (25.3)	4.4 (4.3)	<0.005
Diastolic	27.9 (12.7)	30.1 (12.2)	1.7 (3.1)	<0.05
PCWP, mmHg	11.2 (6.6)	13.1 (7.1)	1.8 (2.2)	<0.05
Mean RAP, mmHg	7.8 (5.1)	10.8 (4.9)	3.2 (2.5)	0.0001
Heart rate, bpm	79.9 (17.5)	82.5 (15.1)	2.6 (8.2)	NS

5.2.4 Statistics

Statistical analysis was performed in MATLAB (release 2017b, The Mathworks, Inc., Natick, Massachusetts, United States). A paired t -test with a confidence level of 95% was performed to determine the effect of passive leg raising on invasive measurements and ultrasound estimations.

5.3 Results

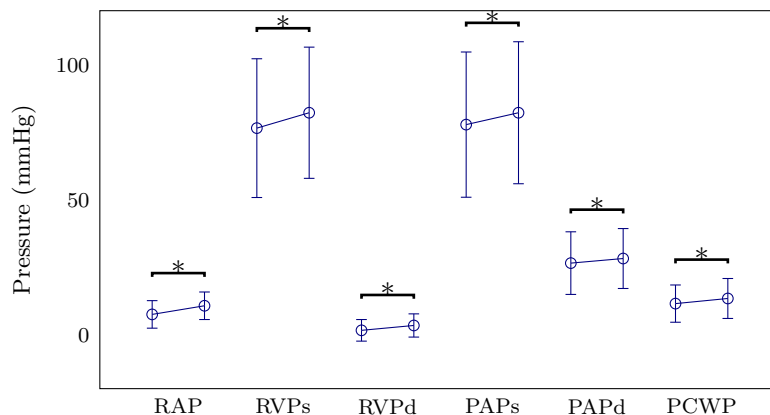
5.3.1 Study population

From January 2018 until May 2018, twenty-three subjects were included in the total population. The first subset consisted of eleven subjects with invasive pressure measurements who underwent passive leg raising. The second subset consisted of eight subjects who underwent invasive pressure measurement, passive leg raising and had adequate CW Doppler envelopes. The third subset consisted of five subjects who underwent invasive pressure measurements, passive leg raising and had adequate PW Doppler envelopes.

5.3.2 Measured RV pressure

In Table 5.1, average pressures as obtained prior to passive leg raising and during passive legs raised are displayed, these results are visualized in Figure 5.2. Per subject, an average of 55 beats were evaluated in baseline condition, an average of 40 beats were evaluated in passive legs raised condition.

The effect of PLR on RV pressure



Invasive pressure measurement prior to PLR (left) and with passive legs raised (right)

Figure 5.2: Visual representation of invasive pressure measurement prior to passive leg raising and during passive legs raised. The x axis represents measurement of all pressures in baseline and passive legs raised condition. Mean right atrial pressure (RAP), systolic right ventricular pressure (RVPs), diastolic right ventricular pressure (RVPd), systolic pulmonary artery pressure (PAPs), diastolic pulmonary artery pressure (PAPd) and pulmonary capillary wedge pressure (PCWP) are displayed. The y axis represents measured pressure in mmHg. Mean values are displayed with the open dot and the error bars represent standard deviation. Significant differences between the conditions were annotated using an asterisk (*).

5.3.3 Ultrasound estimated RV pressure

CW Doppler images containing tricuspid regurgitation velocity were acquired. Baseline and passive legs raised condition were compared. Per subject an average of 9 beats were included for analysis in the baseline condition and an average of 7 beats were included for analysis in the leg raise condition. In Table 5.2, average ultrasound derived pressures as obtained prior to passive leg raising and during passive legs raised are displayed.

In Figure 5.3, the change in estimated maximal RV pressure and estimated end systolic RV pressure as an effect on passive leg raising can be observed. As can be observed, detected ultrasound estimation of RV pressure yielded positive as well as negative changes in RV pressure comparing baseline condition to legs raised condition. Invasive systolic RV pressure only increased as an effect to of passive leg raising with a mean of 4.6 mmHg in a range of 0.2-8.6 mmHg.

5.3.4 Ultrasound estimated stroke volume and end systolic volume

PW Doppler images containing systolic pulmonic valve flow were acquired. Baseline and passive legs raised condition were compared. Per subject an average of 12 beats were included for analysis in the baseline condition and an average of 8 beats were included for analysis in the leg raise condition. In Table 5.2, average US derived stroke volume and end systolic volume as obtained prior to passive

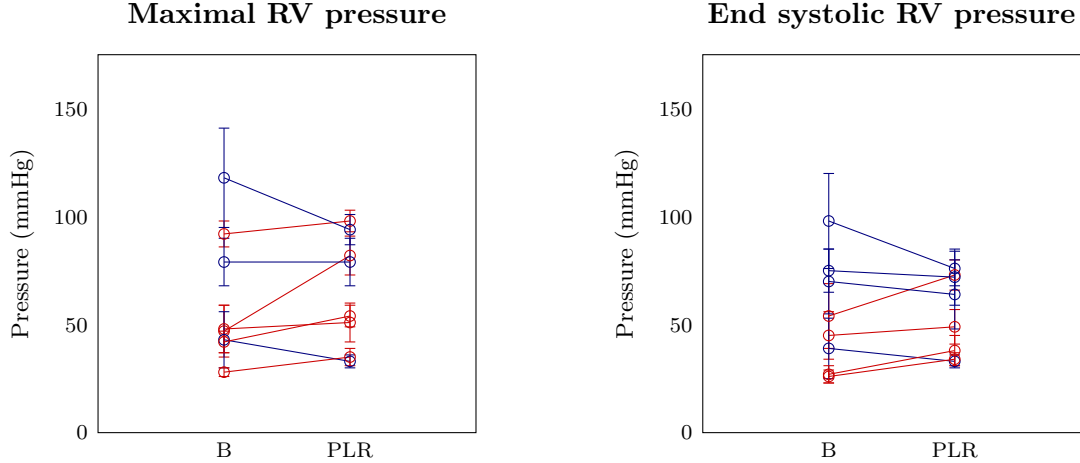


Figure 5.3: Visual representation of maximal RV pressure and end systolic RV pressure estimated using ultrasound in baseline condition and in leg raised condition per subject. The x-axis represents subject condition, the y-axis represents pressure in mmHg. A dot represents mean value, the errorbar represents standard deviation and the line connects obtained values in the same subject. As can be observed, in some subjects estimated pressure increases (red), whereas in other subjects estimated pressure decreases (blue).

Table 5.2: Mean (standard deviation) quantities obtained in baseline condition and leg raise condition. No significant difference was proven between the quantities as measured in both conditions.

	Baseline	Passive legs raised
RVP _{max}	62 (31)	66(26)
RVP _{es}	53 (25)	55 (19)
SV	112 (39)	128 (32)
ESV	124 (40)	133 (22)

leg raising and during passive legs raised are displayed.

5.4 Discussion

Fluid responsiveness of critically ill patients is often tested using a passive legs raise maneuver. Passive legs raising increases cardiac output in healthy and critically ill patients. [117] Comparison between subjects with ejection fraction <40 and $EF >45$ revealed different effect between the groups. In the group with reduced ejection fraction, ejection fraction significantly increased, whereas cardiac output did not. In the group with normal ejection fraction, ejection fraction remained the same and cardiac output increased significantly. [107] Both groups increased in RV systolic pressure, however no significant difference was measured. Difference between our study and [107], is the fact that we measured RV systolic pressure in the initial phase of passive legs raising. The effect of passive legs raising is known to decrease after 1 minute [110]. Therefore the effect of passive legs raising measured in our study is more visible.

A mean increase in diastolic RV pressure of 2 mmHg was also observed during our study. However,

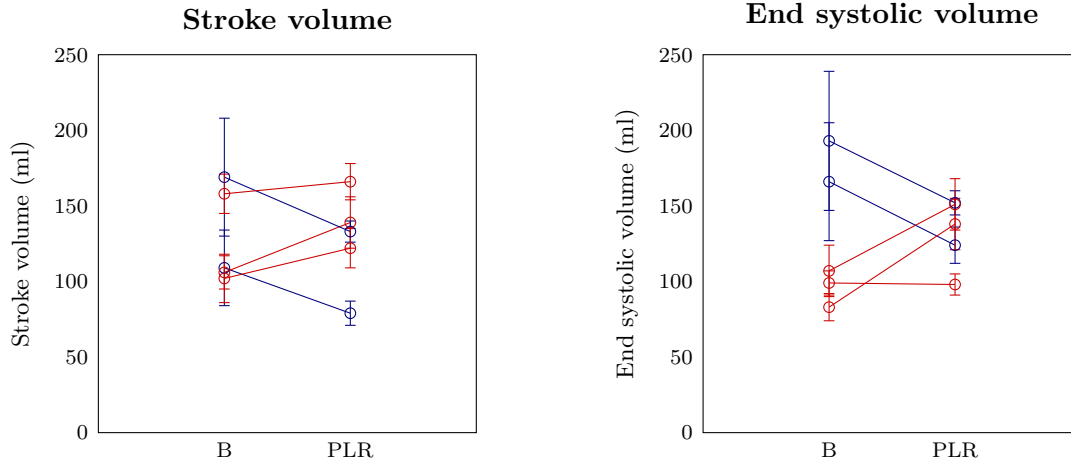


Figure 5.4: Visual representation of stroke volume and end systolic volume estimated using ultrasound in baseline condition and in leg raised condition per subject. The x-axis represents subject condition, the y-axis represents volume in ml. A dot represents mean value, the errorbar represents standard deviation and the line connects obtained values in the same subject. As can be observed, in some subjects estimated volume increases (red), whereas in other subjects estimated volume decreases (blue).

we found a significant mean difference of 6 mmHg, whereas systolic pressure in [107] only increased with 2 mmHg.

5.4.1 RV systolic pressure

As an effect on passive legs raising systolic RV pressure and systolic pulmonary artery pressure increase as measured during right heart catheterization. This physiological effect can be explained by increased stroke volume due to increased venous return. The effect of passive leg raising on mean measured RV systolic pressure can be observed using ultrasound. However, intra subject comparison showed that the increase in pressure is not always detected. Also ultrasound derived RV pressure underestimated real RV pressure. It has to be kept in mind that differences in measured pressure in baseline condition and passive legs raised condition may be subjected to different alignment of the CW Doppler beam with the direction of flow in the tricuspid orifice, as discussed in Chapter 4.

RV systolic pressure increases during passive legs raised as an effect of increased stroke volume. The magnitude of effect in pressure depends on the magnitude of increased stroke volume. In a ICU setting, respiratory induced pulse pressure variation is used as a clinical guideline to determine fluid responsiveness. A decrease in pulse pressure variation as an effect of a passive leg raise maneuver, indicates increased stroke volume. Therefore, pulse pressure variation may be used as an indicator of RV systolic pressure increases. If ultrasound derived pressure does not change or even decreases in combination with decreased pulse pressure variation, misalignment of the CW Doppler scan line is strongly indicated.

Because passive leg raise must be performed in our protocol to obtain pressure volume loops under different loading conditions, the subject must remain in supine position. This limits the alignment of the tricuspid regurgitation jet with the CW Doppler scan line. Due to a passive leg raise maneuver, the heart might slightly rotate or move in the thoracic cavity, thereby also affecting alignment of the CW Doppler scan line.

5.4.2 RV stroke volume and end systolic volume

As can be observed in the results, increase and decrease in ultrasound derived stroke volume occurs. However, the invasive pressure measurement only indicates an increase in stroke volume, as pressure significantly increases comparing baseline condition and passive legs raised condition. These difference in stroke volume may be explained by the velocity profile over the pulmonic valve. Due to increased afterload, this velocity profile differs per scan line. During the measurements, the PW Doppler scan line was positioned in the middle of the pulmonic valve and sample volume was placed such that closing click and opening click could be observed. However, if the systolic pulmonic valve flow profile contains high velocity antegrade flow and high velocity retrograde flow, as observed in patients with pulmonary hypertension, only a slight deviation in the placement of the PW Doppler scan line is expected to induce a large variation in obtained velocity profile.

5.4.3 Implications of observed effects on multiple beat RV-PA coupling

RV systolic pressure significantly increases as an effect on passive leg raising. As measured using ultrasound Doppler, RV stroke volume does not always increase. This might be the effect the limited time frame of the US measurement during passive leg raising measurement quality is less. Due to the altered systolic flow profile in pulmonary hypertension, slight deviation in PW Doppler scan line might also severely affect the pulmonic valve velocity time integral, whereof stroke volume is computed. After the initial phase of passive leg raising, the effect of passive leg raising on cardiac output and RV systolic pressure known to decrease.

5.5 Conclusion

Invasive RV systolic pressure measurement demonstrates increased RV systolic pressure during passive legs raised compared to prior to passive leg raising. Ultrasound estimation failed to detect this change, most likely due to misalignment of the CW Doppler scan line with the direction of the tricuspid regurgitation jet. The expected increase in stroke volume and end systolic volume as an effect of passive leg raise was not observed in all subjects. Overall, ultrasound did not always detect change in RV pressure, stroke volume and end systolic volume as an effect of passive leg raise.

Chapter 6

Determining right ventricular – pulmonary vascular coupling using ultrasound

6.1 Introduction

Ultrasound parameters describing right heart function only reflect RV afterload or RV systolic function. However, interaction between RV afterload and RV systolic function cannot yet be quantified using US. Interaction between the RV and pulmonary artery, can be quantified by RV-PA coupling.

RV-PA coupling is defined as the ratio of ventricular elastance to arterial elastance. Ventricular elastance describes ventricular contractility, whereas arterial elastance describes the pulsatile and steady component of RV afterload. RV-PA coupling can be derived from a pressure volume loop using a single beat method and multiple beat method.

The multiple beat method relies on the acquisition of multiple pressure volume loops under different loading conditions. Ventricular elastance is then determined as the slope of the end systolic pressure volume relation (ESPVR), which is estimated using multiple pressure volume loops. Multiple beat ventricular elastance is then defined as:

$$E_{es,mb} = \frac{ESP_2 - ESP_1}{ESV_2 - ESV_1} \quad (6.1)$$

where end systolic pressure (ESP) and end systolic volume (ESV) are obtained in two different preload conditions.

The single beat method obviates the need to alter preload to determine ventricular elastance [16,38]. Isovolumic phases of the cardiac cycle are used to extrapolate maximal end systolic pressure as would occur during an isovolumic beat. Single beat ventricular elastance ($E_{es,sb}$) is defined as:

$$E_{es,sb} = \frac{ESP_{iso} - ESP}{SV} \quad (6.2)$$

Where ESP_{iso} is estrapolated maximal pressure generated during a theoretical isovolumic contraction, ESP is end systolic pressure and SV is stroke volume.

Table 6.1: Required parameters for the estimation of RV-PA coupling using a single beat method or multiple beat method. For the multiple beat method, quantities must be obtained in two preload conditions.

	Single beat	Multiple beat	
Condition	Baseline	Baseline	Passive leg raised
Pressure estimates	End systolic RV pressure	End systolic RV pressure	End systolic RV pressure
	Right atrial pressure	Right atrial pressure	Right atrial pressure
	Isovolumic RV-pressure		
Volumic estimates	Stroke volume	Stroke volume	Stroke volume
	End systolic volume	End systolic volume	

Both the single and multiple beat method define E_a as:

$$E_a = \frac{ESP}{SV} \quad (6.3)$$

where ESP is end systolic pressure and SV is stroke volume.

An overview of the required parameters to determine RV-PA coupling using a single beat method or a multiple beat method is listed in Table 6.1.

6.2 Methods

6.2.1 Study population

The determination of single beat gold standard RV-PA coupling, single beat ultrasound derived RV-PA coupling and multiple beat ultrasound derived RV-PA coupling. Therefore, three subsets of the population described in Chapter 4 were formed.

The first subset consisted of twelve subjects who underwent invasive pressure measurements and cardiac MRI. The second subset consisted of ten subjects with adequate baseline CW Doppler profile, baseline PW Doppler profile and baseline two dimensional evaluation of the RV. The third subset consisted of five subjects with adequate CW Doppler profile, PW Doppler profile and two dimensional evaluation of the RV in the baseline condition and PLR condition.

6.2.2 MRI, right heart catheterization and RV focused ultrasound

Cardiac MRI was performed as described in Chapter 3, clinical right heart catheterization and RV focused ultrasound was performed as described in Chapter 3 and 4. The RV-focused ultrasound protocol was performed prior to and during passive legs raised. Using the algorithms described in Chapter 3 and 4, ultrasound derived stroke volume, end systolic volume and RV end systolic pressure were estimated. Thereof ventricular elastance and arterial elastance were determined according to Equation 6.1, 6.2 and 6.3.

6.2.3 Offline data analysis

Using MATLAB (release 2017b, The Mathworks, Inc., Natick, Massachusetts, United States), systolic RV-RA pressure gradient was determined. Automatic detection of systolic PW Doppler profile and CW Doppler profile was performed. A detailed description of automatic PW Doppler velocity profile detection and CW Doppler velocity profile detection and comparison of different processing methods is included in Appendices B-D. Briefly, the algorithm used during data analysis is based on the detection of both velocity profiles is based on pixel intensity. The obtained signal was smoothed using cubic spline interpolation.

MRI and right heart catheterization derived quantities

From the invasive RV pressure measurements, mean end systolic RV pressure and isovolumic RV pressure were obtained. Mean end systolic RV pressure in combination with median isovolumic RV pressure were used in combination with MRI derived stroke volume to determine single beat RV-PA coupling.

Ultrasound derived quantities

CW Doppler images and PW Doppler images were obtained prior to passive leg raising and with passive legs raised. Automatic detection of the pulmonic valve velocity time integral as described in Chapter 3 was performed to obtain stroke volume. Fractional area change of the RV outflow tract and RV body were manually determined and end systolic volume was computed according to the method described in Chapter 3. Automatic detection of RV systolic pressure, end systolic RV pressure and isovolumic RV pressure was performed as described in Chapter 4.

Median stroke volume, end systolic volume, end systolic pressure and isovolumic pressure of all acquired measurements per subject were used to determine RV-PA coupling. Mean end systolic RV pressure was chosen to serve as end systolic pressure.

6.2.4 Statistics

Statistical analysis was performed in MATLAB (release 2017b, The Mathworks, Inc., Natick, Massachusetts, United States). Linear regression was performed to determine correlation between gold standard single beat RV-PA coupling and ultrasound derived RV-PA coupling. Regression was determined using the function regress. R-square was determined. R-squared >0.8 implicates proper correlation between estimated values. Bland-Altman analysis was performed to determine the difference between gold standard RV-PA coupling measurement and ultrasound RV-PA coupling estimation.

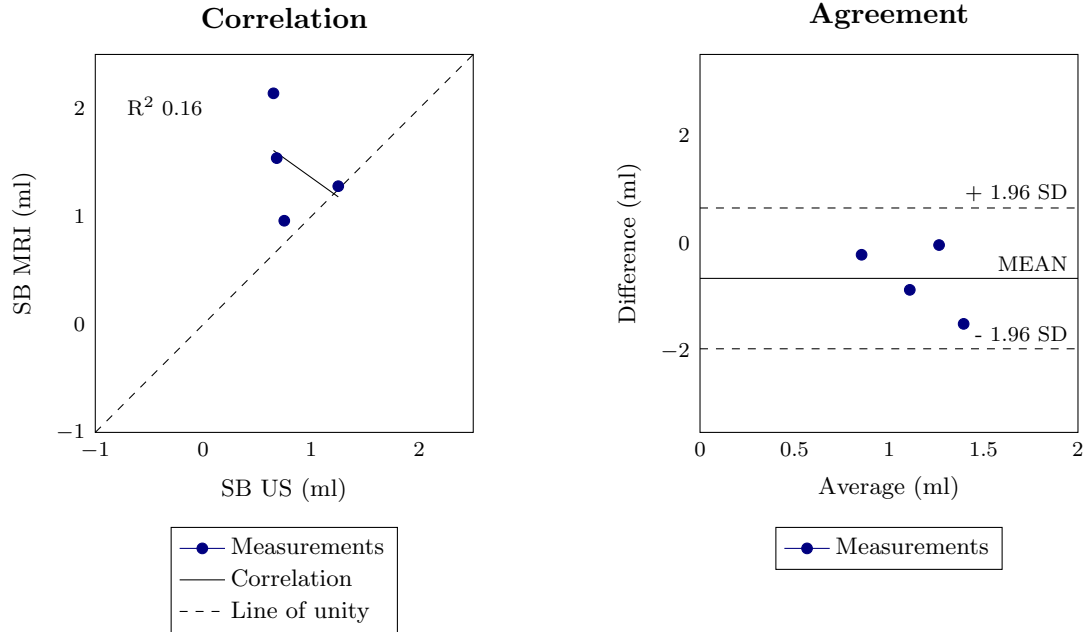


Figure 6.1: Correlation (left) and Bland-Altman (right) analysis between gold standard RV-PA coupling and single beat ultrasound derived RV-PA coupling. **Left panel:** Correlation plot. The blue dots represents measurement data, the solid line represents correlation line and the dashed line represents the line of unity. R-squared value is displayed in the plot area. **Right panel:** Bland-Altman analysis. The blue dots represent measurement data, the solid line represents mean mean difference between the two measurement methods and the dashed lines represents limits of agreement.

6.3 Results

6.3.1 Study population

From January 2018 until May 2018, twenty-three subjects were included in the total population. Clinical characteristics of the population are depicted in Chapter 4. Subgroups were formed; in the first subset twelve subjects were included, in the second subset ten subjects were included and in the third subset five subjects were included. In four subjects, gold standard RV-PA coupling and single beat ultrasound derived RV-PA coupling was determined. In three subjects, gold standard RV-PA coupling and multiple beat ultrasound derived RV-PA coupling was determined. These subjects were included for statistical analysis.

6.3.2 Ultrasound derived RV-PA coupling

In Table 6.2, mean and standard deviation values and range of all methods to derive RV-PA coupling are depicted. Single beat US derived RV-PA coupling was closest to gold standard RV-PA coupling, as can be observed in Figure 6.1 and 6.2. Difference in arterial elastance in the baseline condition and leg raised condition is displayed in Figure 6.3.

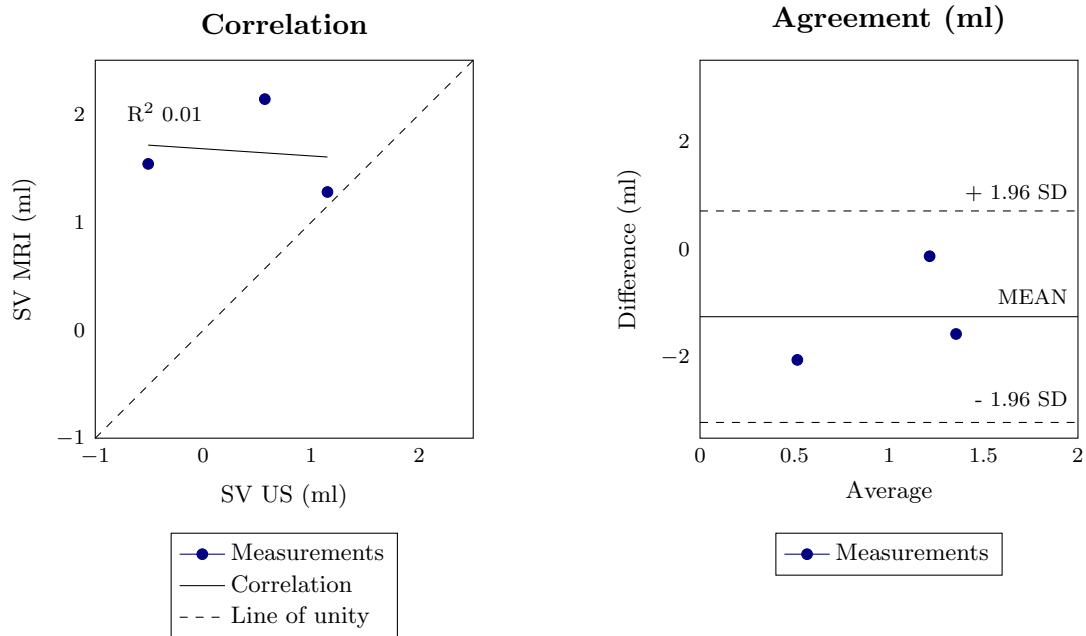


Figure 6.2: Correlation (left) and Bland-Altman (right) analysis between gold standard RV-PA coupling and multiple beat ultrasound derived RV-PA coupling. **Left panel:** Correlation plot. The blue dots represents measurement data, the solid line represents correlation line and the dashed line represents the line of unity. R-squared value is displayed in the plot area. **Right panel:** Bland-Altman analysis. The blue dots represent measurement data, the solid line represents mean mean difference between the two measurement methods and the dashed lines represents limits of agreement.

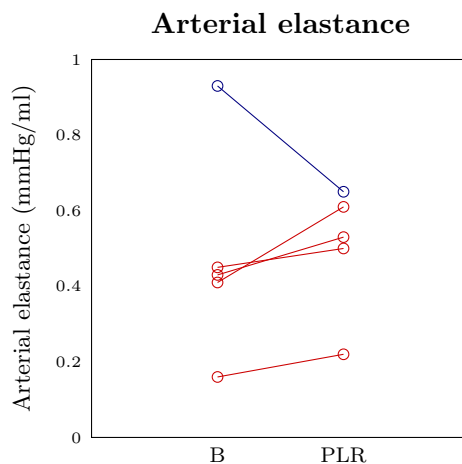


Figure 6.3: Visual representatin of arterial elastance (E_a) in the baseline condition and in leg raised condition per subject. The x-axis represents subject condition, the y-axis represents arterial elastance in mmHg/ml. A dot represents determined arterial elastance and the line connects determined values in the same subjects. As can be observed, in some subjects determined arterial elastance increases (red), whereas in other subjects determined arterial elastance decreases (blue).

Table 6.2: Mean (standard deviation) and [range] of estimated ventricular elastance (Ees), arterial elastance (Ea) and RV-PA coupling (Ees/Ea) using a gold standard single beat method ($SBmri$), single beat ultrasound method ($SBus$) and multiple beat ultrasound method ($MBus$) are displayed.

	SBmri (n=12)		SBus (n=10)		MBus (n=5)	
Ees	1.17 (0.64)	[0.34 2.63]	0.51 (0.37)	[0.18 1.44]	-0.56 (1.27)	[-2.7 0.5]
Ea	0.72 (0.32)	[0.35 1.42]	0.46 (0.29)	[0.16 1.14]	0.32 (0.14)	[0.16 0.45]
Ees/Ea	1.59 (0.43)	[0.96 2.14]	1.25 (0.90)	[0.65 3.48]	-3.23 (7.56)	[-16.68 1.15]

6.4 Discussion

Gold standard derived single beat RV-PA coupling estimates and ultrasound derived single beat RV-PA coupling estimates in this study showed similar results as described in literature. [36,118,119] The multiple beat method performed a lot worse. In two subjects, obtained RV-PA coupling values lay within a physiological reasonable range. However, negative RV-PA coupling, as observed in two subjects, implies that the RV can not generate any power to overcome RV afterload. This was not the case in the study population, as all subjects maintained cardiac output.

6.4.1 Single beat ultrasound derived RV-PA coupling

A single beat method to determine RV-PA coupling was first described in the left ventricle. [120,121] The single beat method was proven applicable to the right ventricle. [16,118,119,122,123] Our results show comparable results of gold standard derived RV-PA coupling and single beat ultrasound derived RV-PA coupling within the range reported in literature. Therefore, the proposed single beat method to derive RV-PA coupling using ultrasound adequately reflect RV-PA coupling.

Comparing the single beat method to the multiple beat method, less parameters have to be estimated and measurements can be obtained in a baseline condition. Also, the estimation of right atrial pressure might be obviated, as the single beat method uses the difference between isovolumic pressure and end systolic pressure. The difference between end systolic RV pressure and isovolumic RV pressure is not affected by the addition of RA pressure. Future research directed on further validation of a single beat ultrasound method to derive RV-PA coupling, should also assess this factor. [124]

6.4.2 Multiple beat ultrasound derived RV-PA coupling

In the initial description of the multiple beat validates the model by ranging end systolic RV pressure between 5 and 50 mmHg. [32] The Valsalva maneuver has been proposed and tested to obviate invasive vena cava occlusion to obtain PV loops under different preload conditions. [36,37,123] In these studies, obtained pressure volume loops range over 20-40 mmHg. In our study, passive leg raising only affects RV pressure with a mean of 2 mmHg. Therefore, the multiple beat US derived RV-PA coupling is expected to be subjected to error in a higher degree. This is reflected in our

results, a large variation between obtained pressure volume loops in the baseline condition and PLR condition exists. Determining RV-PA coupling using a multiple beat method based on the effect of the Valsalva maneuver requires optimal subject cooperation during the measurements. From critically ill patients at the ICU, this level of cooperation is not expected to be feasible due to deep sedation or delirium.

Arterial elastance was different comparing the baseline condition and passive legs raised condition. As estimated arterial elastance differed between the conditions, one of the assumptions whereon the multiple beat method is based is violated. Therefore, the obtained physiologically inadequate RV-PA coupling values can be explained. Difference in arterial elastance may be due to the fact the multiple pressure volume loops were obtained on average 10 minutes apart. However, in pulmonary hypertension, arterial elastance is not expected to fluctuate a lot due to a constant highly increased RV afterload.

6.4.3 Study limitation

A major limitation of this study is the fact that gold standard RV-PA coupling was not determined by simultaneous RV pressure and volume measurements. In healthy subjects, RV-PA coupling values fluctuates over time. However, in patients with pulmonary hypertension, RV-PA coupling is expected to be more stable over time due to the higher demand of the pulmonary vasculature. Therefore, cardiac contractility is expected to be about equal during right heart catheterization and cardiac MRI.

6.4.4 Added value of the determination of RV-PA coupling in the ICU

Animal studies demonstrate the ability RV-PA coupling to describe interaction between the right ventricle and pulmonary vasculature. Progressive and gradual increase in RV afterload affect RV-PA coupling and reflect a coupled state and uncoupled states. [38,125–128] In humans, this physiological concept is shown to be true. [36,122] Healthy RV-PA coupling is a ratio above 1 and when the ratio is around unity, optimal coupling is present. [43,119,122,125,129] Ventricular elastance has been shown to be an intrinsic parameter independent to loading condition to describe ventricular contractility. [17,30,130] Arterial elastance has been shown to be an intrinsic parameter to describe RV afterload. [39–42,131] In critically ill patients, RV-PA coupling, ventricular elastance and arterial elastance is expected to be affected by hemodynamic treatment and mechanical ventilation. Therefore, obtaining RV-PA coupling value can further personalize treatment.

6.5 Conclusion

Single beat US derived RV-PA coupling performs more similar with gold standard RV-PA coupling than multiple beat US derived RV-PA coupling does. Therefore, single beat US derived RV-PA

coupling shows more potential and is therefore a recommended focus for future research. However, first a valid derivation of quantities determining RV-PA coupling using ultrasound is required. Next, validation of the single beat ultrasound method to derive RV-PA coupling is recommended in the ICU setting. Theoretically, RV-PA coupling should be able to reflect hemodynamic changes due to therapy. Subsequent research should be conducted to determine whether this is true.

Chapter 7

Preliminary investigation into the feasibility of ultrasound method to determine right ventricular pulmonary vasculature coupling in the ICU.

7.1 Introduction

A new method can be theoretically and technically valid but its feasibility in a clinical setting is equally important. A clinically attractive technique is a technique that is easy to implement in daily care, not time consuming and one that can be performed with limited instruction.

To determine RV-PA coupling using ultrasound, the different methods described in the previous chapters require the estimation of specific quantities. The described multiple beat method to determine RV-PA coupling requires the estimation of RV stroke volume, RV end systolic volume and RV systolic pressure. The described single beat method requires RV stroke volume, RV systolic pressure and extrapolated RV isovolumic pressure. Whether all quantities can be determined provides insight in the feasibility of the ultrasound method to derive RV-PA coupling.

Required views to determine RV-PA coupling using a single- or multiple beat method are:

1. Parasternal long axis (PLAX) to obtain two-dimensional images of the RV outflow tract. By the use of these images, fractional area change of the RV outflow tract is determined.
2. Parasternal short axis (PSAX) at height of the aortic valve to obtain the PW Doppler velocity profile over the pulmonic valve and two-dimensional images of the pulmonic valve. By the use of these images, RV stroke volume is determined.
3. Apical four chamber (AP4CH) to obtain two-dimensional images of the RV body and the CW Doppler velocity profile over the tricuspid valve. By the use of these images fractional area change of the RV body, RV systolic pressure and extrapolated RV isovolumic pressure are determined.

Next to obtaining all required views, tricuspid regurgitation must be present. Tricuspid regurgitation must be holosystolic, parallel alignment of the CW Doppler scan line with the flow direction of the tricuspid regurgitation jet and the observer must be able to observe the complete outer border of the CW Doppler spectral profile.

Patients with atrial fibrillation were not included for screening. Atrial fibrillation affects the RR-interval. By affecting RR-interval, cardiac filling time and cardiac ejection time. Also, contraction pattern differ beat to beat, resulting in poorly comparable cardiac contractions. Due to poorly comparable cardiac contraction, valid matching of pressure profile and volume profile was expected to be difficult. Therefore, these patients were excluded for screening in this preliminary investigation.

In this chapter, preliminary screening is described to gain insight in the feasibility of an ultrasound method to determine RV-PA coupling. Therefore, success rate of a complete measurement is determined.

7.2 Methods

From September 2017 until February 2018 and from 24th of April 2018 until 8th of June 2018, mechanically ventilated patients were screened on the presence of tricuspid regurgitation and the ability to acquire a complete measurement. A complete measurement was defined as the ability to obtain PLAX, PSAX and AP4CH view. In combination with the occurrence of tricuspid regurgitation, RV-PA coupling can be determined. Adequate tricuspid regurgitation envelope was defined as stated in the introduction of this chapter.

The shortened RV-focused protocol was performed with a clinically approved SonoSite (Edge II, 2015, Fujifilm SonoSite Inc., Bothell, USA) ultrasound machine with a clinical cardiac probe (5-1). In the period from April to June, patients were screened with the intention to determine whether the patient could be included for further data analysis. Further data analysis would be initiated when all views could be obtained and tricuspid regurgitation was present.

7.2.1 Further data acquisition

A complete measurement in combination with a clinical indication for a passive leg raise maneuver were the requirements for further data acquisition. The complete shortened RV-focused protocol should then be performed three times. The first time just prior to passive leg raise (baseline condition 1), the second time when legs are raised (passive legs raised condition) and the third time when the legs are laid down again (baseline condition 2).

Each time the RV-focused protocol was performed, two-dimensional images were acquired in all

Table 7.1: Clinical characteristics of the screened population.

Characteristic	
Total population, n	73
Age, y, mean (SD)	64.6 (13.4)
Gender, Male, n (%)	46.0 (63.0)
Body mass index, kg/m ² , mean (SD)	28.2 (6.2)
Tricuspid insufficiency, n (%)	36 (55.4)
Cardiothoracic surgery, n (%)	31 (42.4)

views. Images of the PW Doppler profile over the pulmonic valve and CW Doppler profile over the tricuspid valve were acquired. All images were acquired for at least three subsequent heart beats and stored at the ultrasound machine.

DICOM images were exported from the ultrasound machine and offline data analysis provided fractional area change of the RV outflow tract, fractional area change of the RV body, pulmonic valve diameter, RV stroke volume and RV systolic pressure. For all conditions, these quantities were determined using MATLAB.

7.2.2 Effect of cardiothoracic surgery

During the screening, it became apparent that cardiothoracic surgery may be a major factor affecting success rate of a complete measurement. Therefore, correlation between the amount of obtained views and cardiothoracic surgery was determined. Subgroup analysis was performed to determine the success rate of a complete measurement in subjects with cardiothoracic surgery and without cardiothoracic surgery.

7.2.3 Screening adequacy

In 48 patients, trained specialists from the Department of Cardiology in the VU medical center performed cardiac ultrasound and reported the presence and severity of tricuspid regurgitation. Severity was graded as trace, mild, moderate or severe by the cardiologist. [46] The results of the cardiologist were compared to the results as obtained from the screening. From these results, screening adequacy of the detection of tricuspid regurgitation was determined.

7.3 Results

In total of 73 subjects the complete RV-focused ultrasound protocol was screened in the complete period. From September until February, 29 subjects were included. From April until June, 44 subjects were included. The only significant difference between the two groups was the amount of subjects who underwent cardiothoracic surgery. Clinical characteristics are displayed in Table 7.1.

Obtained views with prevalence TI

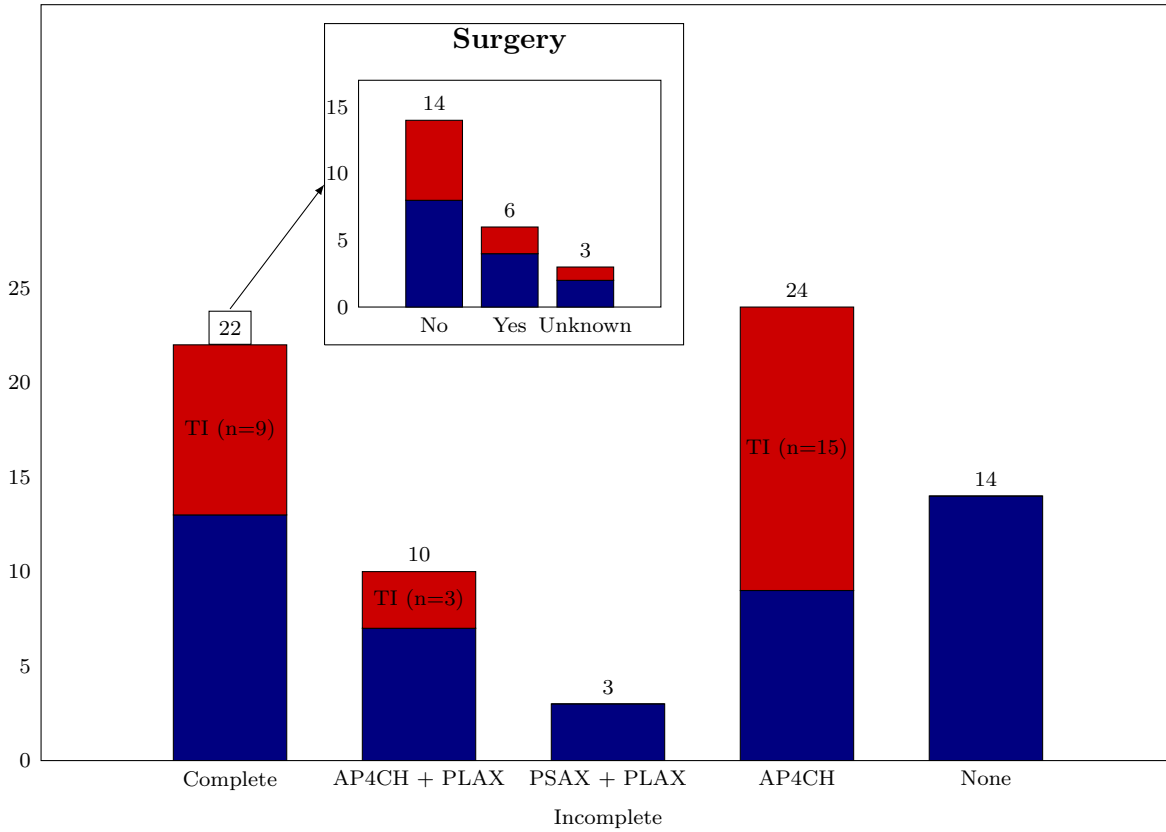


Figure 7.1: Visual representation obtained views and the prevalence of tricuspid regurgitation. The x axis represents the combination of acquired views and the y axis corresponds to the number of subjects. The red part of the bar plot indicates the amount of tricuspid regurgitation and the complete bar represents the amount of subjects in which the views could be obtained. In only 9 (12%) subjects, the complete measurement could be performed.

7.3.1 Further data acquisition

No patient was included for further data acquisition. In two screened subjects between April 2018 and June 2018 all required views could be obtained. However, in the first subject, passive leg raising was clinically contraindicated due to hypertension. In the other subject, inclusion was contraindicated due to irregular cardiac rhythm due to the occurrence of ventricular runs.

Figure 7.1 displays all subjects categorized according completeness of the measurement. As can be observed in the category of the incomplete measurement, AP4CH view was acquired the most and PSAX the least.

Table 7.2: Comparison of screening to medical history of the subjects. The severity of tricuspid regurgitation (TR), true positive (TP), false negative (FN), true negative (TN) and false positive (FP) tricuspid regurgitation were assessed. If no view could be obtained, this was separately stated. The subdivision of severity of tricuspid regurgitation shows that a trace of tricuspid regurgitation was most often missed.

Severity TR	TP	FN	No view
Trace	3	7	5
Mild	9	2	2
Moderate	5	1	1
Severe	1	0	0

7.3.2 Effect of cardiothoracic surgery

No significant correlation exists between amount of obtained views and cardiothoracic surgery. As can be observed in the subplot of Figure 7.1, the amount of subjects with cardiothoracic surgery wherein a complete measurement could be obtained was lower compared to subjects without cardiothoracic surgery. Subgroup analysis showed that success rate in cardiothoracic surgery subjects was 7% whereas success rate was 17 % in subjects without cardiothoracic surgery.

7.3.3 Screening adequacy

In Table 7.2, results of the comparison between screening performed at the ICU to the reports of trained specialists are stated. As can be observed from the table, not all patients with tricuspid regurgitation were adequately detected, mainly in the group of a trace tricuspid regurgitation. Absence of tricuspid regurgitation was adequately detected, no false positive cases were determined.

7.4 Discussion

As can be observed from the results, success rate of a complete measurement is low. A single beat ultrasound method to derive RV-PA coupling was feasible in 12% of the total population. Based on clinical contraindication, a passive leg raise maneuver may not always be performed. Most often the limiting factor was the inability to acquire pulmonic valve flow. When no measurement could be obtained in the PSAX view, subcostal or right parasternal short axis view were tried to obtain pulmonic valve flow. However, also these views were often inadequate to obtain pulmonic valve flow and acquisition of the pulmonic valve diameter would be less accurate due to lower spatial resolution. As pulmonic valve flow must be obtained for both a single beat method and multiple beat method to determine RV-PA coupling, feasibility of both methods is the same.

Presence of thoracic drains and the surgical thoracic wounds affect optimal probe position by decreasing thoracic surface where the US probe can be positioned. It is also expected that in patients with a high body mass index, the US probe cannot be easily positioned between ribs, thereby di-

minishing the acoustic window. A subcostal view is then complicated by the existence of abdominal fat. To overcome these limiting factors, esophageal US is proposed as an alternative method to acquire all measurements. However, compared to transthoracic US, esophageal US is more invasive and less easy applicable.

Tricuspid regurgitation was not always detected. This might be the effect of difference in ultrasound machine used for screening and used by the Department of Cardiology. The ultrasound machine used by the Department of Cardiology has a higher spatial resolution, thereby improving the detection of a trace of tricuspid regurgitation. Comparison between the ultrasound machine used in the ICU and by the Department of Cardiology in the detection of tricuspid regurgitation is therefore recommended.

The screening presented in this chapter was performed by one observer. Next to feasibility of the method, repeatability and consistency of the measurement is related to the validity of US derived RV-PA coupling determination. Low inter observer variability and intra observer variability must be obtained to adequately implement the measurement method in the ICU.

Patients with atrial fibrillation were excluded from screening based on the large variation in beat to beat RR interval. However, based on RR-interval, comparable cardiac contractions may be matched and used for the determination of RV-PA coupling. In order to determine whether RV-PA coupling can be validly determined in patients with atrial fibrillation using ultrasound, the ultrasound method to derive RV-PA coupling should first be validated and tested in the ICU.

7.5 Conclusion

The inability to detect pulmonic valve flow, necessary for stroke volume estimation, was the major limitation to obtain a complete measurement in the ICU department. Without the determination of stroke volume, even the single beat method to determine RV-PA coupling would be unfeasible. Further research is recommended to determine inter observer variability, intra observer variability and assesses the effect of US machine on the detection of tricuspid regurgitation for the determination of RV-PA coupling in the ICU.

Part IV

General discussion and conclusion

Patients admitted to the ICU require optimal personalized care for all organ systems. Care of the circulatory system is a primary concern. Evaluation of left heart function is common, evaluation of right heart function much less so. Yet, the right heart is also affected by hemodynamic treatment, and mechanical ventilation may also compromise its function. Therefore, frequent right heart evaluation would provide additional information to optimize personal care. Yet, a non-invasive, bedside, affordable and frequently applicable technique to determine right ventricular function and especially right ventricular-pulmonary vasculature interactions does not exist.

This thesis focused on an ultrasound method for the determination of RV-PA coupling. The simplifying assumptions underlying this method were carefully documented. Validity and feasibility were investigated. The single beat method provides comparable results to RV-PA coupling measured with the gold standard method (Chapter 6). However, the estimation of stroke volume, end systolic volume, systolic pressure and isovolumic pressure (Chapter 3, 4 and 5) is inaccurate. The validity of ultrasound derived RV-PA coupling therefore remains questionable. Given its potential clinical value, further research should focus on diminishing estimation errors.

Currently, the use of ultrasound derived RV-PA coupling is only recommended for intra subject comparison. Changes in RV-PA coupling might reflect the effect of treatment. It is still unknown whether ultrasound derived RV-PA coupling reflects changes in RV-PA interaction. Therefore, further data acquisition in the ICU is indicated. Data acquisition should focus on the ability of ultrasound derived RV-PA coupling to reflect treatment effect.

However, preliminary investigation of feasibility of the ultrasound method showed that data acquisition in the ICU is challenging. An ultrasound based method requires at least tricuspid regurgitation and the estimation of systolic pulmonic valve flow. As described in Chapter 7, these measurements could only be obtained in 12% of the population. This predicts poor applicability in the complete ICU population.

To our knowledge, validity and feasibility of ultrasound derived RV-PA coupling was not extensively studied. In a few articles in books, possibility of such a method is discussed [118,124,132] but never thoroughly described. Authors describe the possibility, but only report preliminary results. The results of Hobson et al. [124] imply valid use of ultrasound derived RV-PA coupling, opening the doors to considerable possibilities. Results presented in this thesis point in the same direction. However, cautious use of derived RV-PA coupling values and extensive future research is strongly indicated.

In the clinical ICU setting, right heart evaluation is often bypassed. However, single quantities as obtained in this study might provide the physician with additive information about right heart

function, even in absence of the computation of RV-PA coupling. Assessing the effect of treatment on the pulmonic valve velocity time integral, maximal velocity of tricuspid regurgitation and two-dimensional area changes is expected to reflect individual changes in RV stroke volume, RV afterload and RV ejection fraction. The addition of these values to standard clinical ultrasound would provide the physician with detailed information about the right heart and is therefore strongly recommended.

Transthoracic ultrasound as used in this study is hindered by the presence of extra thoracic fat, ribs, patient position, thoracic drains and thoracic wounds. These factors can be circumvented by the use of esophageal ultrasound, thereby potentially increasing the feasibility of US derived RV-PA coupling. However, esophageal ultrasound is more invasive and less easily applicable. Therefore, the method is less attractive compared to transthoracic ultrasound. However, esophageal ultrasound may help establish validity of the method and expand its applicability among the complete ICU population.

In conclusion, and based on the data and results presented in this thesis, RV-PA coupling can theoretically be derived using ultrasound. However, large estimation errors limit its practical applicability for now. The single beat method seems to obtain the most promising results. Future research should be aimed at reducing estimation errors and the ability of ultrasound derived RV-PA coupling to describe treatment effects.

Appendices

Appendix A

Descriptive diagrams

Both the multiple beat and single beat method are depicted in a descriptive model. Where the multiple beat method requires the estimation of stroke volume, end systolic volume and RV systolic pressure from ultrasound, the single beat requires the estimation of stroke volume and RV systolic pressure. A descriptive diagram of both methods is displayed in A.3.

To validate both methods, baseline US volume data was compared to MRI and baseline pressure data was compared to baseline invasive pressure measurements. Chapter 3 describes the validity of US derived volume and Chapter 4 described the validity of US derived pressure. A descriptive diagram of the validation of the method is displayed in Figure A.1

To determine the effect of PLR on invasive pressure measurements, baseline and PLR conditions were compared. To determine whether this effect could be measured using US, baseline volume and pressure estimates were compared to PLR volume and pressure estimates. These effects are described in Chapter 5.

In the subset of patients who underwent PLR, single beat and multiple beat RV-PA coupling were determined. In the subset of patients who underwent RHC and MRI, gold standard single beat RV-PA coupling was determined and compared to US derived single beat RV-PA coupling. The derivation of RV-PA coupling is described in Chapter 6. Different methods to derive RV-PA coupling with their measurement methodologies are displayed in Figure A.2.

The computation of the estimates, stroke volume, end systolic volume and systolic pressure, required to derive RV-PA coupling, is displayed in Figure A.4. The interaction between different estimates can be observed in this diagram.

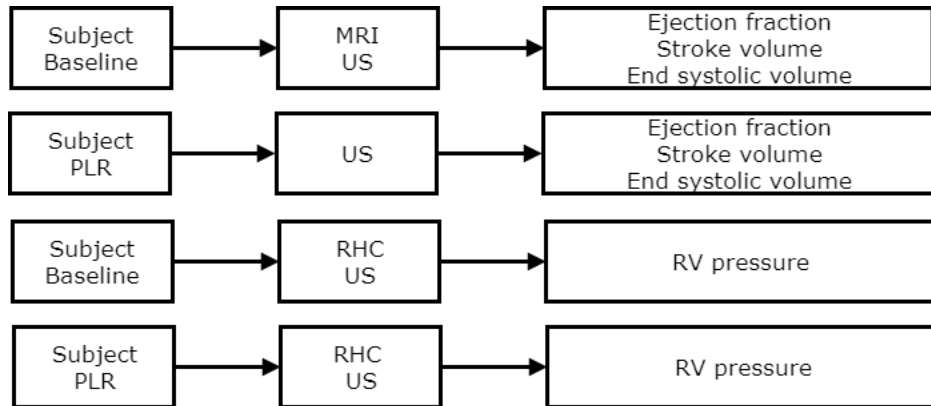


Figure A.1: Descriptive diagram of the quantities estimated during this study.

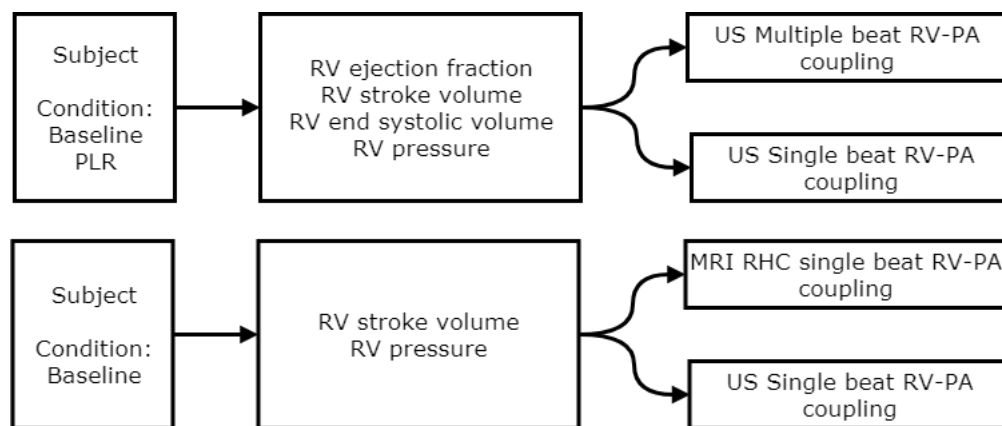


Figure A.2: Descriptive diagram of the derivation of the different RV-PA coupling estimates by the different measurements methods.

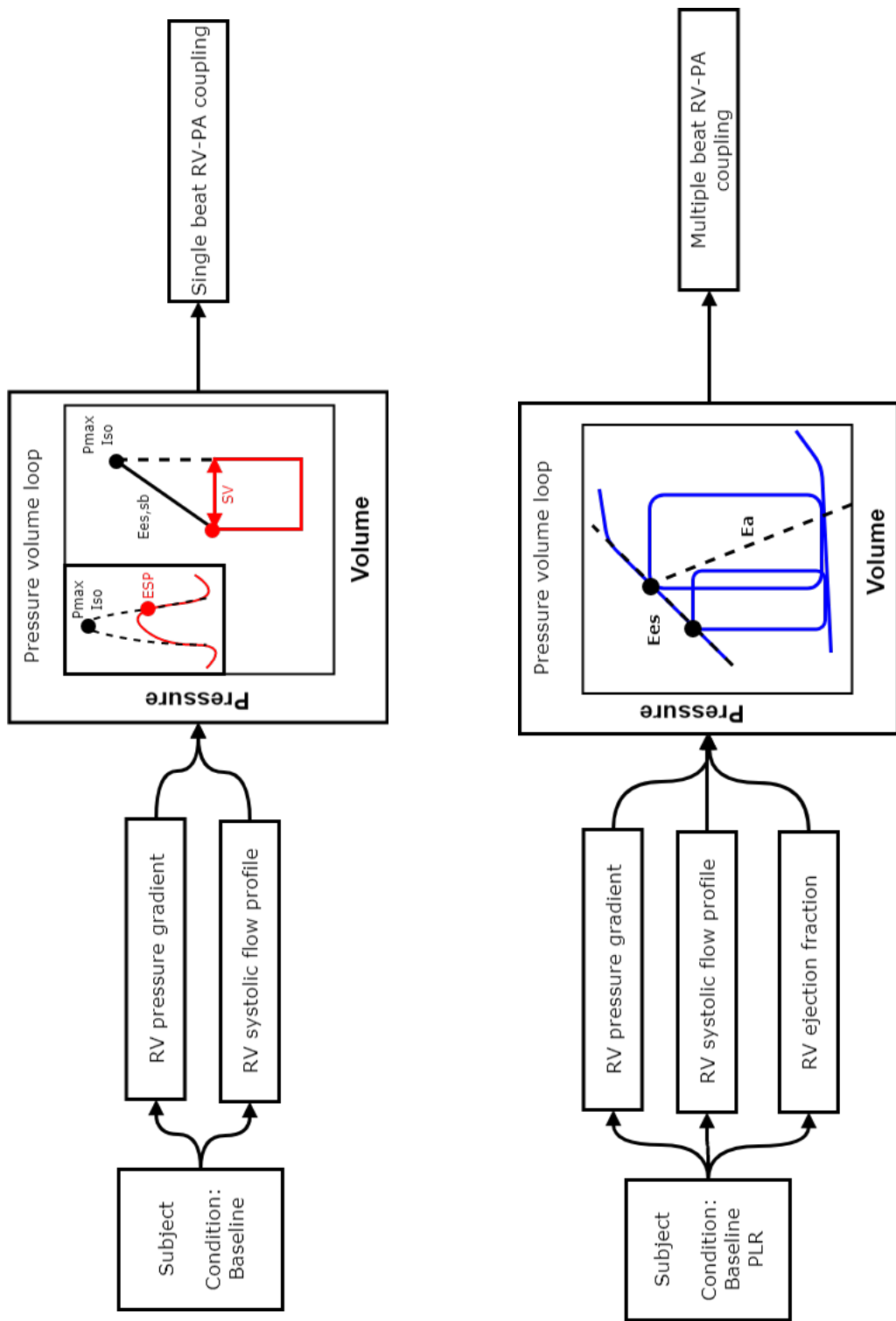


Figure A.3: Descriptive diagram of the single beat method (left) and the multiple beat method (right).

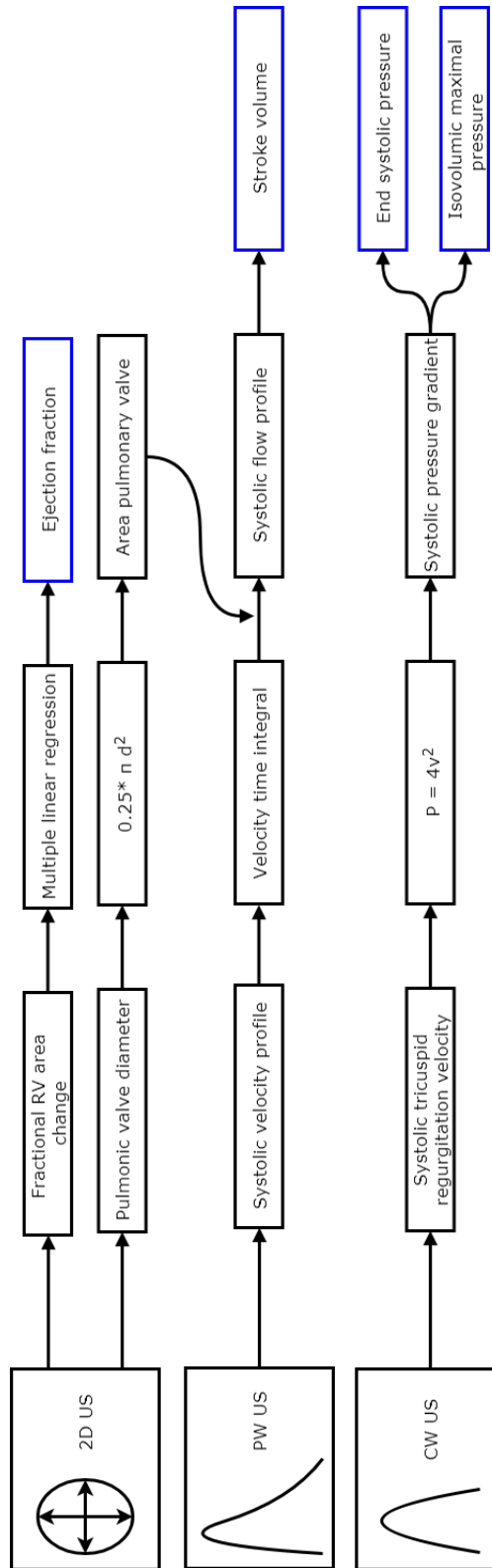


Figure A.4: Descriptive diagram of the derivation of different estimates from the ultrasound measurements.

Appendix B

Framework for the automatic detection of PW Doppler velocity profile and CW Doppler velocity profile

Using the PHILIPS CX50 US machine, PW Doppler velocity profiles and CW Doppler velocity profiles were acquired. Data was exported from the machine as raw DICOM images. DICOM images were first converted to MAT files and loaded into MATLAB. The basic frame work of the automatic detection of the velocity profiles is described in this appendix. Used methods to determine SV from PW Doppler velocity profiles and RVSP from CW Doppler velocity profiles are described in Appendix C and Appendix D. A framework of the automatic detection is presented in Figure.. DICOM image preprocessing, RR-interval detection and velocity profile detection is described in this Appendix.

B.1 Automatic R wave detection

On each DICOM image, the ECG is displayed. To automatically determine RR interval in the image, first the ECG was extracted from the image based on color recognition. Due to the low resolution of the ECG, a method based on the derivative as used in the Pan-Tompkins method for QRS detection was not sufficient. Therefore, R peaks were defined as the peaks occurring at the upper 98% quantile and S peaks were defined as the peaks occurring at the lower quantile of 1% of the ECG data. Assuming equal amount of R and S peaks, R and S peaks were matched to their complex based on pixel location. After defining R and S peaks, P, Q and T peaks were determined from the ECG.

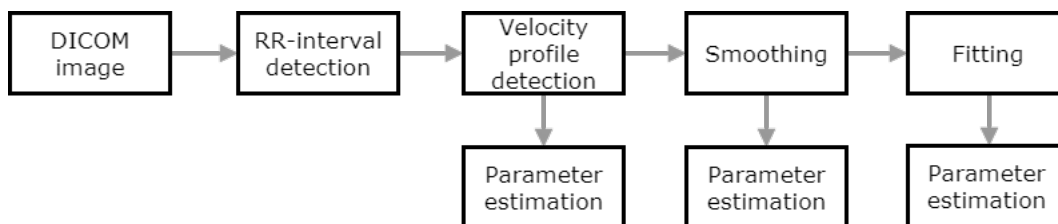


Figure B.1: Descriptive diagram of post processing of the DICOM image to the estimated parameter.

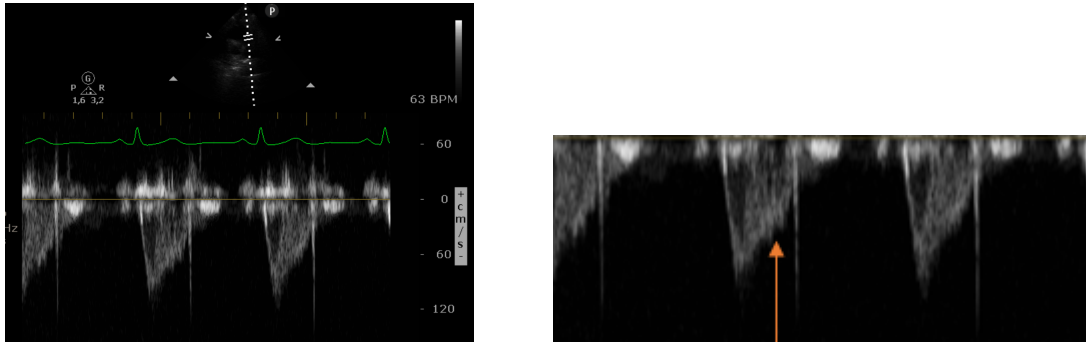


Figure B.2: Pulsed wave Doppler images, a complete image is displayed left, the direction of the detection of the envelope is displayed in the right figure.

B.2 Velocity profile extraction

After determining the velocity axis using optical character recognition, pixel velocity was determined. Thereafter, the zero line was detected. Measured pulmonic valve flow velocities and tricuspid regurgitation velocities move away from the probe. Therefore, all information above the zero line line was excluded from analysis.

The outer border of the velocity profile was detected based on pixel intensity. Therefore, the image was first binarized, with an intensity threshold of 10%. Pixel intensity below 10% were set to zero. The first pixel exceeding 10% were detected per image column from the bottom of the image, as visualized with the red arrow in Figure B.2. Maximal velocity was determined and stored.

Appendix C

Comparison manual and automatic PW profile

The PV velocity profile was determined as explained in Appendix B. The performance of automatic detected velocity profiles was compared to manual detection of the PV Doppler profile. The method obtaining the most similar results compared to manual PV Doppler velocity was then selected to establish PV loops.

C.1 Manual PV Doppler velocity quantification

The MATLAB function `imfreehand` was used for the manual detection of the PV Doppler profile. Corresponding coordinates of the drawn line in the image were converted to velocity.

C.2 Automatic curve detection

Three methods for the automatic quantification of PV Doppler flow were compared. The first method contained no further processing. The second method consisted of the application of cubic spline interpolation. The third method consisted of the fitting of the raw curve to a combination of two polynomials. [133] Maximal PV Doppler velocity was used as the junction between the two polynomials. The ascending part of the PV Doppler velocity was fitted to a third order polynomial. The descending part of the PV Doppler velocity profile was fitted to a fourth order polynomial. In the occurrence of a mid-systolic notch [61, 66], the descending part of the PV Doppler velocity profile was fitted to a sixth order polynomial. The mid-systolic notch was manually detected.

Systolic flow was determined by the detection of the R peak in the ECG and the closing click. Onset of systolic flow was determined as the R peak. End of systolic flow was determined at the closing click. The closing click was defined at the index with the highest positive derivative between the T-wave top and T-wave end. If no closing click was present in the velocity profile, the index of the end of the manual curve was used as the end of systolic flow. The velocity profile was set to zero during the diastolic phase of the cardiac cycle.

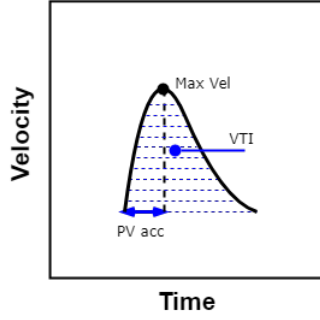


Figure C.1: Schematic representation of pulmonic valve acceleration time (PV acc), maximal pulmonic valve velocity (Max Vel) and the velocity time integral (VTI, area under the curve)

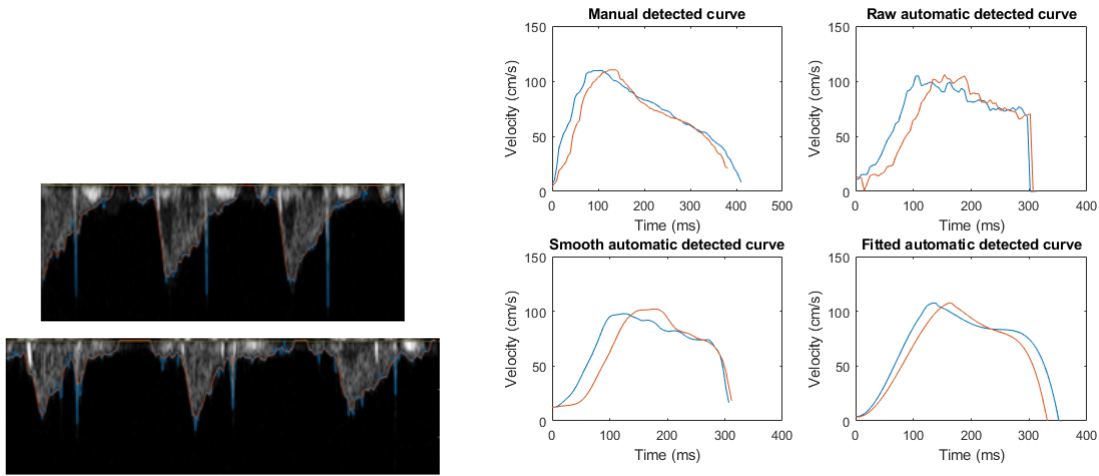


Figure C.2: Left: pulsed wave Doppler images with raw curve (blue) and smoothed curve (red). Right: Pulsed wave Doppler automatically detected curves by the different automatic detection algorithm. The manual detected profile, raw detected profile, smoothed detected profile and fitted detected profile are displayed.

C.3 Statistics

The effect of processing of the raw obtained was determined by the comparison of maximal PV velocity, PV acceleration time and PV velocity time integral. PV acceleration time was determined as the time between the onset of systolic flow until the maximal systolic velocity. The velocity time integral was determined as the integral of the velocity profile. In Figure C.1 these parameters are schematically represented.

Bland-Altman analysis was used to determine the agreement between manual velocity profile detection and automatic velocity profile detection. Correlation and linear regression were used to assess correlation between manual velocity profile detection and automatic velocity profile detection. R-squared was determined.

Table C.1: Mean (standard deviation) values of the estimated velocity time integral (VTI), pulmonic valve acceleration time (PVacc) and maximal velocity (Maxvel).

Parameter	Detection method			
	Manual	Smooth	Raw	Fit
VTI, cm	18,3 (6,0)	15,5 (5,2)	15,8 (5,2)	17,4 (8,6)
Pvacc, ms	136,3 (44,3)	175,8 (59,0)	156,7 (60,0)	180,1 (92,2)
Maxvel, cm/s	78,7 (21,6)	72,7 (21,2)	82,5 (24,9)	90,7 (26,9)

Table C.2: R-squared value and mean difference per estimated velocity time integral (VTI), pulmonic valve acceleration time (PVacc) and maximal velocity (Maxvel). Values are presented as the mean difference and corresponding limits of agreement.

	VTI			Pvacc			Maxvel		
	Smooth	Raw	Fit	Smooth	Raw	Fit	Smooth	Raw	Fit
Rsquare	0,67	0,65	0,63	0,31	0,21	0,23	0,55	0,41	0,35
Mean difference	2,59	2,26	0,62	-38,31	-19,10	-41,89	4,97	- 5,25	-13,20
Limit of agreement	2,9	3,0	3,3	46,7	53,2	59,2	13,3	17,9	21,8

C.4 Results

In 23 subject the RV focused protocol was performed. In 2 subjects, the PV Doppler velocity profile could not be visualized. Of all obtained PW Doppler images, 321 heart beats were analyzed. Thereof 253 were adequate for analysis. From these 253 beats, 11 beats had a notched velocity profile. Success rate to acquire an adequate PW Doppler profile ranged per subject from 0 to 100%. An average success rate of 72% was obtained.

An example of unprocessed PV Doppler velocity profile and smoothed PV Doppler velocity profile can be observed in the left panel of Figure C.2. As can be observed, smoothing of the obtained velocity profile provided a less noisy appearance which is more like a manually drawn envelope.

In Figure C.2 the difference between manual detected PV Doppler velocity profile, unprocessed automatic detected PV Doppler velocity profile, smoothed automatic detected PV Doppler velocity profile and fitted automatic detected PV Doppler velocity profile is displayed. Table C.1 displays mean and std of the different methods. R square is displayed in Table C.2.

C.5 Conclusion

Automatic detection of the PV velocity profile in combination with postprocessing using cubic spline interpolation has a superior correlation to manual detection of the PV velocity profile. Therefore, the smoothed PV velocity profile will be used for further establishment of the PV loops.

Appendix D

Comparison manual and automatic CW Doppler profile

The tricuspid regurgitation velocity profile was determined as explained in Appendix B. The performance of automatic detected velocity profiles was compared to manual detection of the tricuspid regurgitation velocity profile. The method obtaining the most similar results compared to manual tricuspid regurgitation velocity profile was then selected to establish PV loops.

D.1 Manual tricuspid regurgitation Doppler velocity quantification

The MATLAB function *imfreehand* was used for the manual detection of the tricuspid regurgitation velocity profile. Corresponding coordinates of the drawn line in the image were converted to velocity.

D.2 Automatic curve detection

Three methods for the automatic quantification of PV Doppler flow were compared. The first method contained no further processing. The second method consisted of the application of cubic spline interpolation. The third method consisted of the fitting the complete unprocessed velocity profile, the complete smoothed velocity profile and parts of the smoothed velocity profile to a sine wave.

Using a constrained least squares algorithm, the complete velocity profiles were fitted to a sine wave. In some subjects, partially inadequate tricuspid regurgitation velocity profile were obtained (see Figure D.1 middle panel). Automatic detection and subsequent fitting then results in an underestimation of the tricuspid regurgitation profile. Therefore, parts of the smoothed signal were used to determine a fit. The first part of the smoothed velocity profile was selected, until the first derivative became zero and the second part consisted of the last part with a negative first derivative. Based on the least error to measured data and maximal estimated velocity, one of the fits was selected for further analysis.

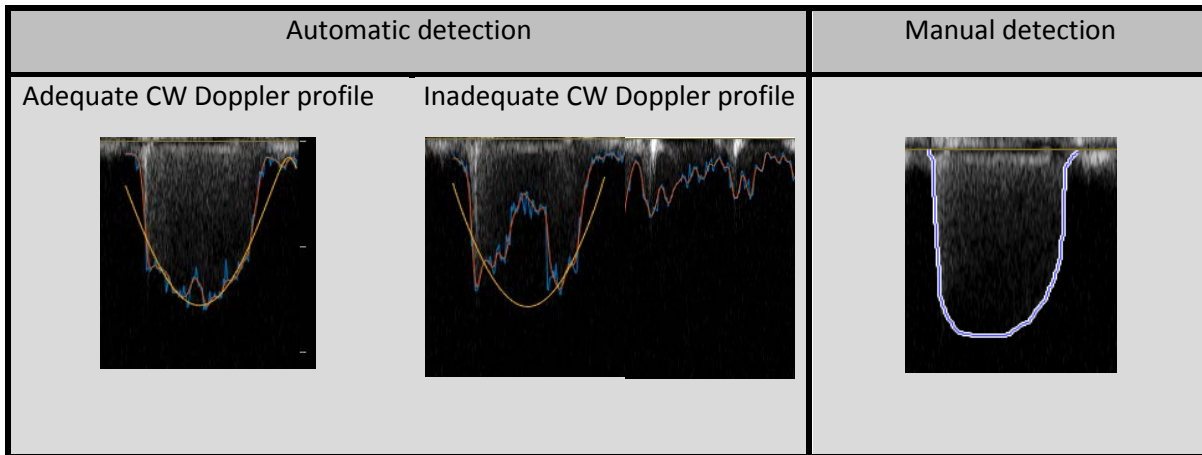


Figure D.1: Continuous wave Doppler images with manual detected envelope, raw envelope (blue) and smoothed envelope (red).

D.3 Statistics

The effect of processing of the raw obtained was determined by the comparison of maximal tricuspid regurgitation velocity derived RV pressure, normalized index of the occurrence of RVSP and maximal pressure change and minimal pressure change during systole. Maximal tricuspid regurgitation velocity and its corresponding index were automatically determined. The first derivative was used to determine maximal pressure change and minimal pressure change during systole. Bland-Altman analysis was used to determine the agreement between manual velocity profile detection and automatic velocity profile detection. Correlation and linear regression were used to assess correlation between manual velocity profile detection and automatic velocity profile detection. R-squared was determined.

D.4 Results

In 23 subject the RV focused protocol was performed. In 2 subjects, tricuspid regurgitation could not be visualized. Of all obtained CW Doppler images, 306 heart beats were analyzed. Thereof 145 CW Doppler profiles were adequate for analysis. Of all adequate beats, 6 beats were recorded to be fitted according to technique 1, 67 to technique 2 and 72 to technique 3. Overall success rate to acquire an adequate CW Doppler profile ranged per subject from 0% to 100%. An average success rate of 37% was achieved.

An example of a manually detected tricuspid regurgitation Doppler velocity profile, unprocessed tricuspid regurgitation Doppler velocity profile and smoothed tricuspid regurgitation Doppler velocity profile can be observed in Figure D.1. As can be observed, smoothing of the obtained velocity

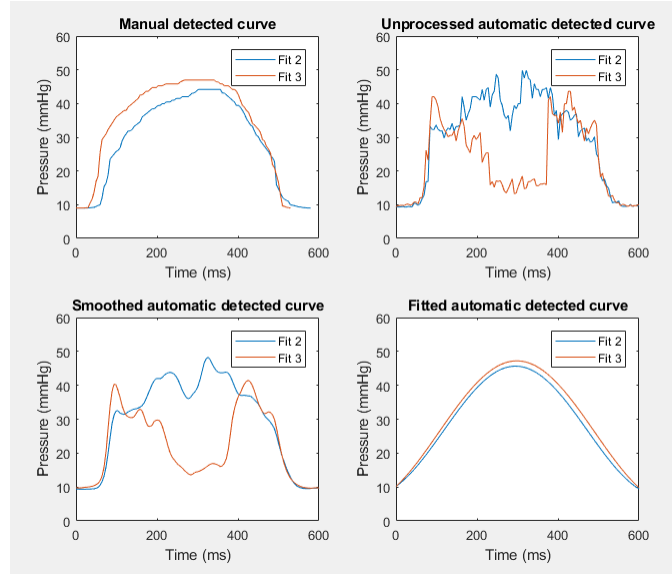


Figure D.2: Continuous wave Doppler automatically detected curves by the different automatic detection algorithm. The manual detected profile, raw detected profile, smoothed detected profile and fitted detected profile are displayed.

Table D.1: Mean (standard deviation) values of the estimated velocity time integral (VTI), pulmonic valve acceleration time (PVacc) and maximal velocity (Maxvel).

Parameter	Detection method			
	Manual	Smooth	Raw	Fit
RVSPmax, mmHg	54,1 (23,3)	46,6 (32,3)	48,9 (32,8)	42,2 (33,2)
RVSPidx, %systole	0,32 (0,08)	0,29 (0,20)	0,29 (0,12)	0,60 (0,14)
dP/dtmax, mmHg/s	1943 (1031)	660 (401)	1947 (1190)	153 (161)
dP/dtmin, mmHg/s	-1284 (802)	-2013 (3582)	-2650 (3594)	-157 (160)

profile provided a less noisy appearance which is more like a manually drawn envelope. An example of all estimated curves with an adequate and a semi adequate CW Doppler profile is displayed in Figure D.2. Mean values and the standard deviation of the obtained parameters are stated in Table D.1. R-squared, mean difference and limit of agreements are displayed in Table D.2 and D.3.

D.5 Conclusion

Based on the results, the use of the raw automatic detection is indicated. However, because of the noisy appearance of the unprocessed tricuspid regurgitation velocity profile, maximal pressure change during systole and minimal pressure change during diastole are most likely to be based on a noisy change instead of the pressure change in the ventricle. Therefore, the smoothed tricuspid regurgitation velocity profile will be used for further establishment of the PV loops.

Table D.2: R-squared value and mean difference per estimated maximal RV systolic pressure (RVSPmax) and the normalized time where RVSP max is detected (RVSPidx). Values are presented as the mean difference and corresponding limits of agreement (LOA).

	RVSPmax			RVSPidx		
	Smooth	Raw	Fit	Smooth	Raw	Fit
Rsquare	0,56	0,58	0,50	0,05	0,09	0,04
Mean difference (LOA)	7,57 (21,5)	5,17 (21,37)	11,91 (23,42)	0,02 (0,20)	0,05 (0,18)	0,04 (0,13)

Table D.3: R-squared value and mean difference per estimated maximal pressure change during contraction (dP/dt_{max}) and maximal pressure change during relaxation (dP/dt_{min}). Values are presented as the mean difference and corresponding limits of agreement (LOA).

	dP/dt_{max}			dP/dt_{min}		
	Smooth	Raw	Fit	Smooth	Raw	Fit
Rsquare	0,09	0,05	0,04	0,01	0,01	0,21
Mean difference (LOA)	-325 (2502)	-1298 (2538)	1226 (794)	1223 (939)	-356 (1344)	1831 (956)

Bibliography

- [1] Clifford R Greyson. Right heart failure in the intensive care unit. *Current opinion in critical care*, 18(5):424–431, 2012.
- [2] Christopher King, Christopher W May, Jeffrey Williams, and Oksana A Shlobin. Management of right heart failure in the critically ill. *Critical care clinics*, 30(3):475–498, 2014.
- [3] Massimiliano Foschi, Michele Di Mauro, Fabrizio Tancredi, Carlo Capparuccia, Renata Petroni, Luigi Leonzio, Silvio Romano, Sabina Gallina, Maria Penco, Mario Cibelli, et al. The dark side of the moon: The right ventricle. *Journal of Cardiovascular Development and Disease*, 4(4):18, 2017.
- [4] Corey E Ventetuolo and James R Klinger. Management of acute right ventricular failure in the intensive care unit. *Annals of the American Thoracic Society*, 11(5):811–822, 2014.
- [5] Anton Vonk Noordegraaf, Berend E Westerhof, and Nico Westerhof. The relationship between the right ventricle and its load in pulmonary hypertension. *Journal of the American College of Cardiology*, 69(2):236–243, 2017.
- [6] Lawrence G Rudski, Wyman W Lai, Jonathan Afilalo, Lanqi Hua, Mark D Handschumacher, Krishnaswamy Chandrasekaran, Scott D Solomon, Eric K Louie, and Nelson B Schiller. Guidelines for the echocardiographic assessment of the right heart in adults: a report from the american society of echocardiography. *Journal of the American Society of Echocardiography*, 23(7):685–713, 2010.
- [7] Pia Trip, Nicolaas Westerhof, and Anton Vonk Noordegraaf. Function of the right ventricle. In *The Right Heart*, pages 9–18. Springer, 2014.
- [8] Robert Naeije. Physiology of the pulmonary circulation and the right heart. *Current hypertension reports*, 15(6):623–631, 2013.
- [9] D. Burkhoff. Mechanical properties of the heart and its interaction with the vascular system. Course material, 2002.
- [10] Walter F Boron and Emile L Boulpaep. *Medical Physiology, 2e Updated Edition E-Book: with STUDENT CONSULT Online Access*. Elsevier Health Sciences, 2012.
- [11] Nicolaas Westerhof, Nikos Stergiopoulos, and Mark IM Noble. *Snapshots of hemodynamics: an aid for clinical research and graduate education*. Springer Science & Business Media, 2010.
- [12] Jonathan C Kentish, Henk EDJ ter Keurs, Lucio Ricciardi, Jeroen JJ Bucx, and Mark IM Noble. Comparison between the sarcomere length-force relations of intact and skinned trabeculae from rat right ventricle. influence of calcium concentrations on these relations. *Circulation research*, 58(6):755–768, 1986.
- [13] R Naeije. From frank-starling relationships to ventriculo-arterial coupling. *Anaesthesia, Pain, Intensive Care and Emergency Medicine—APICE*, pages 449–459, 2005.
- [14] SJ Sarnoff, JH Mitchell, JP Gilmore, and JP Remensnyder. Homeometric autoregulation in the heart. *Circulation research*, 8(5):1077–1091, 1960.
- [15] Kasper Dennis, Fauci Anthony, Hauser Stephen, Longo Dan, Jameson J. Larry, and Loscalzo Joseph. *Harrison’s Principles of Internal Medicine, 19e*, volume 1. McGraw-Hill Education, 19 edition, 2015.

- [16] Serge Brimiouille, Pierre Wauthy, Patricia Ewalenko, Benoit Rondelet, Françoise Vermeulen, François Kerbaul, and Robert Naeije. Single-beat estimation of right ventricular end-systolic pressure-volume relationship. *American Journal of Physiology-Heart and Circulatory Physiology*, 284(5):H1625–H1630, 2003.
- [17] Louis J Dell’Italia and Richard A Walsh. Application of a time varying elastance model to right ventricular performance in man. *Cardiovascular research*, 22(12):864–874, 1988.
- [18] Guido Claessen, Piet Claus, Marion Delcroix, Jan Bogaert, Andre La Gerche, and Hein Heidbuchel. Interaction between respiration and right versus left ventricular volumes at rest and during exercise: a real-time cardiac magnetic resonance study. *American Journal of Physiology-Heart and Circulatory Physiology*, 306(6):H816–H824, 2014.
- [19] Shareen Kaur Jaijee. Non-invasive assessment of right ventricular function in health and in acute and chronic pulmonary arterial hypertension. -, 2016.
- [20] WILLIAM P Santamore and JOHN N Amooore. Buffering of respiratory variations in venous return by right ventricle: a theoretical analysis. *American Journal of Physiology-Heart and Circulatory Physiology*, 267(6):H2163–H2170, 1994.
- [21] William R Milnor, C Richard Conti, Kenneth B Lewis, and Michael F O’rourke. Pulmonary arterial pulse wave velocity and impedance in man. *Circulation research*, 25(6):637–649, 1969.
- [22] Nabil Saouti, Nico Westerhof, Frank Helderma, J Tim Marcus, Anco Boonstra, Pieter E Postmus, and Anton Vonk-Noordegraaf. Right ventricular oscillatory power is a constant fraction of total power irrespective of pulmonary artery pressure. *American journal of respiratory and critical care medicine*, 182(10):1315–1320, 2010.
- [23] Stefano Ghio, Sandra Schirinzi, and Silvia Pica. Pulmonary arterial compliance: How and why should we measure it? *Global Cardiology Science and Practice*, page 58, 2015.
- [24] Diana M Tabima, Jennifer L Philip, and Naomi C Chesler. Right ventricular-pulmonary vascular interactions. *Physiology*, 32(5):346–356, 2017.
- [25] L.J. Rubin and W. Hopkins. Classification and prognosis of pulmonary hypertension in adults, 2018.
- [26] J Ressler, D Urbanova, J Widimský, B Ošťádal, V Pelouch, and J Prochazka. Reversibility of pulmonary hypertension and right ventricular hypertrophy induced by intermittent high altitude hypoxia in rats. *Respiration*, 31(1):38–46, 1974.
- [27] B Ostadal and F Kolar. Cardiac adaptation to chronic high-altitude hypoxia: beneficial and adverse effects. *Respiratory physiology & neurobiology*, 158(2-3):224–236, 2007.
- [28] Hiroyuki Suga, Kiichi Sagawa, and Artin A Shoukas. Load independence of the instantaneous pressure-volume ratio of the canine left ventricle and effects of epinephrine and heart rate on the ratio. *Circulation research*, 32(3):314–322, 1973.
- [29] Hiroyuki Suga and Kiichi Sagawa. Instantaneous pressure-volume relationships and their ratio in the excised, supported canine left ventricle. *Circulation research*, 35(1):117–126, 1974.
- [30] Kiichi Sagawa, Hiroyuki Suga, Artin A Shoukas, and Kenneth M Bakalar. End-systolic pressure/volume ratio: a new index of ventricular contractility. *American Journal of Cardiology*, 40(5):748–753, 1977.
- [31] Toshiyuki Noda, CP Cheng, Pieter P De Tombe, and William C Little. Curvilinearity of lv end-systolic pressure-volume and dp/dtmax-end-diastolic volume relations. *American Journal of Physiology-Heart and Circulatory Physiology*, 265(3):H910–H917, 1993.
- [32] W Lowell Maughan, Artin A Shoukas, Kiichi Sagawa, and Myron L Weisfeldt. Instantaneous pressure-volume relationship of the canine right ventricle. *Circulation research*, 44(3):309–315, 1979.

- [33] RM Shoucri. Pressure-volume relation in the right ventricle. *Journal of biomedical engineering*, 15(2):167–169, 1993.
- [34] Kenneth A Brown and Roy V Ditchey. Human right ventricular end-systolic pressure-volume relation defined by maximal elastance. *Circulation*, 78(1):81–91, 1988.
- [35] Louis J Dell’Italia and William P Santamore. Can indices of left ventricular function be applied to the right ventricle? *Progress in cardiovascular diseases*, 40(4):309–324, 1998.
- [36] Ryan J Tedford, James O Mudd, Reda E Girgis, Stephen C Mathai, Ari L Zaiman, Traci Houston-Harris, Danielle Boyce, Benjamin W Kelemen, Anita C Bacher, Ami A Shah, et al. Right ventricular dysfunction in systemic sclerosis associated pulmonary arterial hypertension. *Circulation: Heart Failure*, pages CIRCHEARTFAILURE–112, 2013.
- [37] Steven Hsu, Brian A Houston, Emmanouil Tampakakis, Anita C Bacher, Parker S Rhodes, Stephen C Mathai, Rachel L Damico, Todd M Kolb, Laura K Hummers, Ami A Shah, et al. Right ventricular functional reserve in pulmonary arterial hypertension. *Circulation*, pages CIRCULATIONAHA–116, 2016.
- [38] Alessandro Bellofiore and Naomi C Chesler. Methods for measuring right ventricular function and hemodynamic coupling with the pulmonary vasculature. *Annals of biomedical engineering*, 41(7):1384–1398, 2013.
- [39] Raymond P Kelly, Chih-Tai Ting, Tsong-Ming Yang, Chung-Peng Liu, W Lowell Maughan, Mau-Song Chang, and David A Kass. Effective arterial elastance as index of arterial vascular load in humans. *Circulation*, 86(2):513–521, 1992.
- [40] Julio A Chirinos, Ernst R Rietzschel, Prithvi Shiva-Kumar, Marc L De Buyzere, Payman Zamani, Tom Claessens, Salvatore Geraci, Prasad Konda, Dirk De Bacquer, Scott R Akers, et al. Effective arterial elastance is insensitive to pulsatile arterial load. *Hypertension*, 64(5):1022–1031, 2014.
- [41] Patrick Segers, Nikos Stergiopoulos, and Nico Westerhof. Relation of effective arterial elastance to arterial system properties. *American Journal of Physiology-Heart and Circulatory Physiology*, 282(3):H1041–H1046, 2002.
- [42] Denis Chemla, Isabelle Antony, Yves Lecarpentier, and Alain Nitenberg. Contribution of systemic vascular resistance and total arterial compliance to effective arterial elastance in humans. *American Journal of Physiology-Heart and Circulatory Physiology*, 285(2):H614–H620, 2003.
- [43] Alberto Pagnamenta, Céline Dewachter, Kathleen McEntee, Pierre Fesler, Serge Brimiouille, and Robert Naeije. Early right ventriculo-arterial uncoupling in borderline pulmonary hypertension on experimental heart failure. *Journal of applied physiology*, 109(4):1080–1085, 2010.
- [44] Richard G Axell, Simon J Messer, Paul A White, Colm McCabe, Andrew Priest, Thaleia Statopoulou, Maja Drozdzyńska, Jamie Viscasillas, Elizabeth C Hinchy, James Hampton-Till, et al. Ventriculo-arterial coupling detects occult rv dysfunction in chronic thromboembolic pulmonary vascular disease. *Physiological reports*, 5(7), 2017.
- [45] Adriaan Oosterom and Thomas Franciscus Oostendorp. *Medische fysica*. Elsevier Gezondheidszorg, 2008.
- [46] Patrizio Lancellotti, Luis Moura, Luc A Pierard, Eustachio Agricola, Bogdan A Popescu, Christophe Tribouilloy, Andreas Hagendorff, Jean-Luc Monin, Luigi Badano, Jose L Zamorano, et al. European association of echocardiography recommendations for the assessment of valvular regurgitation. part 2: mitral and tricuspid regurgitation (native valve disease). *European Journal of Echocardiography*, 11(4):307–332, 2010.
- [47] Paul G Yock and Richard L Popp. Noninvasive estimation of right ventricular systolic pressure by doppler ultrasound in patients with tricuspid regurgitation. *Circulation*, 70(4):657–662, 1984.
- [48] Marvin Berger, Susan R Hecht, Andrew van Tosh, and Umadevi Lingam. Pulsed and continuous wave doppler echocardiographic assessment of valvular regurgitation in normal subjects. *Journal of the American College of Cardiology*, 13(7):1540–1545, 1989.

- [49] David Stewart, Robert B Leman, Jackie Kaiser, and Douglas L Mann. Catheter-induced tricuspid regurgitation*: Incidence and clinical significance. *Chest*, 99(3):651–655, 1991.
- [50] Patrizio Lancellotti, Christophe Tribouilloy, Andreas Hagedorff, Bogdan A Popescu, Thor Edvardsen, Luc A Pierard, Luigi Badano, and Jose L Zamorano. Recommendations for the echocardiographic assessment of native valvular regurgitation: an executive summary from the european association of cardiovascular imaging. *European Heart Journal–Cardiovascular Imaging*, 14(7):611–644, 2013.
- [51] WA Zoghbi, M Enriquez-Sarano, E Foster, PA Grayburn, CD Kraft, RA Levine, P Nihoyannopoulos, CM Otto, MA Quinones, H Rakowski, et al. American society of echocardiography: recommendations for evaluation of the severity of native valvular regurgitation with two-dimensional and doppler echocardiography: A report from the american society of echocardiography’s nomenclature and standards committee and the task force on valvular regurgitation, developed in conjunction with the american college of cardiology echocardiography committee, the cardiac imaging committee, council on clinical cardiology, the american heart association, and the european society of cardiology working group on echocardiography, represented by. *European Journal of Echocardiography*, 4(4):237–261, 2003.
- [52] Allan L Klein, Darryl J Burstow, A Jamil Tajik, Prince K Zachariah, Charles P Taliercio, Catherine L Taylor, Kent R Bailey, and James B Seward. Age-related prevalence of valvular regurgitation in normal subjects: A comprehensive color flow examination of 118, volunteers. *Journal of the American Society of Echocardiography*, 3(1):54–63, 1990.
- [53] Jagmeet P Singh, Jane C Evans, Daniel Levy, Martin G Larson, Lisa A Freed, Deborah L Fuller, Birgitta Lehman, and Emelia J Benjamin. Prevalence and clinical determinants of mitral, tricuspid, and aortic regurgitation (the framingham heart study). *The American journal of cardiology*, 83(6):897–902, 1999.
- [54] Ajit P Yoganathan, Edward G Cape, Hsing-Wen Sung, Frank P Williams, and Abdul Jimoh. Review of hydrodynamic principles for the cardiologist: applications to the study of blood flow and jets by imaging techniques. *Journal of the American College of Cardiology*, 12(5):1344–1353, 1988.
- [55] Luca Lanzarini, Alessandra Fontana, Elena Lucca, Carlo Campana, and Catherine Klersy. Noninvasive estimation of both systolic and diastolic pulmonary artery pressure from doppler analysis of tricuspid regurgitant velocity spectrum in patients with chronic heart failure. *American heart journal*, 144(6):1087–1094, 2002.
- [56] Javier F Aduen, Ramon Castello, Marcelo M Lozano, George N Hepler, Cesar A Keller, Francisco Alvarez, Robert E Safford, Julia E Crook, Michael G Heckman, and Charles D Burger. An alternative echocardiographic method to estimate mean pulmonary artery pressure: diagnostic and clinical implications. *Journal of the American Society of Echocardiography*, 22(7):814–819, 2009.
- [57] Yan Topilsky, Christophe Tribouilloy, Hector I Michelena, Sorin Pislaru, Douglas W Mahoney, and Maurice Enriquez-Sarano. Pathophysiology of tricuspid regurgitation. *Circulation*, 122(15):1505–1513, 2010.
- [58] Halfdan Ihlen, JP Amlie, J Dale, Kolbjorn Forfang, Sigurd Nitter-Hauge, JE Otterstad, Svein Simonsen, and Erik Myhre. Determination of cardiac output by doppler echocardiography. *Heart*, 51(1):54–60, 1984.
- [59] Herbert Dittmann, Wolfram Voelker, Karl-Ruediger Karsch, and Ludger Seipel. Influence of sampling site and flow area on cardiac output measurements by doppler echocardiography. *Journal of the American College of Cardiology*, 10(4):818–823, 1987.
- [60] David B Northridge, Iain N Findlay, John Wilson, Esther Henderson, and Henry J Dargie. Non-invasive determination of cardiac output by doppler echocardiography and electrical bioimpedance. *Heart*, 63(2):93–97, 1990.
- [61] Angel López-Candales and Kathy Edelman. Shape of the right ventricular outflow doppler envelope and severity of pulmonary hypertension. *European Heart Journal-Cardiovascular Imaging*, 13(4):309–316, 2011.

- [62] Frank Helderma, Gert-Jan Mauritz, Kirsten E Andringa, Anton Vonk-Noordegraaf, and J Tim Marcus. Early onset of retrograde flow in the main pulmonary artery is a characteristic of pulmonary arterial hypertension. *Journal of Magnetic Resonance Imaging*, 33(6):1362–1368, 2011.
- [63] Gert Reiter, Ursula Reiter, Gabor Kovacs, Bernhard Kainz, Karin Schmidt, Robert Maier, Horst Olschewski, and Rainer Rienmueller. Magnetic resonance-derived 3-dimensional blood flow patterns in the main pulmonary artery as a marker of pulmonary hypertension and a measure of elevated mean pulmonary arterial pressureclinical perspective. *Circulation: Cardiovascular Imaging*, 1(1):23–30, 2008.
- [64] Mitsuo Matsuda, Tatsuhiko Sekiguchi, Yasuro Sugishita, Kenji Kuwako, Keiji Iida, and Iwao Ito. Reliability of non-invasive estimates of pulmonary hypertension by pulsed doppler echocardiography. *Heart*, 56(2):158–164, 1986.
- [65] Youichiroh Furuno, Yasuo Nagamoto, Masasuke Fujita, Tohru Kaku, Syugo Sakurai, and Akio Kuroiwa. Reflection as a cause of mid-systolic deceleration of pulmonary flow wave in dogs with acute pulmonary hypertension: comparison of pulmonary artery constriction with pulmonary embolisation. *Cardiovascular research*, 25(2):118–124, 1991.
- [66] Shailendra P Kushwaha, Qin-Hua Zhao, Qian-Qian Liu, Wen-Hui Wu, Lan Wang, Ping Yuan, Rui Zhang, and Zhi-Cheng Jing. Shape of the pulmonary artery doppler-flow profile predicts the hemodynamics of pulmonary hypertension caused by left-sided heart disease. *Clinical cardiology*, 39(3):150–156, 2016.
- [67] Murilo Foppa, Garima Arora, Philimon Gona, Arman Ashrafi, Carol J Salton, Susan B Yeon, Susan J Blease, Daniel Levy, Christopher J O’Donnell, Warren J Manning, et al. Right ventricular volumes and systolic function by cardiac magnetic resonance and the impact of sex, age, and obesity in a longitudinally followed cohort free of pulmonary and cardiovascular diseaseclinical perspective: The framingham heart study. *Circulation: Cardiovascular Imaging*, 9(3):e003810, 2016.
- [68] Nadine Kawel-Boehm, Alicia Maceira, Emanuela R Valsangiacomo-Buechel, Jens Vogel-Claussen, Evrim B Turkbey, Rupert Williams, Sven Plein, Michael Tee, John Eng, and David A Bluemke. Normal values for cardiovascular magnetic resonance in adults and children. *Journal of Cardiovascular Magnetic Resonance*, 17(1):29, 2015.
- [69] Veli-Pekka Harjola, Alexandre Mebazaa, Jelena Čelutkienė, Dominique Bettex, Hector Bueno, Ovidiu Chioncel, Maria G Crespo-Leiro, Volkmar Falk, Gerasimos Filippatos, Simon Gibbs, et al. Contemporary management of acute right ventricular failure: a statement from the heart failure association and the working group on pulmonary circulation and right ventricular function of the european society of cardiology. *European journal of heart failure*, 18(3):226–241, 2016.
- [70] Chunguang Ken Cao and Timothy S Newman. A new framework for recovery of shape of the right ventricle from gbp spect images. In *Proceedings of the 43rd annual Southeast regional conference-Volume 2*, pages 404–405. ACM, 2005.
- [71] FP Czegledy and J Katz. A new geometric description of the right ventricle. *Journal of biomedical engineering*, 15(5):387–391, 1993.
- [72] Peter J Leary, Christopher E Kurtz, Catherine L Hough, Mary-Pierre Waiss, David D Ralph, and Florence H Sheehan. Three-dimensional analysis of right ventricular shape and function in pulmonary hypertension. *Pulmonary circulation*, 2(1):34–40, 2012.
- [73] Karima Addetia, Francesco Maffessanti, Megan Yamat, Lynn Weinert, Akhil Narang, Benjamin H Freed, Victor Mor-Avi, and Roberto M Lang. Three-dimensional echocardiography-based analysis of right ventricular shape in pulmonary arterial hypertension. *European Heart Journal-Cardiovascular Imaging*, 17(5):564–575, 2015.
- [74] Aparna Srinivasan, Jiwon Kim, Omar Khalique, Alexi Geevarghese, Melissa Rusli, Tara Shah, Antonino Di Franco, Javid Alakbarli, Samantha Goldberg, Meenakshi Rozenstrauch, et al. Echocardiographic linear

- fractional shortening for quantification of right ventricular systolic function—a cardiac magnetic resonance validation study. *Echocardiography*, 34(3):348–358, 2017.
- [75] Lamyaa Elsayed Allam, Ahmed Mohammed Onsy, and Hylan Ahmed Ghalib. Right ventricular outflow tract systolic excursion and fractional shortening: Can these echocardiographic parameters be used for the assessment of right ventricular function? *Journal of Cardiovascular Echography*, 27(2):52, 2017.
- [76] Masashi Yamaguchi, Toshihiro Tsuruda, Yuki Watanabe, Hisamitsu Onitsuka, Kuniko Furukawa, Takeshi Ideguchi, Junji Kawagoe, Tetsunori Ishikawa, Johji Kato, Makoto Takenaga, et al. Reduced fractional shortening of right ventricular outflow tract is associated with adverse outcomes in patients with left ventricular dysfunction. *Cardiovascular ultrasound*, 11(1):19, 2013.
- [77] Chandra Srinivasan, Ritu Sachdeva, W Robert Morrow, S Bruce Greenberg, and Himesh V Vyas. Limitations of standard echocardiographic methods for quantification of right ventricular size and function in children and young adults. *Journal of Ultrasound in Medicine*, 30(4):487–493, 2011.
- [78] Rika Takemoto, Hiroki Oe, Satoko Ugawa, Norihisa Toh, Nobuhisa Watanabe, Yasuharu Tanabe, and Hiroshi Ito. Right ventricular fractional area change obtained in different echocardiographic views of right heart; comparison with right ventricular ejection fraction by cardiac magnetic resonance imaging, 2013.
- [79] Jannet F Lewis, Lawrence C Kuo, Jean G Nelson, Marian C Limacher, and Miguel A Quinones. Pulsed doppler echocardiographic determination of stroke volume and cardiac output: clinical validation of two new methods using the apical window. *Circulation*, 70(3):425–431, 1984.
- [80] Bruno Valtier, Bernard P Cholley, Jean-pierre Belot, JEAN-EMMANUEL de la COUSSAYE, Joaquim Mateo, and Didier M Payen. Noninvasive monitoring of cardiac output in critically ill patients using transesophageal doppler. *American journal of respiratory and critical care medicine*, 158(1):77–83, 1998.
- [81] Micah R Fisher, Paul R Forfia, Elzbieta Chamera, Traci Houston-Harris, Hunter C Champion, Reda E Girgis, Mary C Corretti, and Paul M Hassoun. Accuracy of doppler echocardiography in the hemodynamic assessment of pulmonary hypertension. *American journal of respiratory and critical care medicine*, 179(7):615–621, 2009.
- [82] Iain R Crossingham, Daniel R Nethercott, and Malachy O Columb. Comparing cardiac output monitors and defining agreement: A systematic review and meta-analysis. *Journal of the Intensive Care Society*, 17(4):302–313, 2016.
- [83] SW Chong and Philip J Peyton. A meta-analysis of the accuracy and precision of the ultrasonic cardiac output monitor (uscom). *Anaesthesia*, 67(11):1266–1271, 2012.
- [84] M Okamoto, K Miyatake, N Kinoshita, H Sakakibara, and Y Nimura. Analysis of blood flow in pulmonary hypertension with the pulsed doppler flowmeter combined with cross sectional echocardiography. *Heart*, 51(4):407–415, 1984.
- [85] Sonia MF Mesquita, Claudia RP Castro, Nana M Ikari, Sérgio A Oliveira, and Antonio Augusto Lopes. Likelihood of left main coronary artery compression based on pulmonary trunk diameter in patients with pulmonary hypertension. *The American journal of medicine*, 116(6):369–374, 2004.
- [86] SY Ho and P Nihoyannopoulos. Anatomy, echocardiography, and normal right ventricular dimensions. *Heart*, 92(suppl 1):i2–i13, 2006.
- [87] Per Lindqvist, Michael Henein, and Elsadig Kazzam. Right ventricular outflow-tract fractional shortening: an applicable measure of right ventricular systolic function. *European Journal of Echocardiography*, 4(1):29–35, 2003.
- [88] Jesper Kjaergaard, Claus Leth Petersen, Andreas Kjaer, Bente Krogsgaard Schaadt, Jae K Oh, and Christian Hassager. Evaluation of right ventricular volume and function by 2d and 3d echocardiography compared to mri. *European journal of echocardiography*, 7(6):430–438, 2006.

- [89] Philip J Currie, James B Seward, Kwan-Leung Chan, Derek A Fyfe, Donald J Hagler, Douglas D Mair, Guy S Reeder, Rick A Nishimura, and A Jamil Tajik. Continuous wave doppler determination of right ventricular pressure: a simultaneous doppler-catheterization study in 127 patients. *Journal of the American College of Cardiology*, 6(4):750–756, 1985.
- [90] Georgeann K Groh, Philip T Levy, Mark R Holland, Joshua J Murphy, Timothy J Sekarski, Craig L Myers, Diana P Hartman, Rebecca D Roiger, and Gautam K Singh. Doppler echocardiography inaccurately estimates right ventricular pressure in children with elevated right heart pressure. *Journal of the American Society of Echocardiography*, 27(2):163–171, 2014.
- [91] Jonathan D Rich, Sanjiv J Shah, Rajiv S Swamy, Anna Kamp, and Stuart Rich. Inaccuracy of doppler echocardiographic estimates of pulmonary artery pressures in patients with pulmonary hypertension: implications for clinical practice. *Chest*, 139(5):988–993, 2011.
- [92] Takuma Hioka, Sanae Kaga, Taisei Mikami, Kazunori Okada, Michito Murayama, Nobuo Masauzi, Masahiro Nakabachi, Hisao Nishino, Shinobu Yokoyama, Mutsumi Nishida, et al. Overestimation by echocardiography of the peak systolic pressure gradient between the right ventricle and right atrium due to tricuspid regurgitation and the usefulness of the early diastolic transpulmonary valve pressure gradient for estimating pulmonary artery pressure. *Heart and vessels*, 32(7):833–842, 2017.
- [93] Michael S Firstenberg, Erik E Abel, Thomas J Papadimos, and Ravi S Tripathi. Nonconvective forces: a critical and often ignored component in the echocardiographic assessment of transvalvular pressure gradients. *Cardiology research and practice*, 2012, 2012.
- [94] Per Ask, Dan Loyd, and Bengt Wranne. Regurgitant flow through heart valves: a hydraulic model applicable to ultrasound doppler measurements. *Medical and Biological Engineering and Computing*, 24(6):643–646, 1986.
- [95] Alessandro Giardini and Theresa A Tacy. Non-invasive estimation of pressure gradients in regurgitant jets: an overdue consideration. *European Journal of Echocardiography*, 9(5):578–584, 2008.
- [96] Edward G Cape, Michael Jones, Izumi Yamada, Michael D VanAuker, and Lilliam M Valdes-Cruz. Turbulent/viscous interactions control doppler/catheter pressure discrepancies in aortic stenosis. *Circulation*, 94(11):2975–2981, 1996.
- [97] Florence H Sheehan and Per Lindqvist. Echocardiography of chronic right heart failure. In *The Right Ventricle in Health and Disease*, pages 209–248. Springer, 2015.
- [98] Michael J Miller, Raymond G McKay, James J Ferguson, Peter Sahagian, Shoichiro Nakao, Patricia C Come, and William Grossman. Right atrial pressure-volume relationships in tricuspid regurgitation. *Circulation*, 73(4):799–808, 1986.
- [99] Jeffrey B Geske, Dawn C Scantlebury, James D Thomas, and Rick A Nishimura. Hemodynamic evaluation of severe tricuspid regurgitation. *Journal of the American College of Cardiology*, 62(20):e441, 2013.
- [100] Rick A Nishimura, Catherine M Otto, Robert O Bonow, Blase A Carabello, John P Erwin, Robert A Guyton, Patrick T O’Gara, Carlos E Ruiz, Nikolaos J Skubas, Paul Sorajja, et al. 2014 aha/acc guideline for the management of patients with valvular heart disease: executive summary: a report of the american college of cardiology/american heart association task force on practice guidelines. *Journal of the American College of Cardiology*, 63(22):2438–2488, 2014.
- [101] Shinichi Minagoe, Shahbudin H Rahimtoola, and P Anthony N Chandraratna. Significance of laminar systolic regurgitant flow in patients with tricuspid regurgitation: a combined pulsed-wave, continuous-wave doppler and two-dimensional echocardiographic study. *American heart journal*, 119(3):627–635, 1990.
- [102] Frederick C Cobey, Maria Fritock, Frederick W Lombard, Donald D Glower, and Madhav Swaminathan. Severe tricuspid valve regurgitation: a case for laminar flow. *Journal of cardiothoracic and vascular anesthesia*, 26(3):522–524, 2012.

- [103] Yu Zhang, Yuanyuan Wang, Weiqi Wang, and Bin Liu. Doppler ultrasound signal denoising based on wavelet frames. *IEEE transactions on ultrasonics, ferroelectrics, and frequency control*, 48(3):709–716, 2001.
- [104] Yufeng Zhang, Le Wang, Yali Gao, Jianhua Chen, and Xinling Shi. Noise reduction in doppler ultrasound signals using an adaptive decomposition algorithm. *Medical engineering and physics*, 29(6):699–707, 2007.
- [105] David G Platts, Manan Vaishnav, Darryl J Burstow, Christian Hamilton Craig, Jonathan Chan, John L Sedgwick, and Gregory M Scalia. Contrast microsphere enhancement of the tricuspid regurgitant spectral doppler signal—is it still necessary with contemporary scanners? *IJC Heart & Vasculature*, 17:1–10, 2017.
- [106] Michael Thomas and John Shillingford. The circulatory response to a standard postural change in ischaemic heart disease. *British heart journal*, 27(1):17, 1965.
- [107] Massimo Bertolissi, Ugo Da Broi, Franca Soldano, and Flavio Bassi. Influence of passive leg elevation on the right ventricular function in anaesthetized coronary patients. *Critical Care*, 7(2):164, 2003.
- [108] David H Wong, Kevin K Tremper, June Zaccari, Jadwiga Hajduczek, Halappa N Konchigeri, and Steve M Hufstедler. Acute cardiovascular response to passive leg raising. *Critical care medicine*, 16(2):123–125, 1988.
- [109] David Osman, Christophe Ridel, Patrick Ray, Xavier Monnet, Nadia Anguel, Christian Richard, and Jean-Louis Teboul. Cardiac filling pressures are not appropriate to predict hemodynamic response to volume challenge. *Critical care medicine*, 35(1):64–68, 2007.
- [110] Bart F Geerts, Lara van den Bergh, Theo Stijnen, Leon PHJ Aarts, and Jos RC Jansen. Comprehensive review: is it better to use the trendelenburg position or passive leg raising for the initial treatment of hypovolemia? *Journal of clinical anesthesia*, 24(8):668–674, 2012.
- [111] Xavier Monnet, Mario Rienzo, David Osman, Nadia Anguel, Christian Richard, Michael R Pinsky, and Jean-Louis Teboul. Passive leg raising predicts fluid responsiveness in the critically ill. *Critical care medicine*, 34(5):1402–1407, 2006.
- [112] Thierry Boulain, Jean-Michel Achard, Jean-Louis Teboul, Christian Richard, Dominique Perrotin, and Guy Ginies. Changes in bp induced by passive leg raising predict response to fluid loading in critically ill patients. *Chest*, 121(4):1245–1252, 2002.
- [113] Matthieu Biais, Lionel Vidil, Philippe Sarrabay, Vincent Cottenceau, Philippe Revel, and François Sztark. Changes in stroke volume induced by passive leg raising in spontaneously breathing patients: comparison between echocardiography and vigileoTM/flotracTM device. *Critical Care*, 13(6):R195, 2009.
- [114] F Andrew Gaffney, Bruce C Bastian, Erwin R Thal, James M Atkins, and C Gunnar Blomqvist. Passive leg raising does not produce a significant or sustained autotransfusion effect. *The Journal of trauma*, 22(3):190–193, 1982.
- [115] Bouchra Lamia, Ana Ochagavia, Xavier Monnet, Denis Chemla, Christian Richard, and Jean-Louis Teboul. Echocardiographic prediction of volume responsiveness in critically ill patients with spontaneously breathing activity. *Intensive care medicine*, 33(7):1125–1132, 2007.
- [116] Thomas GV Cherpanath, Alexander Hirsch, Bart F Geerts, Wim K Lagrand, Mariska M Leeftang, Marcus J Schultz, and AB Johan Groeneveld. Predicting fluid responsiveness by passive leg raising: a systematic review and meta-analysis of 23 clinical trials. *Critical care medicine*, 44(5):981–991, 2016.
- [117] BF Geerts, LPHJ Aarts, AB Groeneveld, and JRC Jansen. Predicting cardiac output responses to passive leg raising by a peep-induced increase in central venous pressure, in cardiac surgery patients. *British journal of anaesthesia*, 107(2):150–156, 2011.
- [118] Rebecca R Vanderpool, Michael R Pinsky, Robert Naeije, Christopher Deible, Vijaya Kosaraju, Cheryl Bunner, Michael A Mathier, Joan Lacomis, Hunter C Champion, and Marc A Simon. Rv-pulmonary arterial coupling predicts outcome in patients referred for pulmonary hypertension. *Heart*, 101(1):37–43, 2015.

- [119] Javier Sanz, Ana García-Alvarez, Leticia Fernández-Friera, Ajith Nair, Jesús G Mirelis, Simonette T Sawit, Sean Pinney, and Valentin Fuster. Right ventriculo-arterial coupling in pulmonary hypertension: a magnetic resonance study. *Heart*, 98(3):238–243, 2012.
- [120] Kenji Sunagawa, Akira Yamada, Yutaka Senda, Yutaka Kikuchi, Motoomi Nakamura, Tetsutaro Shibahara, and Yoshiaki Nose. Estimation of the hydromotive source pressure from ejecting beats of the left ventricle. *IEEE Transactions on Biomedical Engineering*, (6):299–305, 1980.
- [121] Hideaki Senzaki, Chen-Huan Chen, and David A Kass. Single-beat estimation of end-systolic pressure-volume relation in humans: a new method with the potential for noninvasive application. *Circulation*, 94(10):2497–2506, 1996.
- [122] Titus Kuehne, Sevim Yilmaz, Paul Steendijk, Phillip Moore, Maarten Groenink, Maythem Saaed, Oliver Weber, Charles B Higgins, Peter Ewert, Eckard Fleck, et al. Magnetic resonance imaging analysis of right ventricular pressure-volume loops: in vivo validation and clinical application in patients with pulmonary hypertension. *Circulation*, 110(14):2010–2016, 2004.
- [123] Ryo Inuzuka, Steven Hsu, Ryan J Tedford, and Hideaki Senzaki. Single-beat estimation of right ventricular contractility and its coupling to pulmonary arterial load in patients with pulmonary hypertension. *Journal of the American Heart Association*, 7(10):e007929, 2018.
- [124] Nicholas E Hobson and Kendall S Hunter. Ventricular-vascular coupling in the pulmonary circulation. In *Right Ventricular Physiology, Adaptation and Failure in Congenital and Acquired Heart Disease*, pages 53–68. Springer, 2018.
- [125] Pieter R Fourie, André R Coetzee, and Chris T Bolliger. Pulmonary artery compliance: its role in right ventricular-arterial coupling. *Cardiovascular research*, 26(9):839–844, 1992.
- [126] Pierre Wauthy, Alberto Pagnamenta, Fabio Vassalli, Robert Naeije, and Serge Brimiouille. Right ventricular adaptation to pulmonary hypertension: an interspecies comparison. *American Journal of Physiology-Heart and Circulatory Physiology*, 286(4):H1441–H1447, 2004.
- [127] Alexandre Ghuysen, Bernard Lambermont, Philippe Kolh, Vincent Tchana-Sato, David Magis, Paul Gerard, Véronique Mommens, Nathalie Janssen, Thomas Desaive, and Vincent D’orio. Alteration of right ventricular-pulmonary vascular coupling in a porcine model of progressive pressure overloading. *Shock*, 29(2):197–204, 2008.
- [128] Julien Guihare, Francois Haddad, David Boulate, Benoît Decante, Andre Y Denault, Joseph Wu, Philippe Hervé, Marc Humbert, Philippe Dartevelle, Jean-Philippe Verhoye, et al. Non-invasive indices of right ventricular function are markers of ventricular-arterial coupling rather than ventricular contractility: insights from a porcine model of chronic pressure overload. *European Heart Journal–Cardiovascular Imaging*, 14(12):1140–1149, 2013.
- [129] Kenji Sunagawa, W Lowell Maughan, and Kiichi Sagawa. Optimal arterial resistance for the maximal stroke work studied in isolated canine left ventricle. *Circulation research*, 56(4):586–595, 1985.
- [130] Brian Oommen, Mustafa Karamanoglu, and Sándor J Kovács. Modeling time varying elastance: the meaning of “load-independence”. *Cardiovascular Engineering: An International Journal*, 3(4):123–130, 2003.
- [131] Patrick Segers, Nikos Stergiopoulos, Nico Westerhof, Patrick Wouters, Philippe Kolh, and Pascal Verdonck. Systemic and pulmonary hemodynamics assessed with a lumped-parameter heart-arterial interaction model. *Journal of Engineering Mathematics*, 47(3-4):185–199, 2003.
- [132] Mandeep R Mehra, Myung H Park, Michael J Landzberg, and Aaron B Waxman. The normal and abnormal right heart: Introduction to a clinical classification. In *The Right Heart*, pages 1–5. Springer, 2014.
- [133] H Kalinic, S Loncaric, M Cikes, A Baltabaeva, C Parsai, J Separovic, I Cikes, GR Sutherland, and Bart Bijmens. Analysis of doppler ultrasound outflow profiles for the detection of changes in cardiac function. In *Image and Signal Processing and Analysis, 2007. ISPA 2007. 5th International Symposium on*, pages 326–331. IEEE, 2007.